BIOFEEDBACK DRIVEN MUSCLE COORDINATION

by

Ollie Blake

B.Sc., University of Guelph, 2002
M.Sc., Simon Fraser University, 2012

Thesis Submitted in Partial Fulfillment of the
Requirements for the Degree of
Doctor of Philosophy

in the
Department of Biomedical Physiology and Kinesiology
Faculty of Science

SIMON FRASER UNIVERSITY

Fall 2015

Approval

Name:	**Oliver Blake**
Degree:	**Doctor of Philosophy (Biomedical Physiology & Kinesiology)**
Title:	***Biofeedback Driven Muscle Coordination***
Examining Committee:	**Chair: Dr. Miriam Rosin** Professor

James Wakeling
Senior Supervisor
Professor _____

David Clarke
Supervisor
Assistant Professor _____

Max Donelan
Internal Examiner
Professor
Department of Biomedical Physiology & Kinesiology _____

James Martin
External Examiner
Associate Professor
Department of Exercise and Sport Science
The University of Utah _____

Date Defended/Approved: December 17, 2015

Ethics Statement

The author, whose name appears on the title page of this work, has obtained, for the research described in this work, either:

a. human research ethics approval from the Simon Fraser University Office of Research Ethics,

or

b. advance approval of the animal care protocol from the University Animal Care Committee of Simon Fraser University;

or has conducted the research

c. as a co-investigator, collaborator or research assistant in a research project approved in advance,

or

d. as a member of a course approved in advance for minimal risk human research, by the Office of Research Ethics.

A copy of the approval letter has been filed at the Theses Office of the University Library at the time of submission of this thesis or project.

The original application for approval and letter of approval are filed with the relevant offices. Inquiries may be directed to those authorities.

Simon Fraser University Library
Burnaby, British Columbia, Canada

update Spring 2010

Abstract

Groups of muscles are recruited in various combinations to perform smooth, controlled limb movements. Within these muscle groups, the excitation of a single muscle is commonly the focus of manipulation when attempting to influence limb movement, but it is the coordinated excitation of multiple muscles (muscle coordination) that ultimately determines the limb movement and mechanics. Despite successes with single muscles, the capabilities of manipulating muscle coordination are unknown. Therefore the goal of this research was to develop a tool to purposefully manipulate muscle coordination.

This research is comprised of four studies that collectively facilitated the development of a biofeedback tool to purposefully manipulate muscle coordination in real-time during movement. The first study established a physiologically relevant outcome to be used by the biofeedback tool. The study showed that muscle excitation provides good predictions of changes in metabolic power and could therefore be used to determine the relative mechanical efficiency of different muscle coordination strategies. The second and third studies established a muscle coordination reference frame, specific to the efficiency outcome ascertained in the first study, used to characterize the current and desired end states of muscle coordination. Specifically, muscle coordination patterns, and their associated relative efficiencies, were determined across a range of mechanical demands to distinguish the key features responsible for differences in efficiency that were subsequently used to guide the biofeedback tool.

In the final study, a novel biofeedback tool for manipulating muscle coordination was developed and validated. The underlying algorithm used principal component decomposition of muscle excitation to characterize the changes in muscle coordination at different mechanical demands. The algorithm was modified to be implemented in real-time and the tool was validated by having subjects cycle while receiving feedback comparing their muscle coordination to the reference frame. The results showed that the subjects were successfully able to change muscle coordination to improve the relative efficiency of the movement. Collectively, this research provides a valuable tool for research into motor learning and could be applied to improve rehabilitation and sport performance.

Keywords: Electromyography; Cycling; Motor Control; Excitation; Wavelets; Principal Component Analysis

Acknowledgements

I would like to thank Dr. James Wakeling for allowing me to continue my studies in his laboratory. He has continually encouraged me to stretch my knowledge and ideas in an eventful few years of idea sharing and outdoor pursuits. I am fortunate to have a supervisor that shares a similar outlook that a good work-life balance and plenty of outdoor adventures are vital in research! He leads by example and has shown me that some of the best ideas come when you are out skiing, biking, paddling, running or hiking. Thank you also to my co-supervisor, Dr. Dave Clarke. I was fortunate to have Dave join my committee later in the process and immediately provide valuable input to my research and writing. He has also shown a genuine interest in my continued success by helping me grow my network so that I could find my next research position. Fortunately both James and Dave will be part of the support crew in my next position so I know it will be a success!

Thank you the many people that have worked in the lab over the past four years, shared their knowledge and suffered through my constant chatter. I have benefited greatly from each of them, in particular thank you to Dr. Sabrina Lee, Dr. Courtney Pollock, Dr. Hadi Rahemi, Avleen Randhawa, Taylor Dick, David Ryan, Eleanor Li, Sidney Morrison, Kate Olszewski, Basant Chana and the list goes on, which means I have missed someone.

Most importantly I would like to thank Kristina Rody for her unwavering support and motivation to get me out the door every single day! If not for Kristina I would not have applied for the Vanier Scholarship that funded my research and kept food on the table! A couple of kids, a few publications and four years later, I can only say that WE have been an effective and productive team. Of course my two amazing daughters (Jasmine and Malaika) may not remember this time, but I certainly need to thank them for putting each day into perspective in the simple, happy way that only a toddler can. There is nothing like starting your day with your wife running your daughters in the stroller through the forest to school! With bears, dear, coyotes, racoons and squirrels it is always an adventure!

I would like to acknowledge the funding I received through the Vanier Canada Graduate Scholarship. It was an essential part of my PhD that allowed me to focus on my research and complete my thesis in a timely manner and still have a family.

Table of Contents

List of Tables

List of Figures

Chapter 1.

Introduction

Muscles often work in groups to produce movement. Within these muscle groups, multiple muscles cross the same joint and can be recruited in numerous combinations making it possible to perform a range of smooth controlled limb movements. The manner in which muscle recruitment is coordinated to produce limb movements is reflected in outcome variables such as limb kinematics, energy consumption and mechanical power (Wakeling et al., 2010). For example, we recently demonstrated that the coordination of muscle excitation (muscle coordination) limits both the limb mechanics used to produce power and the efficiency of limb movement (Wakeling et al., 2010). Muscle coordination is therefore an important factor when attempting to manipulate limb movement, such as during rehabilitation and sport performance. However, it is currently unknown whether muscle coordination can be purposefully manipulated.

Muscle excitation refers to the depolarization of the muscle cells by action potentials that results in muscular contractions. Manipulation of muscle excitation using real-time sensory feedback (biofeedback) has been successfully used in areas such as post stroke rehabilitation (Moreland et al., 1998), headache disorders (Nestoriuc et al., 2008) and re-education of pelvic floor musculature (Koh et al., 2008). These manipulation methods predominantly focus on the amplitude and timing of muscle excitation in a single muscle. Although individual muscles are important for movement, it is the amplitude and timing of muscle excitation across multiple muscles that determines the outcome. Furthermore, manipulating a single muscle is unrealistic because other muscles and the coordination amongst muscles are also affected. **Therefore a key objective of this research was to develop and show proof of concept of a biofeedback tool that could evaluate and facilitate the manipulation of muscle coordination.**

Cycling on a stationary ergometer is an appropriate mode to investigate the manipulation of muscle coordination because it provides constrained limb movement in a controlled environment. In addition, during cycling, mechanical demands such as workload and velocity can be decoupled (Wakeling and Horn, 2009; Wakeling et al., 2006), which makes it a good model to examine and account for the effects of mechanical demands on muscle excitation and muscle coordination. Therefore, a series of studies using cycling were designed and conducted to evaluate and manipulate muscle coordination patterns.

1.1. Establishing an Biofeedback Outcome

Efficiency (Blake et al., 2012; Wakeling et al., 2010) and power production (Dorel et al., 2012; Samozino et al., 2007; Wakeling et al., 2010) are two fundamental outcomes of human movement that are influenced by muscle coordination. Mechanical efficiency during movement is a measure of the ability to utilize energy, or metabolic power, to produce mechanical power. Thus mechanical efficiency during movement is dependent on the energy required by the contracting muscles, such that it is reasonable to hypothesize that muscle contractions contain meaningful information about metabolic power. **Hence, the first part of this study aimed to characterize the relationship between muscle excitation and metabolic power in order to use muscle excitation as a measureable outcome of the energetics and relative efficiency of the movement.**

Aerobic metabolism during dynamic activities is commonly estimated using oxygen and carbon dioxide gas exchange, but its temporal resolution is limited by the relatively slow respiration rate. Consequently, information about muscular contractions that influence metabolic power is neglected as these contractions can occur more frequently than the respiration rate. Information about muscular contractions can be detected using surface electromyography (EMG) and therefore EMG must contain information about metabolic power at a higher temporal resolution than gas exchange measures, yet it is unknown if EMG is an appropriate method to estimate changes in metabolic power during non steady-state dynamic activities.

Investigations of the relationship between oxygen uptake ($\dot{V}O_2$) and EMG provide evidence of linear (Arnaud et al., 1997; Bigland-Ritchie and Woods, 1976; Jammes et al., 1998) and non-linear (Hug et al., 2004a) relationships below and above the anaerobic threshold, respectively. The non-linear relationship is partially explained by a proportionally larger increase in EMG than $\dot{V}O_2$ due to a greater reliance on anaerobic metabolism. EMG does not discriminate the energy source and therefore contains information about metabolic power from both aerobic and anaerobic sources. We recently showed that a monotonic increase in metabolic power ($r = 0.86$) is associated with increased EMG intensity from mean values of $\dot{V}O_2$ and EMG calculated at constant workloads (Wakeling et al., 2011). This relationship only indicates that metabolic power is related to EMG intensity during steady-state activities averaged over an extended time. The workload transitions were not investigated and the higher temporal resolution of the EMG was ignored. The purpose of the study in chapter two was therefore to define metabolic changes based on EMG, in non steady-state conditions, by establishing a scientifically meaningful relationship between metabolic power and EMG. **It was hypothesized that a scientifically meaningful relationship exists at a greater temporal resolution than previously determined such that estimates of changes in metabolic power can be determined from the EMG signal and muscle excitation can be used as an energetics outcome by the biofeedback system**.

1.2. Establishing a Biofeedback Reference

Comprehensive understanding of muscle coordination, and changes in muscle excitation of the individual muscles that comprise muscle coordination patterns, is essential to establish a physiologically acceptable reference for the biofeedback system. It is also important to understand the relationships between muscle coordination and mechanical demands, such as cycle frequency and workload, and how these relationships influence desired outcomes such as mechanical efficiency and power production. **The second part of this study, therefore, aimed to determine the responses of muscle excitation and coordination to a wide range of mechanical demands and the subsequent influence on relative mechanical efficiency and power production.**

During multi-muscle contractions, the spatiotemporal characteristics of muscle excitation describe the primary features of muscle coordination. Understanding the effects of workload and cycle frequency on muscle coordination is important to the development of a biofeedback system that aims to facilitate the manipulation of muscle coordination towards outcome measures such as relative mechanical efficiency and power output. Understanding the effects of workload and cycle frequency is important because muscle coordination affects mechanical efficiency (Blake et al., 2012; Wakeling et al., 2010) and power output (Dorel et al., 2012; Samozino et al., 2007; Wakeling et al., 2010), yet few studies have looked at the muscle coordination-workload-cycle frequency relationships across multiple muscles.

Changes in excitation of the muscles that comprise muscle coordination in response to mechanical demands, such as workload and cycle frequency (cadence), differs for each muscle (Ericson et al., 1985; Hug et al., 2004b; Jorge and Hull, 1986; Wakeling and Horn, 2009; Wakeling et al., 2006) and have been reviewed (Hug and Dorel, 2009). Briefly, relative muscle excitation is workload dependent and differs for each muscle (Blake and Wakeling, 2012; Blake et al., 2012; Ericson, 1986; Ericson et al., 1985; Hug et al., 2004b; Jorge and Hull, 1986; Sarre et al., 2003; Wakeling and Horn, 2009; Wakeling et al., 2010). The excitation response of individual muscles to different cadences also varies, with many inconsistencies among the collective research (Ericson, 1986; Ericson et al., 1985; Lucia et al., 2004; Neptune et al., 1997; Neptune et al., 1997; Sarre and Lepers, 2005; Sarre and Lepers, 2007; Sarre et al., 2003; Takaishi et al., 1996; Takaishi et al., 1998; Wakeling and Horn, 2009; Wakeling et al., 2006). Evidence suggests that the relationships between muscle excitation and cadence are workload dependent (MacIntosh et al., 2000), which may explain these inconsistencies since a broad range of workloads were employed. Therefore, in chapter four **we hypothesized that there exists an interactive influence of cadence and workload on muscle excitation that would explain previous inconsistencies reported in the literature with respect to the responses of muscle excitation to changes in cadence**. The timing of muscle excitation is also affected by cadence (Baum and Li, 2003; Dorel et al., 2012; Marsh and Martin, 1995; Neptune et al., 1997; Samozino et al., 2007; Sarre and Lepers, 2005; Sarre and Lepers, 2007; Wakeling and Horn, 2009), and both influenced (Sarre and Lepers,

2007) and not influenced (Jorge and Hull, 1986) by workload, but relatively little research has been completed in this area.

Just as the workload-cadence relationships are important to understand muscle coordination, the influence these relationships have on efficiency is important when attempting to manipulate muscle coordination towards such an outcome. Efficiency in cycling has been reviewed (Ettema and Loras, 2009) and is dependent largely on workload, and to a lesser extent on cadence, and is maximized at increasing cadences for increasing power outputs (Böning et al., 1984; Coast and Welch, 1985; Foss and Hallén, 2004; Hagberg et al., 1981; Seabury et al., 1977). Increasing cadence with workload to obtain greater efficiency may reduce the required muscle excitation, and therefore energy, used by the working muscles, since minimum muscle excitation also occurs at increasing cadences with increasing submaximal workloads (MacIntosh et al., 2000).

Increased relative efficiencies resulting from reductions in muscle excitation may occur due to changes in muscle fibre recruitment. Maximum efficiency has been predicted to occur in cycling at approximately 50 and 150 revolutions per minute (r.p.m.) in slow and fast muscle fibres, respectively (Sargeant, 2007). Maximum efficiency would therefore result from a combination of slow and fast muscle fibres, in a mixed fibre type muscle, at an intermediate cadence (professional endurance cyclists typically cycle at approximately 90-105 r.p.m. (Foss and Hallén, 2004; Lucia et al., 2001; Sargeant, 1994)). Maximizing efficiency by increasing cadence with power output may minimize the inefficient fast muscle fibres required, assuming all slow fibres are active, and operate at a more favorable intermediate velocity for both fibres (Sargeant and Beelen, 1993). Greater relative recruitment of fast muscle fibres at 50 r.p.m. compared to 100 r.p.m. (Ahlquist et al., 1992) lends support to this idea as more fast fibres would be necessary at 50 r.p.m. to compensate for their inability to produce power at low velocities. It has also been suggested that 25% maximum power output could be achieved with only slow muscle fibres at 60 r.p.m., whereas fast fibres would be needed for the same power output at 120 r.p.m. due to the inability of slow fibres to produce power at high velocities (Sargeant, 1994; Sargeant and Beelen, 1993). Indeed, faster muscle fibres are recruited at high cycle frequencies, such as 120 r.p.m., at high and low workloads before slow fibres are fatigued

(Farina et al., 2004). Given these changes in muscle fibre recruitment, in chapter four **we hypothesized that a distinct shift in muscle fibre type recruitment will coincide with maximum relative efficiency and this will be demonstrated by a shift in the frequency content of the EMG signal**.

Muscle and muscle fibre recruitment, and therefore muscle coordination, also influence maximum power output, which is another desirable outcome of the biofeedback system. Maximum power output depends on fibre type composition (Hautier et al., 1996) and in cycling occurs at 110-120 r.p.m. (Beelen and Sargeant, 1991; Dorel et al., 2010; Hautier et al., 1996; Samozino et al., 2007; Sargeant et al., 1981). It has been predicted that these cadences optimize fast and slow muscle fibre recruitment, where each fibre type has distinct maximum power outputs at different velocities (Sargeant and Beelen, 1993). Also, faster muscle fibres contribute more to maximum power output at higher cadences such as those found at 120 r.p.m. (Beelen and Sargeant, 1991). When the whole limb is producing maximum power output it is improbable that all muscles are working at optimal velocities for power production (Van Soest and Casius, 2000) since they have different fibre type distributions and structural properties. Indeed, when cycling at maximum power output the ankle plantar flexor muscles shorten at velocities too slow to produce maximum power (Wakeling et al., 2010), yet the soleus (Sol) is at or near maximum excitation (Dorel et al., 2012) during sprint cycling. The Sol, medial (MG) and lateral (LG) gastrocnemii perform the same joint action at the ankle, yet it is doubtful they share a common optimal contraction velocity for maximum power output since Sol has a higher proportion of slow muscle fibres and different muscle fibre arrangement compared to MG and LG. Further, muscle and muscle fibre recruitment changes at extreme shortening velocities with evidence of preferential fast muscle or fast fibre recruitment at high shortening velocities (Citterio and Agostoni, 1984; Gillespie et al., 1974; Gollnick et al., 1974; Grimby and Hannerz, 1977; Hodson-Tole and Wakeling, 2008a; Hoffer et al., 1981; Jayne and Lauder, 1994; Nardone et al., 1989; Smith et al., 1980; Wakeling et al., 2006).

Restrictions on maximum power production may be the result of muscle fibre activation-deactivation limits despite the existence of preferential fast muscle fibre recruitment. It has been suggested that during fast muscle contractions complete inhibition

of slow fibres, within a mixed fibre type muscle, would be detrimental to power production as they would provide resistance to whole muscle shortening (Josephson and Edman, 1988). Therefore, it is speculated that slow fibres are activated, but deactivated before faster fibres to account for their longer deactivation times (Hodson-Tole and Wakeling, 2008a; Lee et al., 2013; Roberts and Gabaldón, 2008). This is because the time between the end of muscle excitation and subsequent shortening represents an increasing portion of the muscle contraction-relaxation cycle at increasing cycle frequencies. Qualitative graphical evidence of this has been shown (Hodson-Tole and Wakeling, 2008a; Wakeling, 2004), but never quantitatively and statistically. In the current research the muscles were subject to an extreme range of mechanical demands to push the recruitment strategies to their limits, in order to quantitatively and statistically test whether shifts in muscle fibre recruitment occur with derecruitment of slow fibres before fast fibres at the highest cycle frequencies. In chapter three **we hypothesized that early derecruitment of slower muscle fibres during muscle relaxation would occur at the highest cycle frequencies, which would be demonstrated by a relative reduction in the low-frequency component of the EMG intensity at the end of the burst of EMG excitation** (Wakeling and Horn, 2009; Wakeling et al., 2001). Showing early derecruitment of slower muscle fibres would provide further insight into the limitations of muscle coordination on maximum power output.

1.3. Goals & Specific Aims

Recently we demonstrated that limb mechanics, the energy required for limb movement (Wakeling et al., 2010) and the trade-off between efficiency and power production (Kohler and Boutellier, 2005) are linked to limitations and differences in muscle coordination (Blake et al., 2012), yet it is unknown if muscle coordination can be manipulated and altered towards a predetermined resultant pattern. **Therefore the specific aims of this research were:**

Aim (1) In chapter two we aimed to determine how metabolic power is related to muscle excitation across a range of cycling conditions to *establish an outcome for the biofeedback system*.

Aim (2) In chapters three and four we aimed to establish a comprehensive understanding of muscle excitation and coordination across a wide range of muscles and mechanical demands during cycling to *create a muscle coordination reference frame for the biofeedback system*.

Aim (3) In chapter five we aimed to develop and show proof of concept of a working system able to evaluate muscle coordination against a predetermined reference (Aim 2), based on a measurable outcome (Aim 1), and provide real-time biofeedback in order to *elicit changes in coordination used for locomotion*.

Portions of this thesis have previously been published elsewhere. Portions of chapter 2 previously appeared as: (Blake and Wakeling, 2013), portions of chapter 3 previously appeared as: (Blake and Wakeling, 2014) and portions of chapter 4 previously appeared as: (Blake and Wakeling, 2015).

Chapter 2.

Establish a biofeedback outcome: estimating changes in metabolic power from EMG

2.1. Introduction

The first aim of this research was to establish a scientifically meaningful relationship between metabolic power and muscle excitation across a range of mechanical demands. The establishment of a scientifically meaningful relationship was essential in order to use muscle excitation as a measureable outcome of the energetics and relative efficiency of the movement for the biofeedback system described in chapter five.

Contracting muscles require energy and more energy is needed as muscular force production increases. For example, metabolic rates can increase 21 times above resting levels in trained cyclists (Astrand and Rodahl, 1986), which is primarily attributed to the energy supplied to the contracting leg muscles by aerobic and anaerobic sources. Muscle contractions during dynamic activities must therefore contain considerable information about metabolic power.

Aerobic metabolism during dynamic activities is often estimated using oxygen and carbon dioxide gas exchange where the energy utilized by the working muscles reflects the changes in pulmonary oxygen uptake (Poole et al., 1992). Unfortunately measures of metabolic power based on gas exchange are unable to resolve metabolic costs to a resolution greater than the respiration rate. Consequently, information about muscular contractions that influence metabolic power is neglected since these contractions can occur more frequently than the respiration rate.

Portions of this chapter previously appeared as: (Blake and Wakeling, 2013)

Alterations in muscle excitation, namely altered motor unit recruitment and firing rates, are primarily responsible for changes in force during muscular contractions. The alterations in muscle excitation can be detected using surface electromyography (EMG), which provides information about the active muscle by measuring the electrical signals of the motor unit action potentials. Muscle excitation during high speed gait cycles and cycling movements can take less than a second and EMG fluctuates considerably within this time. Muscle excitation measured through EMG must therefore contain information about metabolic power at a higher temporal resolution than gas exchange measures, yet it is unknown if EMG can be used to estimate metabolic power changes during non steady-state dynamic activities.

Previous studies looking at the relationship between oxygen uptake ($\dot{V}O_2$) and EMG have shown evidence of a linear relationship below the anaerobic threshold (Arnaud et al., 1997; Bigland-Ritchie and Woods, 1976; Jammes et al., 1998) and a non-linear relationship above the anaerobic threshold (Hug et al., 2004a). The non-linearity of this relationship is partially explained by a greater increase in EMG than $\dot{V}O_2$ above the anaerobic threshold due to a larger reliance on anaerobic metabolism. More recently we found a significant monotonic increase in metabolic power ($r = 0.86$), estimated from $\dot{V}O_2$ that was associated with increased EMG intensity (Wakeling et al., 2011). Mean values of $\dot{V}O_2$ and EMG intensity were calculated while cycling at or near steady-state at a range of workloads. This relationship only indicates that metabolic power is related to EMG intensity during steady-state activity when averaged over an extended time. The relationships at the workload transitions were not investigated and the higher temporal resolution of the EMG was ignored. Dynamic activities are rarely performed at constant workloads except during controlled experiments. It is therefore important to assess the relationship between metabolic power and EMG in non steady-state conditions.

Oxygen uptake kinetics in response to a stepwise change in workload can be modeled as exponential processes distinguished by changes in arterial and venous blood oxygen content (Jones and Poole, 2005). Oxygen uptake kinetics modeled this way provides good predictions of the oxygen uptake kinetics underlying the breath-by-breath fluctuations. Oxygen demands of the working muscles, in response to the change in

workload, require adequate changes in cardiac output and $\dot{V}O_2$, yet these changes are delayed compared to the EMG signal since the altered venous blood oxygen content takes time to reach the lungs. For example, there exists a time delay of approximately 20 seconds accounting for approximately 20% of the total increase in $\dot{V}O_2$, in response to a stepwise increase in workload, before the primary exponential rise towards steady-state (Whipp et al., 1982).

The purpose of this study was to further define metabolic changes based on EMG by establishing a significant and scientifically meaningful relationship between metabolic power and EMG on a breath-by-breath basis in non steady-state conditions. It was hypothesized that a significant relationship exists at a greater temporal resolution than previously determined and good estimates of changes in metabolic power would be established from the EMG signal. **The objectives therefore were:**

Objective 1) Establish a significant and scientifically meaningful relationship between metabolic power and EMG on a breath-by-breath basis in non steady-state conditions.

Objective 2) Determine if a reduced set of muscles can provide as accurate an estimate metabolic power as the entire set of muscles.

2.2. Methods

Nine competitive male cyclists (age = 41.8 ± 2.7 yr, mass = 77.2 ± 2.2 kg, height = 1.81 ± 0.01 m, $\dot{V}O_{2max}$ = 64.65 mL kg^{-1} min^{-1} , yearly mileage = 9428 ± 1913 km; mean ± S.E.M.) participated in the study. The participants gave their informed written consent, and the ethics committee in accordance with the Office of Research Ethics at Simon Fraser University approved all procedures.

The cycling protocol was completed as described previously (Blake et al., 2012). Briefly, participants cycled continuously for 18 minutes in three minute intervals at 25, 40 and 55% of the power output at $\dot{V}O_{2max}$ in random order followed by 60, 75 and 90% $\dot{V}O_{2max}$, also in random order, while oxygen and carbon dioxide gas exchange and EMG

from 10 leg muscles were recorded. The EMG was resolved into intensities (von Tscharner, 2000) and normalized to the mean intensity for each participant for each muscle across all conditions. Total EMG intensity was calculated as the sum of the EMG intensities from each muscle for each pedal cycle and thus was termed the cycle-by-cycle value.

Breath-by-breath total EMG intensities were determined by taking the mean total EMG intensity of those pedal cycles between each breath. Pedal cycles containing breath measurements were included in the following breath. Metabolic power was calculated from the gas exchange parameters using caloric equivalents of oxygen (Foss et al., 1998). For each subject Pearson correlation coefficients were calculated between the breath-by-breath measures of EMG intensity and metabolic power. Also cross-correlation was used to account for the time delay (t_{delay}) between the onset of EMG and subsequent gas exchange measure of metabolic power. Metabolic power (*P* in Eq. 1) was also estimated from the EMG intensity using a bilinear differential equation (Zajac, 1989) that has been used previously to determine the active state of a muscle from its EMG excitation (Lee et al., 2011). The transfer functions accounted for and were defined by the t_{delay}, time constant of rise in metabolic power (τ) and ratio of rise and decay of metabolic power (β). These constants were determined such that they maximized the correlation between estimations of metabolic power from gas exchange and EMG intensity subject to the following constraints: $0 \leq \tau \leq 100$ breaths, $0 \leq \beta \leq 2$ and $0 \leq t_{delay} \leq 100$ breaths.

$$\frac{d}{dt}\big(P(t)\big) + \left[\frac{1}{\tau}\Big(\beta + [1-\beta]EMG\big(t - t_{\mathrm{delay}}\big)\Big)\right]P(t) = \left(\frac{1}{\tau}\right)EMG(t - t_{\mathrm{delay}}) \tag{1}$$

In a subsequent analysis, different weighting coefficients were applied to the EMG intensity from each muscle to analyze the effect of muscle weighting on the correlation between the estimations of metabolic power from the EMG and gas exchange. Random weightings were assigned to the individual muscles in 5000 different combinations for each subject. These were then used in the transfer function, re-optimizing for the coefficients (τ, β and t_{delay}), to predict metabolic power and re-calculate the estimated metabolic power correlations. Mean weighting coefficients for the 100 highest (H_{cor}) and 100 lowest (L_{cor}) correlated muscle combinations were compared to evaluate the

differences in weightings for each muscle. Two-sided t-tests were conducted between H_{cor} and L_{cor} weighting coefficients for each muscle to determine if the mean values were significantly different. Statistical tests were considered significant at $p \leq 0.05$ and results are reported as mean ± S.E.M..

2.3. Results

The correlation between breath-by-breath temporal resolutions of EMG intensity and metabolic power was r = 0.80 ± 0.02, which improved to r = 0.85 ± 0.02 when accounting for the t_{delay} through cross-correlation. There was a significant correlation (r = 0.91 ± 0.01) between metabolic power determined from the EMG intensity using the transfer functions (Eq. 1) and the metabolic power estimated from $\dot{V}O_2$ (Table 1; Figure 2.1). From the transfer function, the mean t_{delay} between the EMG signal and the subsequent metabolic power was 28.33 ± 4.31 s with a mean β of 0.28 ± 0.07 and τ of 96.11 ± 2.57 breaths (Table 1).

Table 1. Transfer function constants optimized for each subject.

Subject	Time Delay	τ	β	Correlation
1	34.56	100	0.30	0.88
2	16.90	100	0.10	0.88
3	13.20	99	0.20	0.87
4	17.32	79	0.10	0.87
5	48.12	100	0.35	0.93
6	23.65	87	0.25	0.94
7	20.55	100	0.70	0.92
8	34.93	100	0.45	0.94
9	45.72	100	0.05	0.95
Mean	28.33	96.11	0.28	0.91
S.E.M.	4.31	2.57	0.07	0.01

Time delay, transfer function coefficients (τ and β) and correlations for each subject to estimate metabolic power from EMG. The time delay is the time adjustment from the measurement of the EMG signal to the subsequent change in gas exchange parameters.

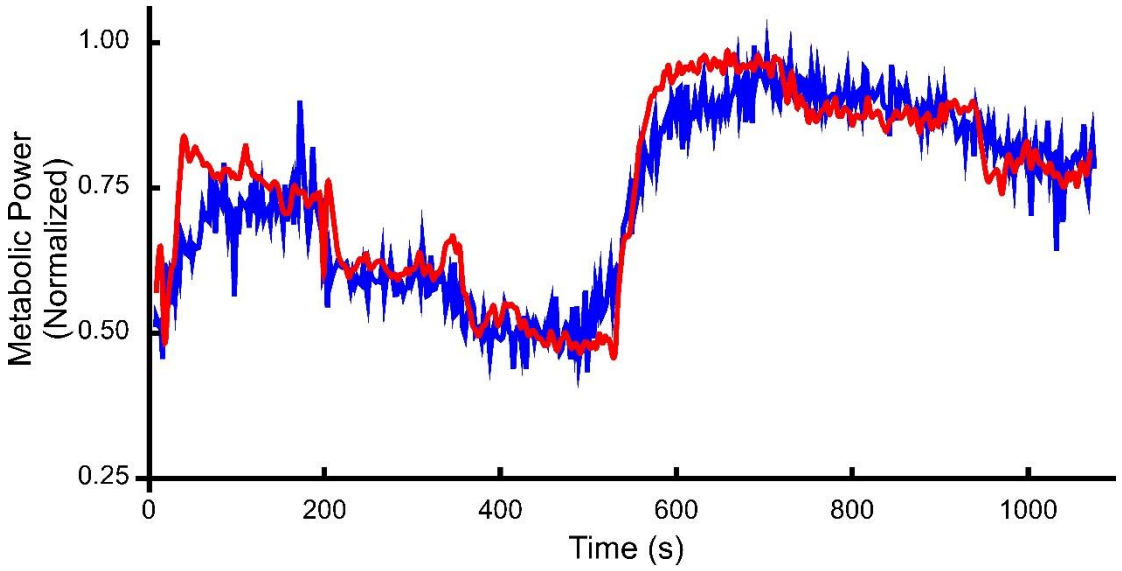

Figure 2-1. Metabolic power calculated from oxygen uptake and EMG.
Metabolic power calculated from oxygen uptake (blue) and estimated metabolic power, calculated from the EMG signal (red) using the transfer function (Eq. 1), for one participant (subject 6). The transfer function was optimized with a time delay of 23.65 s, β of 0.25 and τ of 87 breaths resulting in a correlation of r = 0.94.

Applying different weights to each muscle in the model had a significant effect on the determination of metabolic power as seen by the significantly different mean correlations for H_{cor} and L_{cor} (r = 0.93 ± 0.01 and r = 0.77 ± 0.04 respectively; Figure 2.2B). H_{cor} had the highest mean weightings for vastus medialis (VM, 0.55 ± 0.08; Figure 2.2A), vastus lateralis (VL, 0.49 ± 0.04), semitendinosus (ST, 0.54 ± 0.04), biceps femoris (BF, 0.60 ± 0.07) and gluteus maximus (GM, 0.62 ± 0.07), while L_{cor} had the highest mean weightings for tibialis anterior (TA, 0.72 ± 0.04; Figure 2.2A), medial gastrocnemius (MG, 0.63 ± 0.03) and lateral gastrocnemius (LG, 0.63 ± 0.03). Significantly greater weightings were placed on VM, VL, ST, BF and GM for H_{cor} than for L_{cor} and significantly greater weightings were placed on TA, MG, LG and soleus (Sol) for L_{cor} compared to H_{cor}. The weighting for rectus femoris (RF) was not significantly different between H_{cor} and L_{cor}.

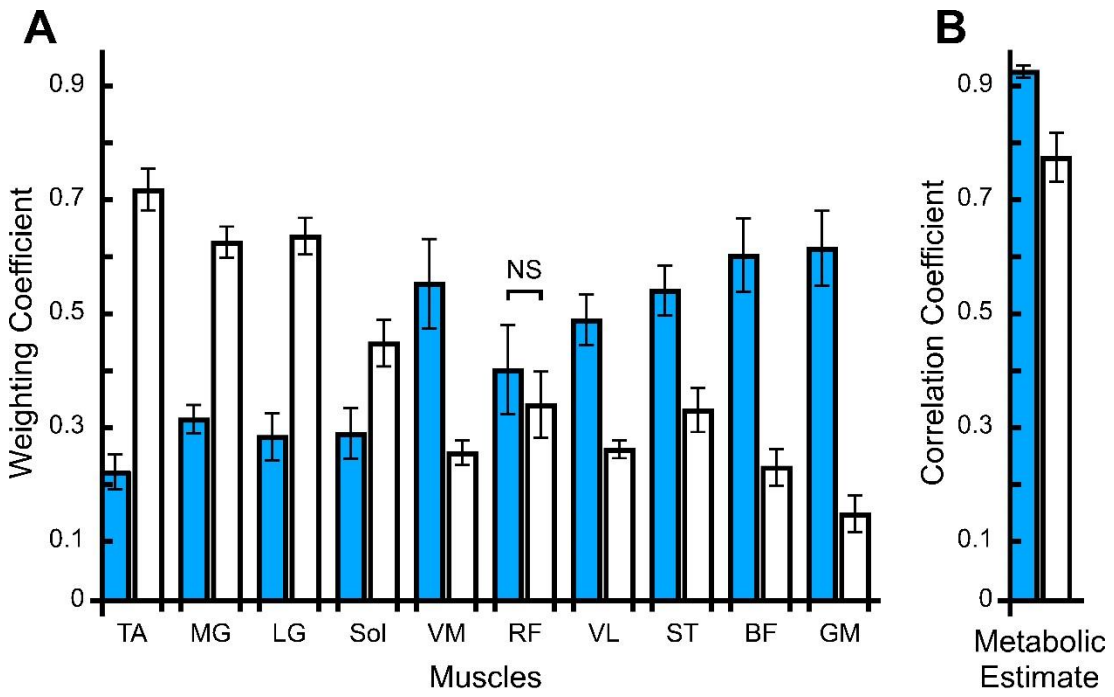

Figure 2-2. Muscle weighting coefficients and resultant metabolic estimates correlated with the metabolic estimates from $\dot{V}O2$.

(A) Mean ± S.E.M. weighting coefficients for each muscle for the highest (H_{cor}; blue) and lowest (L_{cor}; white) 100 correlated estimates of metabolic power. (B) Mean ± S.E.M. correlations between metabolic estimates from $\dot{V}O2$ and both H_{cor} (r = 0.93 ± 0.01) and L_{cor} (r = 0.77 ± 0.04). The correlation and weighting coefficients for H_{cor} and L_{cor} for each muscle were significantly different except for rectus femoris (RF) as indicated (NS).

The muscles with muscle bellies distal to the knee (TA, MG, LG and Sol) displayed less range in EMG intensity across workloads than those proximal to the knee (VM, RF, VL, ST, BF and GM; Figure 2.3). The muscles proximal to the knee showed little change in EMG intensity below 60% $\dot{V}O_{2max}$ and large increases above 60% $\dot{V}O_{2max}$. In most muscles EMG intensity for the 60% $\dot{V}O_{2max}$ condition did not follow the best-fit curve and was significantly higher than the 55% $\dot{V}O_{2max}$ condition.

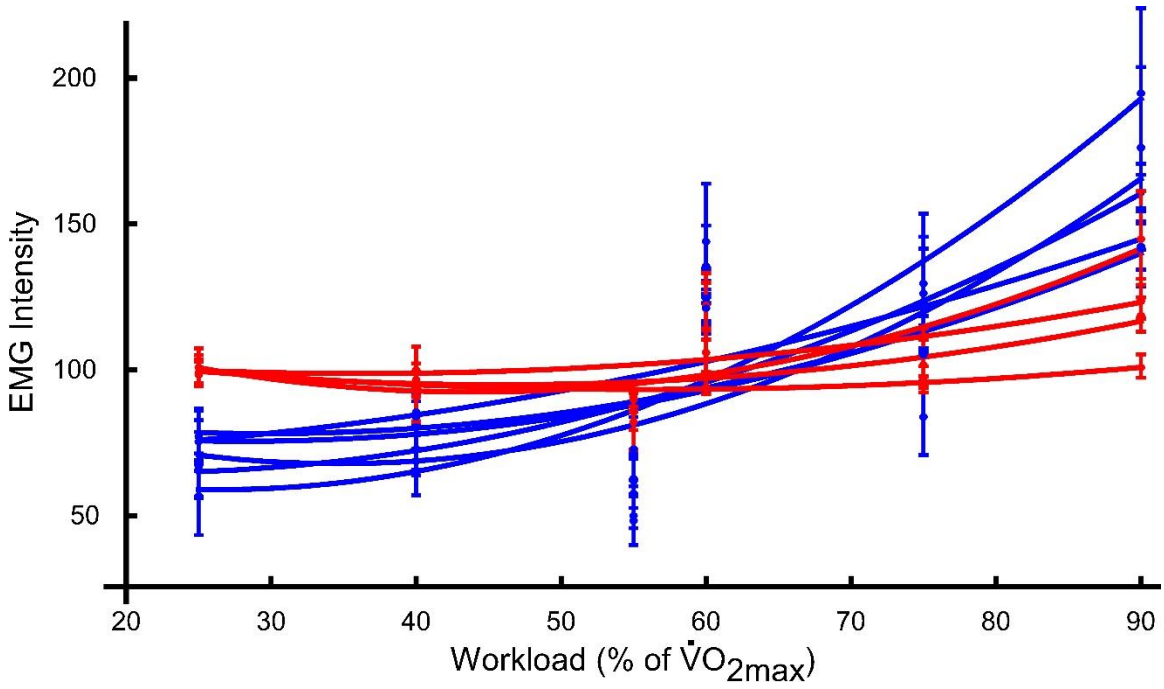

Figure 2-3. Mean EMG intensity for each workload between 25 and 90% $\dot{V}O_{2max}$. Muscles distal to the knee (TA, MG, LG, Sol; red lines) show relatively little change in EMG intensity across workloads and muscles proximal to the knee (VM, RF, VL, ST, BF and GM; blue lines) show relatively large increases in EMG intensity at workloads above 55% $\dot{V}O_{2max}$.

2.4. Discussion

The primary finding of this study was the significant correlation (r = 0.91) between estimates of metabolic power from gas exchange and EMG intensity at a higher temporal resolution than the previously established relationship between metabolic power and EMG intensity (r = 0.86; Wakeling et al. 2011). This relationship was important as it included workload transitions as found in non steady-state conditions and indicates that breath-by-breath EMG intensities provide a good estimate of changes in metabolic power.

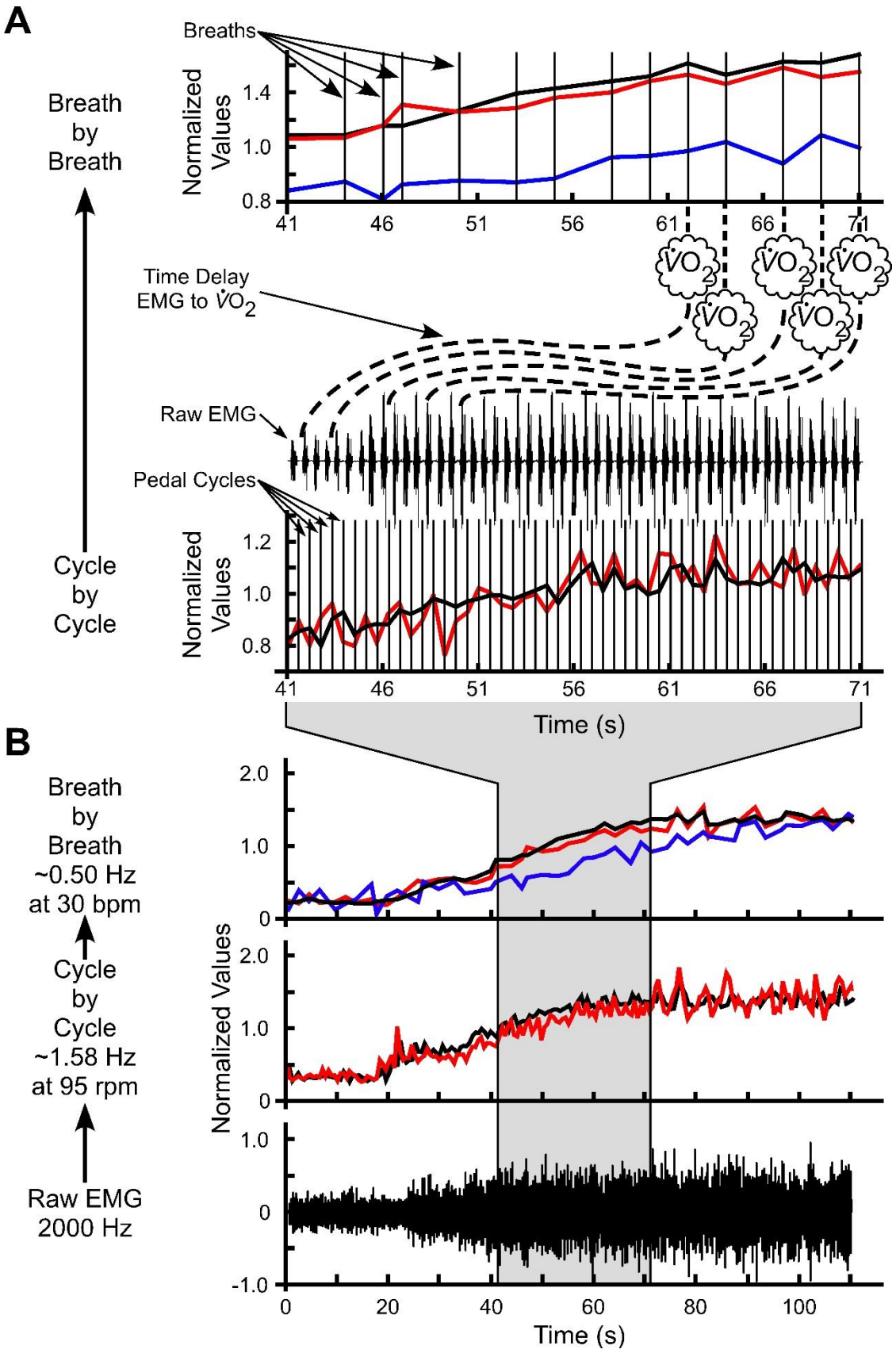
A
Breaths
Normalized Values
1.4
1.0
0.8
41
46
51
56
61
66
71
Breath by Breath
Time Delay EMG to $\dot{V}O_2$
$\dot{V}O_2$
Raw EMG
Pedal Cycles
Cycle by Cycle
1.2
1.0
0.8
Time (s)
B
Breath by Breath ~0.50 Hz at 30 bpm
Cycle by Cycle ~1.58 Hz at 95 rpm
Raw EMG 2000 Hz
2.0
1.0
0
Normalized Values
-1.0
0
20
40
60
80
100
Time (s)

Figure 2-4. Cycle-by-cycle and breath-by-breath temporal resolutions of the EMG and volume of oxygen uptake signals.

(A) Visual representation of 30 seconds of data during a change in workload (power output; solid black line) and the total EMG intensity (EMG; red line) and volume of oxygen uptake ($\dot{V}O_2$; blue line) responses. The cycle-by-cycle figure shows the individual pedal cycles (vertical lines) and the cycle-by-cycle variation in the EMG that is matched well with variation in power output at this temporal resolution. Moving from cycle-by-cycle to the breath-by-breath temporal resolution (mean EMG and power output between breaths) the EMG and power output curves are smoothed since there were 3.19 ± 0.27 pedal cycles per breath across all workloads. Also shown is the time delay (dashed lines) of 28.33 ± 4.31 seconds between a change in the EMG signal and power output and the subsequent change in $\dot{V}O_2$. (B) A global perspective over 110 seconds moving from raw EMG sampled at 2000 Hz to cycle-by-cycle temporal resolution at approximately 1.58 Hz at 95 pedal revolutions per minute (r.p.m.) to breath-by-breath temporal resolution at approximately 0.50 Hz at 30 breaths per minute (bpm). This clearly shows the cycle-by-cycle variation of the EMG and power output that is reduced moving to breath-by-breath resolution, while the primary features of the underlying kinetics are preserved. The EMG, power output and $\dot{V}O_2$ values have been normalized to the mean across the 110 seconds of data

The time-shifted correlation between metabolic power and EMG intensity (r = 0.85) revealed an improved relationship over the initial breath-by-breath correlation (r = 0.80). The t_{delay} from the measured EMG signal to the subsequent $\dot{V}O_2$ realized at the mouth was approximately 12 breaths or 26.20 ± 3.70 seconds. This delay is reasonable given the time delay of approximately 20 seconds attributed to the delay in the transport of blood from the working muscles to the lungs (Whipp et al., 1982). The EMG signal therefore contains metabolic information closer in time to the actual energy use than gas exchange since the t_{delay} is only apparent because the estimated metabolic power was measured at the mouth.

Due to the breath-by-breath fluctuations in both $\dot{V}O_2$ and EMG (Figure 2.4), the activation constants of the transfer functions do not possess significant physiological information. Instead these optimized values smooth the metabolic estimate and highlight the underlying kinetics in order to maximize the correlation. This has a similar effect to previous methods for modeling oxygen uptake using exponential functions that highlight the underlying kinetics of the breath-by-breath fluctuations (Jones and Poole, 2005). There is no physiological explanation to indicate that these fluctuations are directly related to the contractions of the individual muscles, and therefore evident in the EMG signal, since they represent ‘white noise’ and are not important to the overall gas exchange kinetics (Lamarra et al., 1987) and metabolic estimations. Therefore the fundamental information

about metabolic power is contained in the EMG signal and the transfer function (Eq. 1) operates to emphasize the essential features despite the unrelated noise.

The maximum allowable value of τ in the transfer function (Eq. 1) was 100 breaths, yet six subjects had optimized values at this maximum (Table 1). Values greater than 100 breaths were also tested to ensure the resultant correlations were maximized. No subjects displayed appreciable gains in correlation (no difference in r values to the four significant digits reported) with values of τ above 100 breaths. The aim of this study was not to identify specific transfer function constants, but to show a significant relationship between metabolic power estimated from gas exchange and EMG. This aim was accomplished within the constraints imposed on the constants.

There were 3.19 ± 0.27 pedal cycles per breath, which provides a small measure of smoothing, similar to a moving average, for the breath-by-breath EMG intensities when compared to the cycle-by-cycle values. This level of data reduction maintains the important information of the EMG signal while reducing the amount of noise. Determination of an instantaneous measure of metabolic cost remains elusive, but these data and the small number of pedal cycles between breathes suggests that cycle-by-cycle EMG intensity with a time resolution of approximately 0.70 seconds would also provide a reasonable estimate of the $\dot{V}O_2$ kinetics and therefore the metabolic power.

Similar to the findings by Lawrence and De Luca (1983), some muscles displayed non-linear relationships between the EMG signal and force or workload (Figure 2.3). This non-linearity shows that the importance of each muscle is workload dependent. Different weightings were applied to each muscle in order to evaluate its significance to the estimation of metabolic power. Inappropriate weighting resulted in reduced estimations of metabolic power and combinations of all muscles resulted in the best estimates (Figure 2.2). These results provide insight into the most important muscles for accurate metabolic predictions and imply that each muscle has a different role in metabolic power depending on the relative workload intensity. Therefore, when cycling involves a range of workloads, as is the case in this study, it is particularly important to include EMG from many muscles to attain an accurate account of metabolic power.

Muscles proximal to the knee, which include the muscles considered to be the primary power producers in cycling (VL and VM, Ericson 1986), were more heavily weighted in H_{cor}. Eliminating muscles distal to the knee with the lowest weights (TA and Sol) did not improve the metabolic estimations as these muscles had high relative EMG intensities at lower workloads (Figure 2.3). The EMG intensities for the 60% $\dot{V}O_{2max}$ condition are inflated for all muscles (Figure 2.3) since they occurred after the 75% or 90% conditions for some participants. The 75% and 90% conditions occurred with respiration exchange ratios greater than one (Blake et al., 2012) indicating a greater contribution of anaerobic energy sources. With the 60% condition taking place after these workloads and no rest between conditions, there was likely increased fatigue, which is associated with higher levels of EMG intensity (Edwards and Lippold, 1956; Petrofsky, 1979). These inflated values decrease the curvature of the best-fit relationship of EMG intensity across all workloads, especially for those muscles proximal to the knee (Figure 2.3). Despite these limitations the EMG signals contained substantial information about the metabolic power as evidenced by the significant correlation between the metabolic power estimations ($r = 0.91$).

Normalization techniques used to process EMG signals present a limitation to the interpretation of the EMG-metabolic cost relationship. EMG signals are commonly normalized to the trial mean or maximum, or to voluntary isometric or isokinetic contractions (See Burden (2010) for review). Normalization to the trial mean or maximum does not give any indication of the absolute level of muscle contraction and does not permit comparisons between muscles. Alternatively, normalization to the maximal isometric or isokinetic contractions requires an additional test and assumes the maximal neural drive and muscle contraction has been achieved for each muscle. If a maximal contraction is reached, absolute levels of activity as opposed to relative comparisons between muscles could be achieved. Interestingly, imposing 5000 different weighting combinations to the muscle EMG signals only increased the metabolic power estimation correlation from $r = 0.91$ to $r = 0.93$. Changing the weightings is equivalent to using different normalization values for each muscle, and so the 5000 weighting combinations represented 5000 ways to normalize the muscles. The normalization method chosen for this study resulted in close to the best possible normalization for predicting metabolic power from EMG for this cycling task. However, an inappropriate set of normalization

could result in poor results as shown by the significantly reduced correlation of L_{cor} (r = 0.77; Figure 2.2).

This study shows that breath-by-breath changes in EMG across ten leg muscles can be used as a good estimate of changes in metabolic power in non steady-state conditions. Estimations of metabolic changes on a cycle-by-cycle basis may also be reasonable given that breath-by-breath resolution acts as a moving average of approximately three pedal cycles, thereby maintaining the important features of the data. This result has implications for future studies, including those found in the following chapters, and applications involving EMG from large muscle groups during dynamic activities as it provides higher temporal resolution and more real-time predictions of changes in metabolic power than gas exchange measures. Also, metabolic power estimated from gas exchange is used in calculations of mechanical efficiency, which implies that breath-by-breath changes in EMG can also be used to investigate the relationship of mechanical work and metabolic power. Therefore, muscle excitation was utilized by the biofeedback system in chapter five to monitor the impact of different muscle coordination strategies on relative mechanical efficiency.

Chapter 3.

Establishing a muscle coordination reference frame for the biofeedback system: How slower muscle fibres participate at high movement frequencies.

3.1. Introduction

The second aim of this research was to establish a comprehensive understanding of muscle excitation and coordination across a wide range of muscles and mechanical demands during cycling to create a muscle coordination reference frame for the biofeedback system. A comprehensive understanding of muscle coordination across a wide range of mechanical demands is important since the manipulation of muscle coordination facilitated by the biofeedback system relies on knowledge of the current and desired end state of muscle coordination as well as the factors that influence muscle coordination. Therefore, understanding muscle excitation and muscle coordination necessitates the exploration and determination of the way muscle and muscle fibre recruitment, and therefore muscle coordination, responds to changing mechanical demands of the movement.

As one of the extreme mechanical demands, high cycle frequencies require rapid muscle activation-deactivation times and faster muscles and faster muscle fibres are better suited to reach these high cycle frequencies. Maximal cycle frequencies of muscle contraction may be limited by muscle deactivation, particularly in slow muscle fibres, since deactivation is longer than activation (Buchthal et al., 1973; Burke et al., 1973; Lee et al., 2011). However, the size principle of motor unit recruitment (Henneman et al., 1965a; Henneman et al., 1965b) dictates that slower fibres, with longer relaxation times, are deactivated last. While the size principle adequately describes many recruitment

Portions of this chapter previously appeared as: (Blake and Wakeling, 2014)

strategies, alternative strategies may also exist (Citterio and Agostoni, 1984; Gillespie et al., 1974; Gollnick et al., 1974; Grimby and Hannerz, 1977; Hodson-Tole and Wakeling, 2008a; Hoffer et al., 1981; Jayne and Lauder, 1994; Nardone et al., 1989; Smith et al., 1980; Wakeling et al., 2006) when the demands exceed the abilities of the slowest muscle fibres.

The cat paw shake provided an early example of preferential recruitment of fast muscle during high frequency contractions (Smith et al., 1980). The predominantly slow fibred soleus muscle was inactive while the predominantly fast-fibred lateral gastrocnemius was active during the paw shake, which was identified using EMG. The lateral gastrocnemius is a muscle with mixed fibre types, yet, at the time, it was not possible to distinguish the contribution of slow muscle fibres in the muscle. However, it was suggested that recruitment of the slower fibres in the lateral gastrocnemius would be counterproductive to the cyclical action (Smith et al., 1980). In contrast, complete inhibition of slow fibres may be detrimental to the power production for very fast contractions since slow fibres may provide resistance to whole muscle shortening (Josephson and Edman, 1988). Indeed, evidence from a rat study suggests that slow fibres within mixed muscle help the muscle reach higher shortening velocities (Holt et al., 2014).

Techniques to distinguish the activity of different motor unit types from the EMG signal have recently been developed (von Tscharner, 2000; Wakeling and Rozitis, 2004; Wakeling et al., 2002). Wakeling and colleagues (2002) qualitatively showed the presence of preferential recruitment of faster muscle fibres during the cat paw shake in a single muscle, medial gastrocnemius, but was unable to provide quantitative evidence through statistical methods. In addition, a statistically significant shift towards preferential recruitment of faster muscle fibres was displayed in the human medial gastrocnemius at high cycle frequencies independent of the muscle fascicle strain (Wakeling et al., 2006); however, this shift was identified in the middle of the bursts of muscle excitation and was correlated with the muscle fibre strain-rate. Similar findings have subsequently been repeated in the rat (Hodson-Tole and Wakeling, 2008b) and the goat (Lee et al., 2013).

With the inclusion of force measurements, Roberts and Gabaldón (2008) showed shorter muscle relaxation times during running compared to walking in the lateral

gastrocnemius of the turkey independent of strain rate. It was speculated that alterations in muscle fibre recruitment during running, such that faster fibres remain active after deactivation of slow fibres, might explain the shorter relaxation times since the relaxation times should not decrease if dominated by slow fibres as dictated by the size principle (Henneman et al., 1965a; Henneman et al., 1965b). Studies have qualitatively indicated such a recruitment pattern in humans (Wakeling, 2004) and rats (Hodson-Tole and Wakeling, 2008a) running at various speeds, while Lee and co-workers (2013) were unable to confirm a relationship between relaxation rates and muscle fibre recruitment in goats. Despite having been repeatedly suggested, an early derecruitment of slower fibres during muscle relaxation at high cycle frequencies has not yet been demonstrated. The purpose of this study was to investigate if slow muscle fibres are derecruited before fast fibres at the end of muscle excitation during high frequency contractions.

3.2. Methods

3.2.1. Protocol and Data Collection

Eleven males volunteered to participate in the study. All participants gave their informed written consent to participate prior to their participation. All procedures were approved by the ethics committee in accordance with the Office of Research Ethics at Simon Fraser University. Due to the extreme cycle frequencies required, the participants were trained competitive cyclists (mean ± S.E.M.: age = 33.9 ± 3.1 years, mass = 72.8 ± 2.1 kg, height = 179.1 ± 1.9 cm, cycling distance per year = 10773 ± 1575 km).

After a 10-minute warm-up consisting of 5-minutes at 100 W followed by 5-minutes increasing 20 W every minute, the participants cycled at 40, 60, 80, 100, 120, 140, 160 and 180 r.p.m. at each of 100, 200, 300 and 400 Watts. Each trial was 30 seconds in duration followed by 90 seconds rest and the trials were completed in a randomized block design. The conditions were first randomized into blocks by cadence and power output was then randomized within each block. Completing all four power outputs at a single cadence helped facilitate better compliance of the desired cadence. The participants rode an indoor cycle trainer (SRM, Julich, Germany) that was configured as closely as possible to their own racing bicycle, and used their own clipless pedals and shoes.

Muscle excitation of the medial gastrocnemius was monitored continuously using bipolar Ag/AgCl surface EMG electrodes (10mm diameter and 21 mm spacing; Norotrode; Myotronics, Kent, WA) and sampled at 2000 Hz through a 16-bit analog to digital converter (USB-6210; National Instruments, Austin, TX). This muscle was selected as it has previously been used to identify preferential recruitment of faster muscle fibres in response to increasing muscle fascicle strain rates, independent of the level of muscle excitation and muscle fascicle strain (Wakeling et al., 2006). The electrode sites were cleaned with isopropyl and shaved prior to application and the electrodes were secured using stretchable adhesive bandages and tubular net bandages to help reduce movement artifacts. Normal and tangential forces applied to each crank arm, at the pedal-crank arm interface, as well as cycle frequency were measured (Powerforce, Radlabor, Freiburg, Germany) and recorded at 2000 Hz through the same 16-bit analog to digital converter, and subsequently used to calculate power output.

3.2.2. Data Analysis

The EMG signals were resolved into intensities in both time and frequency space using wavelets (j = 0 to 10: von Tscharner, 2000) and divided into individual pedal cycles. If the intensity of the first wavelet (center frequency 6.90 Hz) was the greatest of all wavelets for a particular pedal cycle it was considered to have too much noise from movement artifact and was not analyzed further. For all subsequent analyses wavelet j = 0 was excluded leaving 10 wavelets acting as a band-pass filter between approximately 11 and 432 Hz. Of these “clean” pedal cycles, for each subject and each condition, all cycles within five r.p.m. of the desired cadence were selected and the middle five steady-state cycles were retained. Total EMG intensity per pedal cycle was calculated as the sum of intensities across all wavelets.

In order to evaluate the frequency components during the primary portion of muscle excitation an onset/offset threshold of 5% of the difference between the minimum and maximum EMG intensity was selected. The EMG intensities between the onset and offset were used to determine muscle excitation duration and subsequently interpolated to 100 points per wavelet per pedal cycle for all further analyses. The EMG intensities for each pedal cycle were normalized to unit intensity across the entire spectra and the mean

was subtracted (100 points per wavelet per pedal cycle) in order to maximize the variance from the mean frequency spectra (Ramsay and Silverman, 2005) and analyze the impact of this frequency shift.

PC analysis was used to identify the primary sources of variability within the frequency spectra across all subjects (Wakeling and Rozitis, 2004). A p x N matrix A was constructed with p = 1000 (100 points per wavelet * 10 wavelets) and N = number of pedal cycles. The eigenvector-eigenvalue pairs of the covariance matrix of A were calculated where the eigenvectors represented the PC weightings and the eigenvalues represented the amount of the frequency spectra explained by each PC. The product of the transpose of the matrix composed of the PC weightings (eigenvectors) and the original matrix A produced the loading scores of each pedal cycle on each PC.

The first two PCs explained a significant portion of the variance from the mean and contained polarized positive and negative aspects that displayed shifts in the time and frequency content of the EMG intensity (Figure 3.1A). To visualize the impact of these PCs on each condition the variance from the mean was reconstructed using the vector product of these PC weightings and loading scores (Figure 3.3). It was expected that at the highest cycle frequencies and lowest power outputs there would be an increase in high frequency and decrease in low frequency components at the end of the burst of muscle excitation, signifying earlier offset of low frequencies relative to high frequencies.

3.2.3. Statistics

General linear model analysis of variance (ANOVA) was used to identify the effect of power output and cadence as well as the level of interaction between power output and cadence on EMG intensity with subject as a random factor. A post-hoc Tukey test was performed to determine significant differences between power outputs for a given cadence with respect to EMG intensity. Also, a one-way ANOVA was used to evaluate the effect of condition (cadence-power combination) on EMG intensity with a post-hoc Tukey test to compare EMG intensities across all conditions. Pearson correlation coefficients were determined between all combinations of total EMG intensity, power output, cadence and the first 20 PC loading scores.

General linear model ANOVAs were also used to determine the effects of cadence and power output on the loading scores for each of the first 20 PCs as well as the muscle excitation duration. Post-hoc Tukey tests were performed to identify differences between these durations across all cadences for a given power output and across each power output for a given cadence. In order to test the effects of cadence and power output on the PCs, loading scores for each PC were tested individually as a dependent variable with subject as a random factor and cadence and power output as fixed factors using subject, cadence and power output in a full factorial design.

3.3. Results

The experimental subjects were able complete all cycling conditions (pedal cadences between 40 to 180 r.p.m. at power outputs of 100 to 400 W) and EMG signals were recorded and frequency and timing data were identified. Principal components (PCs) determined from wavelet analysis displayed distinct features in both frequency and timing of the EMG intensities during muscle excitation (Figure 3.1A). In order to identify the influence of alterations in frequency, the data were normalized to unit intensity for each pedal cycle, and the mean across all subjects was subtracted prior to the principal component (PC) analysis with the resulting PCs describing the variance from the mean. The first 20 PCs accounted for almost 70% of the variance with the first two components explaining over 24%. The first and second PCs displayed distinct shifts in both frequency and timing of the peak EMG intensity within each burst of muscle excitation (Figure 3.1A) and loading scores for these components identified the relative amounts of these shifts. The first PC showed a decrease in EMG intensity at high frequencies (peak approximately 170 Hz) earlier in the muscle excitation (approximately 29% of the duration) and an increase in EMG intensity at low frequencies (peak approximately 92 Hz) later in the muscle excitation (approximately 55% of the duration). Conversely, the second PC displayed decreased EMG intensity at low frequency (peak approximately 62 Hz) earlier (35% muscle excitation duration) in the muscle excitation and increased EMG intensity at high frequency later (56% muscle excitation duration).

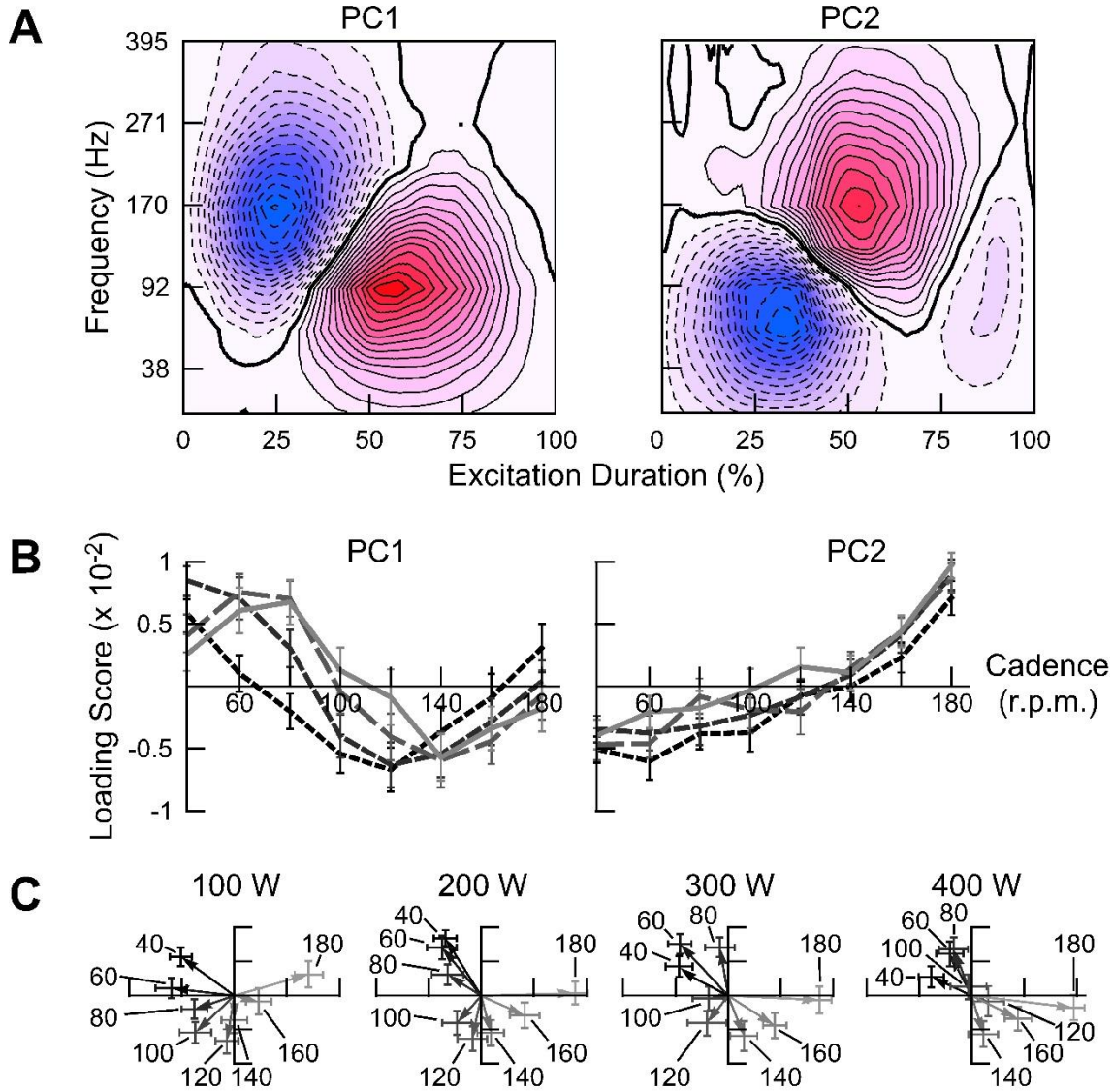
A
PC1
PC2
Frequency (Hz)
395
271
170
92
38
0
25
50
75
100
Excitation Duration (%)
B
PC1
PC2
Loading Score (x 10-2)
1
0.5
-0.5
-1
60
100
140
180
Cadence (r.p.m.)
C
100 W
200 W
300 W
400 W
40
60
80
100
120
140
160
180
A
-1
0
1
B
Power (W)
100
200
300
400
C
PC1 Loading Score (x10-2)
PC2 Loading Score (x10-2)
Cadence (r.p.m.)
40
60
80
100
120
140
160
180

Figure 3-1. Principal component (PC) representations of the time-frequency patterns of the EMG intensity and PC loading scores for each cadence-power output condition.

(A) PC weightings for PC1 and PC2 showing the variance from the mean EMG frequency spectra for medial gastrocnemius during muscle excitation. The EMG intensities are shown relative to the time within each muscle burst (% excitation duration), and their frequency content. Intensities have been normalized to the absolute maximum for each PC and show both increases (positive values - red with solid contour lines) and decreases (negative values - blue with dashed contour lines) in frequency at specific times during excitation. (B) Mean ± S.E.M. loading scores for PC1 and PC2 at each cadence-power output combination. (C) Mean ± S.E.M. loading scores PC2 versus PC1 at each cadence-power output combination. This shows the general pattern of increasing vector angles with increasing cadence at the lowest workloads and negative PC2 and positive PC1 loading scores at low cadences and the opposite at high cadences at the highest workloads.

There was a significant effect of pedalling cadence and no significant effect of crank power output on the EMG intensity. Also, there was a significant correlation between EMG intensity and cadence (r = 0.85) and decreasing differences in EMG intensity for a given cadence at increasing power outputs (Figure 3.2). For example, EMG intensity was significantly different at 40 r.p.m. and not significantly different at 180 r.p.m. for all power outputs (Figure 3.2). EMG intensity for each cadence-power combination showed a monotonic increase from 60 to 120 r.p.m., while the cadences above 120 r.p.m. also displayed a linear increase at a steeper slope (Figure 3.2).

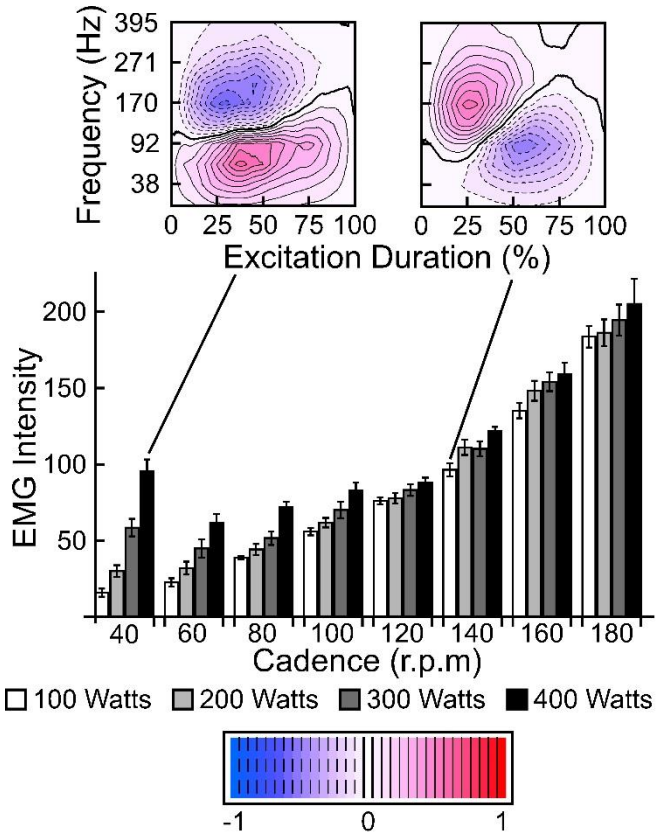

Figure 3-2. EMG intensity for each cadence-power output combination and an example of two principal component representations showing different recruitment patterns.

Mean ± S.E.M. EMG intensity at each cadence-power output combination. The contour plots show reconstructions of the variance from the mean EMG frequency spectra across the muscle excitation duration and have been normalized to the absolute maximum. The 140 r.p.m. at 100 W (right contour plot) condition shows an example of preferential recruitment of faster muscle fibres when compared to the 40 r.p.m. at 400 W condition (left contour plot) due to its increased high frequencies (red with solid contour lines), decreased low frequencies (blue with dashed contour lines) and no significant difference in EMG intensity (bar graph).

There was a significant effect of pedalling cadence on the loading scores for the first two PCs (PC1 and PC2; Figure 3.1B) and 13 of the first 20 PCs, and a significant effect of power output on the loading scores for PC2, but not PC1, and 6 of the first 20 PCs. Vectors created between the first two PC loading scores revealed a circular pattern with increasing cadence at the lowest workloads (Figure 3.1C). In general low cadences had positive PC1 and negative PC2 loading scores, which were reversed at high cadences (Figure 3.1C). Reconstructions of the signal variance of the EMG intensity using the first two PCs for each cadence-power combination can be seen in Figure 3.3 and showed changes in frequency across the burst of muscle excitation. Across all workloads at 40

and 60 r.p.m. the reconstructions showed an increase in EMG intensity at low frequencies (centered around 62-92 Hz) and a decrease in the EMG intensity at high frequencies (centered around 170 Hz). At 80, 100, 120 and 140 r.p.m. there was a distinct shift of the EMG intensity earlier in the burst duration. At 140, 160 and 180 r.p.m. there was an increase in the high frequency and subsequent decrease in the low frequency component of the EMG intensity with the increased high frequency occurring later in the muscle burst at 180 r.p.m.. Additional low frequency components (>62 Hz) appeared at 180 r.p.m. at the same time of muscle excitation (approximately 60-65%) as the increased high frequencies.

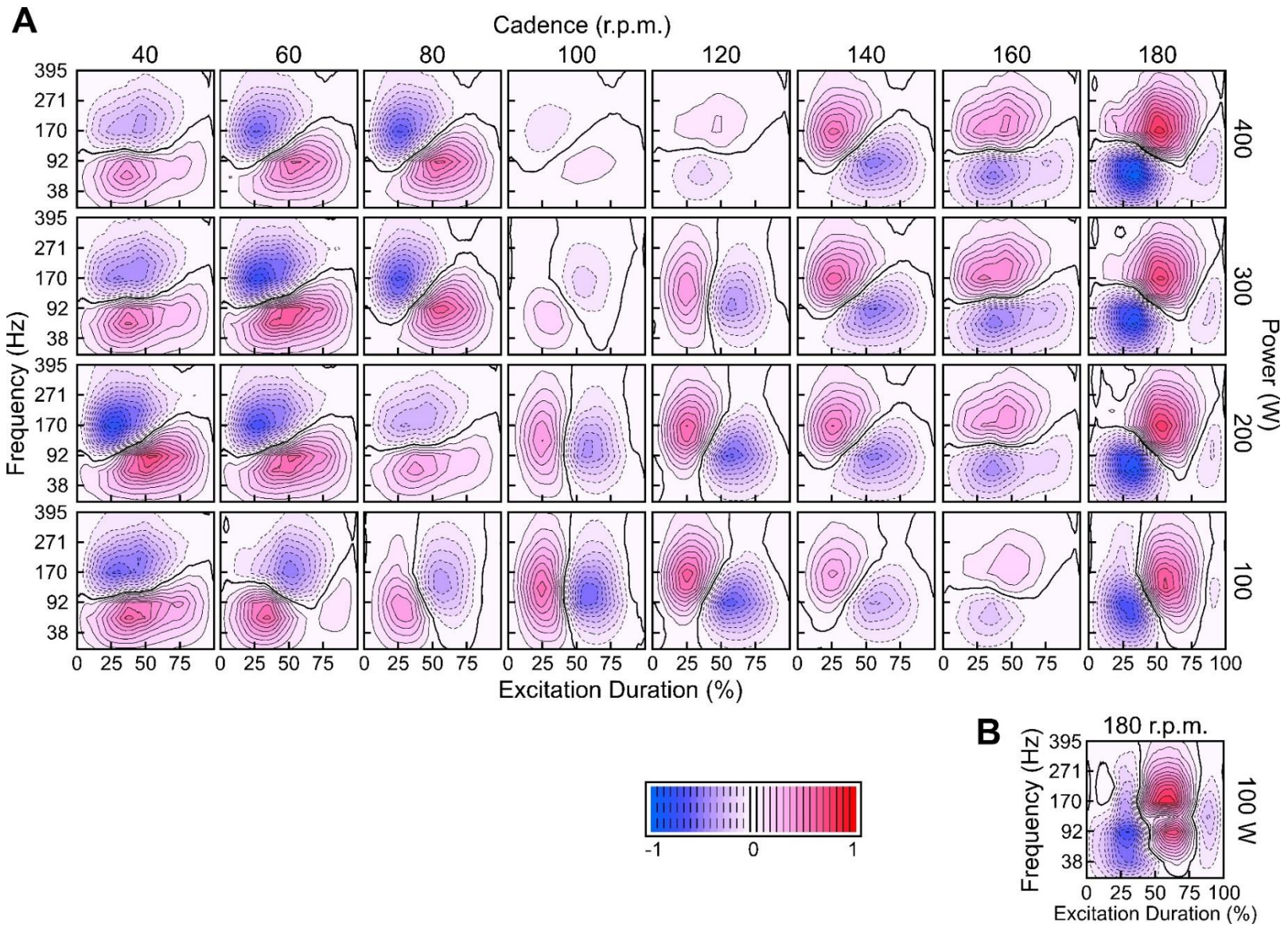
A
Cadence (r.p.m.)
40
60
80
100
120
140
160
180
Frequency (Hz)
395
271
170
92
38
400
300
200
100
Power (W)
0 25 50 75
0 25 50 75 100
Excitation Duration (%)
-1
0
1
B
180 r.p.m.
100 W

Figure 3-3. Principal component reconstructions of the variance from the mean EMG frequency spectra across the muscle excitation duration.

(A) Each time-frequency plot was constructed from the first two PCs at each cadence-power output combination. Values have been normalized to the absolute maximum across all reconstructions and show both increases (positive values - red with solid contour lines) and decreases (negative values - blue with dashed contour lines) in EMG intensity at specific frequencies and at specific times during excitation. This shows the shift in frequency emphasis from low frequencies at the lowest cadences to high frequencies at the highest cadences and finally the addition of low frequencies at 180 r.p.m.. This also shows how the frequency emphasis moves with respect to the time within the burst of muscle excitation. (B) Reconstruction using the first 20 PCs at 180 r.p.m. at 100 W showing the additional low frequency in a distinct band centered at approximately 92 Hz with both the high and low frequencies later in the muscle excitation duration.

The absolute duration of the bursts of muscle excitation decreased from 753.35 +/- 50.39 ms at 40 r.p.m. and 400 W to 151.68 +/- 5.31 ms at 180 r.p.m. and 300 W (Figure 3.4). At all power outputs there was no significant difference in burst duration between 140, 160 and 180 r.p.m., while pedal cycle duration decreased. Also, there was no significant difference in burst duration between power outputs for a given cadence from 100-180 r.p.m..

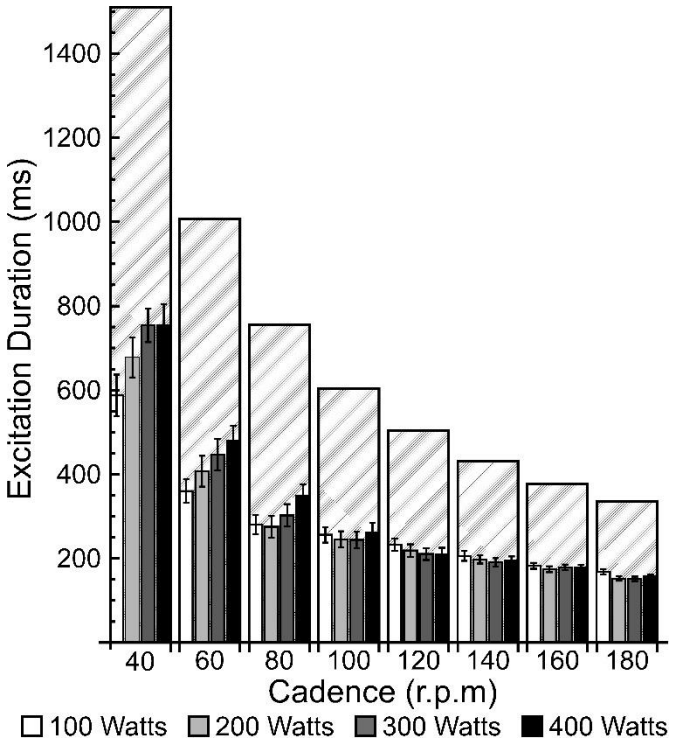

Figure 3-4. Muscle excitation duration at each cadence-power output combination.

Values show mean ± S.E.M. as well as the cycle duration (striped bars). There was no significant difference in muscle excitation duration between 140, 160 and 180 r.p.m., which may represent the minimum duration of the medial gastrocnemius. Therefore, muscle excitation duration was an increasing proportion of the cycle duration at faster cadences.

3.4. Discussion

Preferential recruitment of faster muscle fibres during rapid contractions has been shown in various animal studies, including humans (Citterio and Agostoni, 1984; Gillespie et al., 1974; Gollnick et al., 1974; Grimby and Hannerz, 1977; Hodson-Tole and Wakeling, 2008a; Hoffer et al., 1981; Jayne and Lauder, 1994; Lee et al., 2013; Nardone et al., 1989; Smith et al., 1980; Wakeling et al., 2006). It has been suggested that complete inhibition of slow muscle fibres in a muscle with mixed fibre types would provide resistance to whole muscle shortening and therefore be detrimental to power production for very fast contractions (Josephson and Edman, 1988). Therefore, it has been speculated that slow muscle fibres are activated, but deactivated before faster muscle fibres (Hodson-Tole and Wakeling, 2008a; Lee et al., 2013; Roberts and Gabaldón, 2008). This is to account for their longer deactivation times, since the time between the end of excitation and the end

of muscle shortening represents an increasing portion of the muscle contraction-relaxation cycle at increasing cycle frequencies. Qualitative evidence of this has been shown in humans (Wakeling, 2004) and rats (Hodson-Tole and Wakeling, 2008a), but never quantitatively and statistically. These previous studies indicated graphical evidence for an increase in faster fibre and decrease in slower fibre excitation at the end of a running stride, in contrast to predictions made by the size principle (Henneman et al., 1965a; Henneman et al., 1965b). In this current study we put the muscle through an extreme range of conditions to push the recruitment strategies to their limits, in order to quantitatively and statistically test whether shifts in muscle fibre recruitment occur with derecruitment of slow fibres before fast fibres at the highest cycle frequencies.

Recent developments in EMG decomposition have made it possible to distinguish faster and slower muscle fibres based on the signal frequency with fast and slow muscle fibres producing high and low frequencies, respectively (Elert et al., 1992; Gerdle et al., 1988; Kupa et al., 1995; Solomonow et al., 1990; Wakeling and Horn, 2009; Wakeling and Rozitis, 2004). In addition, by using wavelet analysis it is possible to retain both time and frequency information of the EMG signal to evaluate the changes in frequency with respect to muscle excitation duration (von Tscharner, 2000; Wakeling and Rozitis, 2004; Wakeling et al., 2002). In this study we hypothesized that the early derecruitment of slower muscle fibres during muscle relaxation would occur at the highest cycle frequencies, and this would be demonstrated by a relative reduction in the low-frequency component (60-90 Hz) of the EMG intensity at the end of the burst of EMG excitation (Wakeling and Horn, 2009; Wakeling et al., 2001).

The data revealed a shift of the EMG intensity from low to high frequencies similar to previous findings (Wakeling et al., 2006), a shift of these frequencies relative to the duration of muscle excitation (Figures 3.1A, 3.3), and the addition of low frequency components at the highest pedalling rates (Figures 3.3, 3.5). Changes in EMG frequency between different conditions can be attributed to shifts in muscle fibre recruitment when there is no significant difference in EMG intensity between conditions (Wakeling et al., 2006). For example, this can be seen between the following conditions: 40 r.p.m. at 400 W and 140 r.p.m. at 100 W (Figure 3.2).

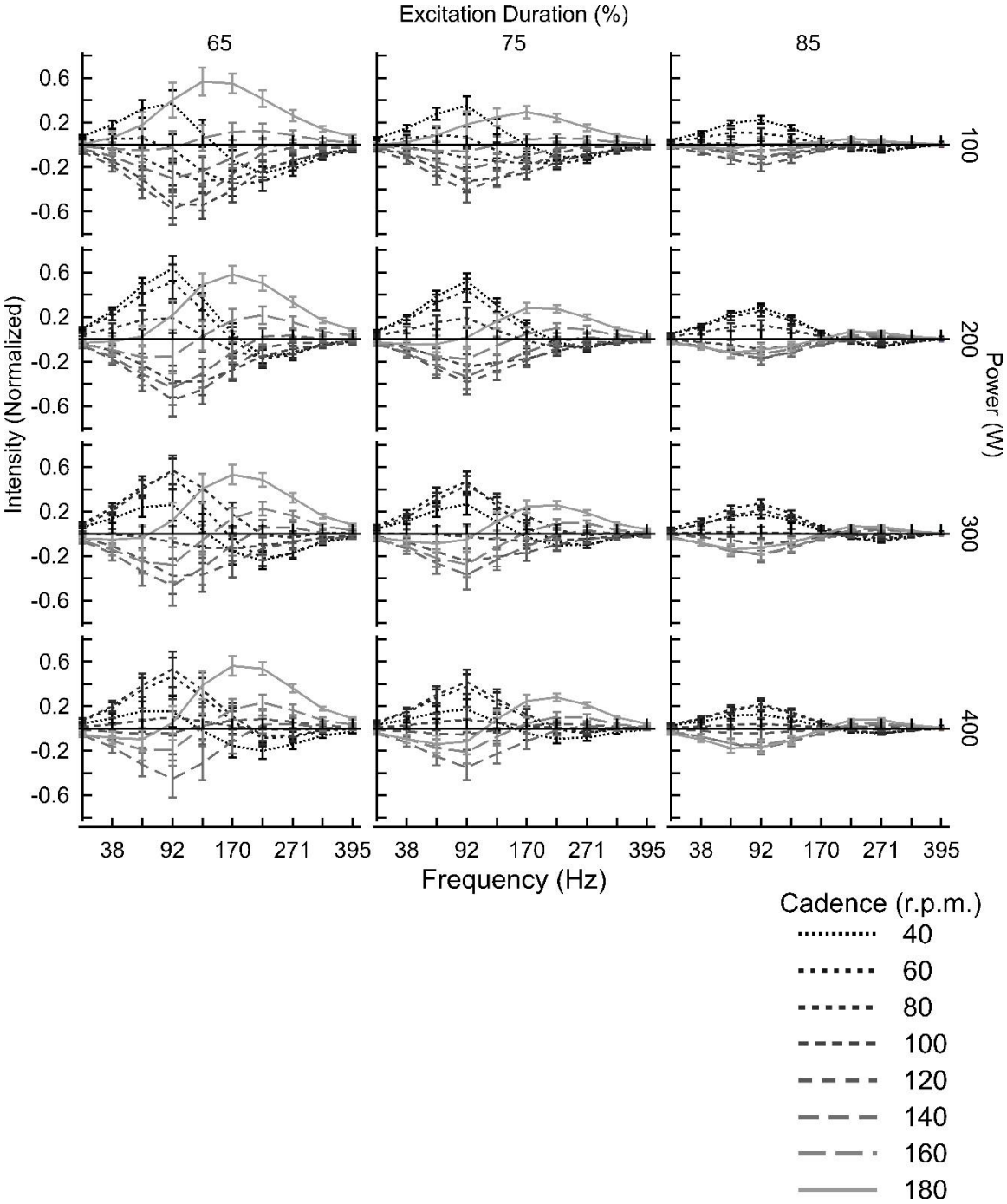
Excitation Duration (%)
65
75
85
100
200
300
400
Power (W)
Intensity (Normalized)
0.6
0.2
-0.2
-0.6
38
92
170
271
395
Frequency (Hz)
Cadence (r.p.m.)
40
60
80
100
120
140
160
180

Figure 3-5. EMG intensity across the frequency spectra at 65, 75 and 85% muscle excitation duration for each cadence at each power output.

This figure shows evidence of early derecruitment of slower muscle fibres at the end of muscle excitation at the highest cycle frequencies. Early derecruitment is shown by the decrease in intensity for lower frequencies and increase in intensity for higher frequencies at the highest cadences (lighter lines), which is in contrast to the increase in intensity for the lower frequencies and decrease in intensity for the higher frequencies at the lowest cadences (darker lines). At 180 r.p.m. (solid line) there is also an increase in lower frequencies when compared to 140 and 160 r.p.m., which is particularly evident at 75% duration. Values shown are mean ± S.E.M..

The first and second PCs represented a large portion of the signal variance and displayed both a shift in frequency and timing (Figure 3.1A) and were significantly affected by cadence (Figure 3.1B). When the first PC loading scores were negative and the second PC loading scores were positive there was a decrease and increase in low and high frequency components of the EMG signal, indicating both a decrease and increase in the contributions of slower and faster muscle fibres, respectively, at the end of muscle excitation (Figure 3.1A). This occurred at 140, 160 and 180 r.p.m. at most workloads (Figure 3.1C), providing evidence of an early derecruitment of slower muscle fibres at the end of muscle excitation, thereby supporting the hypothesis. This increase in high frequency and decrease in low frequency components of the EMG could clearly be seen at 65, 75 and 85% of muscle excitation duration at the highest cycle frequencies (lighter lines in Figure 3.5). This is in contrast to the increase in intensity for the lower frequencies and decrease in intensity for the higher frequencies at the lowest cadences (darker lines in Figure 3.5).

The excitation duration reached a plateau beyond 140 r.p.m. with the shortest duration of 151.68 +/- 20.60 ms (Figure 3.4). This duration plateau may indicate that these cycle frequencies reached or were approaching the minimum muscle excitation duration for the medial gastrocnemius. It has been speculated that pedalling cadences greater than 165 r.p.m. would surpass the maximum shortening velocity of the slow muscle fibres (Sargeant and Beelen, 1993) and since deactivation is longer than activation, during the activation-deactivation cycle of muscle contraction (Buchthal et al., 1973; Burke et al., 1973; Lee et al., 2011), the highest cycle frequencies in this study may exceed the relaxation capabilities of the slowest muscle fibres. The short excitation durations can partially be explained by the ability of the muscle to reach higher cycle frequencies because active shortening accelerates the relaxation dynamics expected from isometric

twitches (Askew and Marsh, 1998; Caiozzo and Baldwin, 1997). As noted, the results indicate that there was also some manipulation of the timing of muscle fibre recruitment relative to muscle excitation that may have helped enable the slow fibres to participate at such high cycle frequencies. As speculated (Hodson-Tole and Wakeling, 2008a; Wakeling, 2004) this could be accomplished through inhibition of the slower fibres by Renshaw cells since the fastest motoneurons have been shown to provide the most stimulus to the Renshaw cells, which in turn inhibit motoneuron activity with the greatest inhibitory influence on the slowest motoneurons (Friedman et al., 1981).

With positive loading scores for the first PC (Figure 3.1B), the 180 r.p.m. conditions at 100 and 200 W displayed an increase in low frequency components of the EMG intensity (Figures 3.3A, 3.5) contrary to the pattern found at 140 and 160 r.p.m. (evident at 75% muscle excitation duration in Figure 3.5). The inclusion of the first 20 PCs, to account for a greater proportion of the signal variance, in a further reconstruction, provided added clarity and showed that the increase in frequency later in the muscle excitation duration was in two distinct bands (centered at approximately 92 and 170 Hz; Figure 3.3B). The addition of lower frequency components, the plateau in excitation duration and the non-linear increase in EMG intensity at 180 r.p.m. indicate that there was greater excitation of the muscle, including slow muscle fibres, to achieve the highest cycle frequency. Previous research has shown that mixed muscles can reach higher maximal shortening velocities than those predicted from extrapolation from a Hill-type (Hill, 1938) model (Close and Luff, 1974; Josephson and Edman, 1988). Indeed, recent evidence in rats suggests that the involvement of slow fibres during contractions of mixed fibre-type muscles helps the muscle reach higher shortening velocities (Holt et al., 2014), which is supported here.

This study provides new evidence to support previous research (Hodson-Tole and Wakeling, 2008a; Wakeling, 2004) showing early derecruitment of slower muscle fibres during high frequency cyclical contractions. In addition, the study provides new evidence in humans, to support findings in rats (Holt et al., 2014), of the contribution of slow muscle fibres in order to achieve the highest cycle frequencies. In summary, changes to the EMG signal, in both frequency and time, provide evidence of modifications of muscle fibre recruitment strategies depending upon the mechanical demands of a movement. Also, the

muscle and muscle fibre responses to the demands imposed by the high cycle frequencies suggest that cadences at and above 140 r.p.m. are approaching the limitations of muscle excitation and therefore may not be appropriate for use by the biofeedback system to manipulate muscle coordination as outlined in chapter five.

Chapter 4.

Establishing a muscle coordination reference frame for the biofeedback system: Muscle Coordination of Human Limb Movement under a Wide Range of Mechanical Demands.

4.1. Introduction

As stipulated in chapter three, the second aim of this research was to establish a comprehensive understanding of muscle excitation and coordination across a wide range of muscles and mechanical demands during cycling to create a muscle coordination reference frame for the biofeedback system. A better understanding of muscle coordination was necessary for the biofeedback system in order to link the current and desired end states of muscle coordination. In particular, with a better understanding of responses of muscle coordination to different mechanical demands, the purposeful manipulation of muscle coordination during human limb movement could be endeavoured.

Human limb movement is achieved through interactions between the neuromuscular and skeletal systems. Movement performance is commonly measured by the resultant mechanical efficiency (ratio of mechanical power output to metabolic power) and power output, both of which are significantly influenced by the coordinated excitation, or muscle coordination, of the muscles involved (Blake et al., 2012; Dorel et al., 2012; Samozino et al., 2007; Wakeling et al., 2010). Therefore, investigating movement performance requires a knowledge of muscle coordination and the muscle coordination responses to a range of mechanical demands.

Portions of this chapter previously appeared as: (Blake and Wakeling, 2015)

The relative excitation of each muscle is both workload (Blake and Wakeling, 2012; Blake and Wakeling, 2013; Blake et al., 2012; Ericson, 1986; Ericson et al., 1985; Hug et al., 2004b; Jorge and Hull, 1986; Sarre et al., 2003; Wakeling and Horn, 2009; Wakeling et al., 2010) and cadence dependent, with many discrepancies in the collective research (Ericson, 1986; Ericson et al., 1985; Lucia et al., 2004; Neptune et al., 1997; Neptune et al., 1997; Sarre and Lepers, 2005; Sarre and Lepers, 2007; Sarre et al., 2003; Takaishi et al., 1996; Takaishi et al., 1998; Wakeling and Horn, 2009; Wakeling et al., 2006). Evidence suggests that individual muscles exhibit workload dependent relationships between muscle excitation and cadence (MacIntosh et al., 2000), which may explain the discrepancies as a wide range of workloads were employed. The timing of muscle excitation has also been shown to be affected by cadence, with several muscles exhibiting a phase advance and/or larger duty cycle with increasing cadence (Baum and Li, 2003; Dorel et al., 2012; Marsh and Martin, 1995; Neptune et al., 1997; Samozino et al., 2007; Sarre and Lepers, 2005; Sarre and Lepers, 2007; Wakeling and Horn, 2009), and both influenced (Sarre and Lepers, 2007) and not influenced (Jorge and Hull, 1986) by workload, but relatively little research has been completed in this area.

The influence of workload and cadence on muscle coordination is important as muscle coordination impacts mechanical efficiency (Blake et al., 2012; Wakeling et al., 2010) and power output (Dorel et al., 2012; Samozino et al., 2007; Wakeling et al., 2010), yet few studies have looked at the spatiotemporal muscle excitation-workload-cadence relationships across multiple muscles. Efficiency in cycling has been reviewed (Ettema and Loras, 2009) and has been shown to be dependent largely on workload and to a lesser extent on cadence, while delta efficiency (ratio of the change in mechanical power to the change in metabolic power) has been shown to be independent of workload (Hansen and Sjogaard, 2007) and both independent (Marsh et al., 2000) and dependent on cadence (Böning et al., 1984; Chavarren and Calbet, 1999; Sidossis et al., 1992). If delta efficiency increases with cadence (Böning et al., 1984; Chavarren and Calbet, 1999) then an increase in power output requires less energy at higher cadences compared to lower cadences (Sargeant and Beelen, 1993). This partially explains evidence that efficiency is maximized at increasing cadences for increasing power outputs (Böning et al., 1984; Coast and Welch, 1985; Foss and Hallén, 2004; Hagberg et al., 1981; Seabury et al., 1977), with the influence of cadence on efficiency decreasing at higher power

outputs (Chavarren and Calbet, 1999; Di Prampero, 2000). Obtaining greater efficiency by increasing cadence with workload may be the result of reduced muscle excitation since minimum muscle excitation also occurs at increasing cadences with increasing submaximal workloads (MacIntosh et al., 2000). Minimum muscle excitation across a group of muscles occurs despite different muscle excitation-workload-cadence relationships seen in individual muscles (Blake and Wakeling, 2013; Hug et al., 2004b; Lawrence and De Luca, 1983; MacIntosh et al., 2000).

Maximum efficiency occurs at cadences below those found at maximum power output and so there is a trade-off between efficiency and power in cycling (Kohler and Boutellier, 2005) that has been linked to differences in muscle coordination (Blake et al., 2012). Maximum efficiency has been predicted to occur at approximately one quarter to one third maximal shortening velocity in slow and fast muscle fibres, which in cycling is predicted to occur at approximately 50 r.p.m. and 150 r.p.m. in slow and fast muscle fibres, respectively (Sargeant, 2007). Maximum efficiency in a mixed fibre type muscle would, therefore, result from some combination of slow and fast muscle fibres at an intermediate cadence. Increasing cadence with power output to maximize efficiency may reflect the need for the additionally recruited faster muscle fibres to operate at higher velocities to maximize their efficiencies (Sargeant and Beelen, 1993). For example, greater relative recruitment of fast muscle fibres at 50 r.p.m. compared to 100 r.p.m. at approximately 335 W has been shown (Ahlquist et al., 1992) and suggests that more fast fibres may be necessary at the lower cadence because of their inability to effectively produce power at low velocities. In addition, it has been suggested that 25% maximum power output could be achieved with only slow muscle fibres at 60 r.p.m., whereas fast fibres would need to be active for the same power output at 120 r.p.m. due to the inability of slow fibres to effectively produce power at high velocities (Sargeant, 1994; Sargeant and Beelen, 1993). Indeed, evidence shows that faster muscle fibres are recruited at high cycle frequencies, such as 120 r.p.m., at high and low workloads (Farina et al., 2004) and at relatively low workloads at 60 r.p.m., before slow fibres are fatigued, (Ivy et al., 1987).

Maximum power output in cycling has been shown to occur at 110-120 r.p.m. (Beelen and Sargeant, 1991; Dorel et al., 2010; Hautier et al., 1996; Samozino et al., 2007; Sargeant et al., 1981) depending on fibre type composition of the individual's muscles

(Hautier et al., 1996). Beelen and Sargeant (1991) provided evidence that faster muscle fibres have a greater contribution to maximum power output at higher cadences such as those found at 120 r.p.m.. With different fibre type distributions and structural properties, it is unlikely that all muscles work at their optimal velocity for power production when the whole limb is producing maximum power output (Van Soest and Casius, 2000). Indeed, evidence shows that when cycling at maximum power output the ankle plantar flexor muscles shorten at velocities too slow to produce maximum power (Wakeling et al., 2010), yet in sprint cycling soleus (Sol) is at or near maximum excitation (Dorel et al., 2012) so it is likely this muscle is operating inefficiently. At extremely high cadences the muscle and muscle fibre recruitment can be further manipulated with evidence, including the previous chapter, of preferential fast muscle or fast fibre recruitment at high shortening velocities (Blake and Wakeling, 2014; Citterio and Agostoni, 1984; Gillespie et al., 1974; Gollnick et al., 1974; Grimby and Hannerz, 1977; Hodson-Tole and Wakeling, 2008a; Hoffer et al., 1981; Jayne and Lauder, 1994; Nardone et al., 1989; Smith et al., 1980; Wakeling and Horn, 2009; Wakeling et al., 2006) and recruitment of additional slow fibres to reach the highest shortening velocities (Blake and Wakeling, 2014; Holt et al., 2014).

The mechanical efficiency and power output of limb movement are significantly influenced by muscle coordination, (Blake et al., 2012; Dorel et al., 2012; Samozino et al., 2007; Wakeling et al., 2010), which is affected by the mechanical demands of the movement. Little is known about the mechanical demand and muscle coordination relationships or their subsequent influence on mechanical efficiency and power output. Therefore, the main objectives of this study were to map the muscle coordination space of ten leg muscles across a wide range of mechanical demands to: 1) determine if muscle excitation responses to changes in cadence are workload dependent and therefore explain previous inconsistencies reported in the literature, 2) determine if critical cadences exist where distinct changes in muscle excitation and muscle coordination can be identified that coincide with maximum relative efficiencies and maximum power output and 3) determine muscle coordination patterns responsible for maximum relative mechanical efficiency. We then aimed to use this knowledge to inform and design a physiologically meaningful reference frame for the biofeedback system to facilitate the manipulation the muscle coordination with respect to relative mechanical efficiency.

4.2. Methods

4.2.1. Protocol and Data Acquisition

Eleven competitively trained male cyclists (mean ± S.E.M.: age = 33.9 ± 3.1 years, mass = 72.8 ± 2.1 kg, height = 179.1 ± 1.9 cm, cycling distance per year = 10773 ± 1575 km) volunteered to participate in the study. All participants gave their informed written consent to participate and the ethics committee in accordance with the Office of Research Ethics at Simon Fraser University approved all procedures.

The participants cycled at cadences of 40, 60, 80, 100, 120, 140, 160 and 180 r.p.m. at each of 100, 200, 300 and 400 W on an indoor cycle trainer (Schoberer Rad Messtechnik (SRM), Julich, Germany). The participants completed a 10-minute warm-up at a freely chosen cadence with 5 minutes at 100 W followed by 5 minutes increasing 20 W each minute. The conditions were first randomized by cadence and then each power output was presented in random order to help ensure compliance of the desired cadence (MacIntosh 2000). The geometry of the cycle trainer was matched to each participant's own bicycle as closely as possible, and they used their own clipless pedals and shoes. Cyclists were instructed to maintain a seated position with hands on the brake hoods while data were collected and each trial was 30 seconds in duration with 90 seconds rest between.

Electomyographic (EMG) signals were recorded continuously from 10 muscles of the right leg (tibialis anterior (TA), MG, LG, Sol, vastus medialis (VM), rectus femoris (RF), vastus lateralis (VL), semitendinosus (ST), biceps femoris (BF) and gluteus maximus (GM)) using bipolar Ag/AgCl surface electrodes with 10 mm diameter and 21 mm spacing (Norotrode; Myotronics, Kent, WA). The skin of the right leg in the location of the electrodes was prepared by removing hair and dead skin and cleaning with isopropyl wipes. The electrodes were fixed to the skin with stretchable adhesive bandages and the entire leg was covered with a tubular net bandage to reduce movement artifacts. The EMG signals were amplified (gain 1000), band-pass filtered (bandwidth 10-500 Hz: Biovision, Wehrheim, Germany) and recorded at 2000 Hz (16-bit analog to digital converter: USB-6210; National Instruments, Austin, TX). Cadence and the effective (normal) and

ineffective (tangential) forces applied to the crank arms were recorded using instrumented pedals (Powerforce, Radlabor, Freiburg, Germany) simultaneously with the EMG. Crank forces were subsequently used to calculate power output.

4.2.2. Data Analysis

The EMG signals were resolved into intensities in both time and frequency space using an EMG-specific wavelet analysis (von Tscharner, 2000). The wavelets had a frequency bandwidth of approximately 11-432 Hz (j = 1-10; (von Tscharner, 2000). EMG intensities for individual muscles were calculated as the sum of intensities across all ten wavelet domains for each time point. The EMG intensities were interpolated to 100 points per muscle per pedal cycle starting at top dead center of the right crank arm rotation and were normalized to the mean for each muscle for each participant across all trials. The total EMG intensity was calculated for each muscle and pedal cycle as the sum of the interpolated intensities. Data from the first five pedal cycles within five r.p.m. of the desired cadence and within 10% of steady-state power output were retained for further analysis. The primary muscle coordination patterns across a pedal cycle were determined using principal component (PC) analysis. Muscle coordination patterns were extracted using the interpolated EMG intensities (100 points per muscle per pedal cycle) as has been described previously (Blake and Wakeling, 2012; Blake et al., 2012; Wakeling and Horn, 2009). In order to visualize the primary differences in muscle coordination for each condition, EMG intensities were reconstructed from the vector sum of the muscle coordination PC's (PC_{mus}) weightings and loading scores for the first 10 principal components (Blake et al., 2012).

Muscle bursts were extracted (using an onset/offset threshold of 5% of the difference between the maximum and minimum EMG intensity: Blake and Wakeling, 2014) and the burst duration and duty cycle (proportion of muscle excitation relative to a complete pedal cycle) were calculated for each muscle for each pedal cycle. For each muscle burst the EMG intensities were interpolated to 100 points for each wavelet (10 wavelets * 100 points = 1000 points per muscle burst) and normalized to the maximum intensity across all wavelets for each muscle for each participant across all trials. The time-frequency patterns were quantified from the interpolated frequency spectra (100 points

per muscle per wavelet per muscle burst) using a Principal Component analysis (Blake and Wakeling, 2014). The first time-frequency PC ($PC_{freq}1$) approximated the mean time-varying frequency spectra with subsequent PC_{freq}'s representing the variation in time and frequency from $PC_{freq}1$. The second and third PC_{freq}'s ($PC_{freq}2$ and $PC_{freq}3$) showed distinct shifts in EMG intensity at different times and frequencies within each muscle burst and were therefore used to calculate vectors in $PC_{freq}3$-$PC_{freq}2$ space using the mean loading scores for each condition. A change in the direction of these vectors for different conditions represents a change in the time-varying frequency of the EMG intensity for each muscle burst.

Relative phase shifts of the EMG intensities for each muscle across a pedal cycle were determined using the Procrustes shift registration method (Ramsay and Silverman, 2005). These were determined separately for cadence and power output by analyzing the shift due to cadence at each power output and the shift due to power output at each cadence. Phase shifts due to cadence and power output were also calculated in a similar manner for the effective, ineffective and resultant pedal forces. Relationships between the mean pedal force per pedal cycle and cadence were determined at each power output for the effective, ineffective and resultant pedal forces. Where a parabolic relationship was evident a best-fit 2^{nd} or 3^{rd} order polynomial was determined for the data using a linear least-squares fit (Mathematica Version 10, Wolfram Research, Inc., Champaign, USA) to estimate the cadence at which minimum pedal forces occurred. The relative efficiency was estimated as the ratio of mechanical power output measured at the pedals to the sum of the total EMG intensities across all muscles where total EMG intensity was used as a proxy for the metabolic power required for cycling (Blake and Wakeling, 2013; Wakeling et al., 2011). The relationships between cadence and both relative efficiency and total EMG intensity across all muscles were determined at each pedal cycle and best-fit polynomials were fit to the data to estimate the cadence at which relative efficiency was maximized and total EMG intensity was minimized.

4.2.3. Statistics

The influence of power, cadence and any interaction between power and cadence on muscle coordination was determined using general linear model analyses of variance

(ANOVA) using each of the first 20 muscle coordination PC's (PC_{mus} loading scores) individually as the dependent variable and subject as a random factor. This same analysis was also completed for the first 10 PC_{freq}'s for each muscle. The effects of cadence and power output on EMG intensity, total EMG intensity across all muscles, relative efficiency, muscle burst duration and duty cycle, mean effective, ineffective and resultant pedal forces and pedal force and EMG intensity phase shifts were evaluated using one-way ANOVAs. Where significant effects were found, Tukey's *post hoc* tests were performed to determine differences between cadences for a particular power output, when cadence was the independent variable, and between power outputs for a given cadence, when power output was the independent variable.

4.3. Results

4.3.1. EMG Intensity & Muscle Coordination

The total EMG intensities and the sum of the total EMG intensities across all muscles were significantly influenced by power output, cadence and the interaction between power and cadence (Figure 4.1E & Figure 4.2). EMG intensity of most muscles displayed an exponential relationship with cadence at low power outputs and a parabolic relationship at high power outputs increasing primarily with cadence independent of power output above 140 r.p.m. (Figure 4.2). There was no significant difference in the total EMG intensity between 40 and 120 (Sol, VM and VL) or 140 r.p.m. (RF, ST, BF and GM) at 100 W and 40 and 120 (VL and ST) or 140 r.p.m. (Sol, GM) at 200 W. In contrast there was no significant difference in the total EMG intensity between 60 and 120 (ST) or 140 r.p.m. (Sol, VM, RF, VL, BF and GM) at 300 W and 60 and 120 (TA, ST and BF) or 140 r.p.m. (Sol, VM and VL) at 400 W with intensities significantly larger outside these cadences. EMG intensity for RF and GM was not significantly different between 80 and 140 r.p.m. at 400 W thus forming a steeper parabolic relationship (Figure 4.2). The total EMG intensities for MG and LG increased predominantly with cadence independent of power output, while the total EMG intensities for VM, VL and BF increased primarily with power output independent of cadence below 140 r.p.m.. The total EMG intensity for TA increased with both power and cadence below 140 r.p.m..

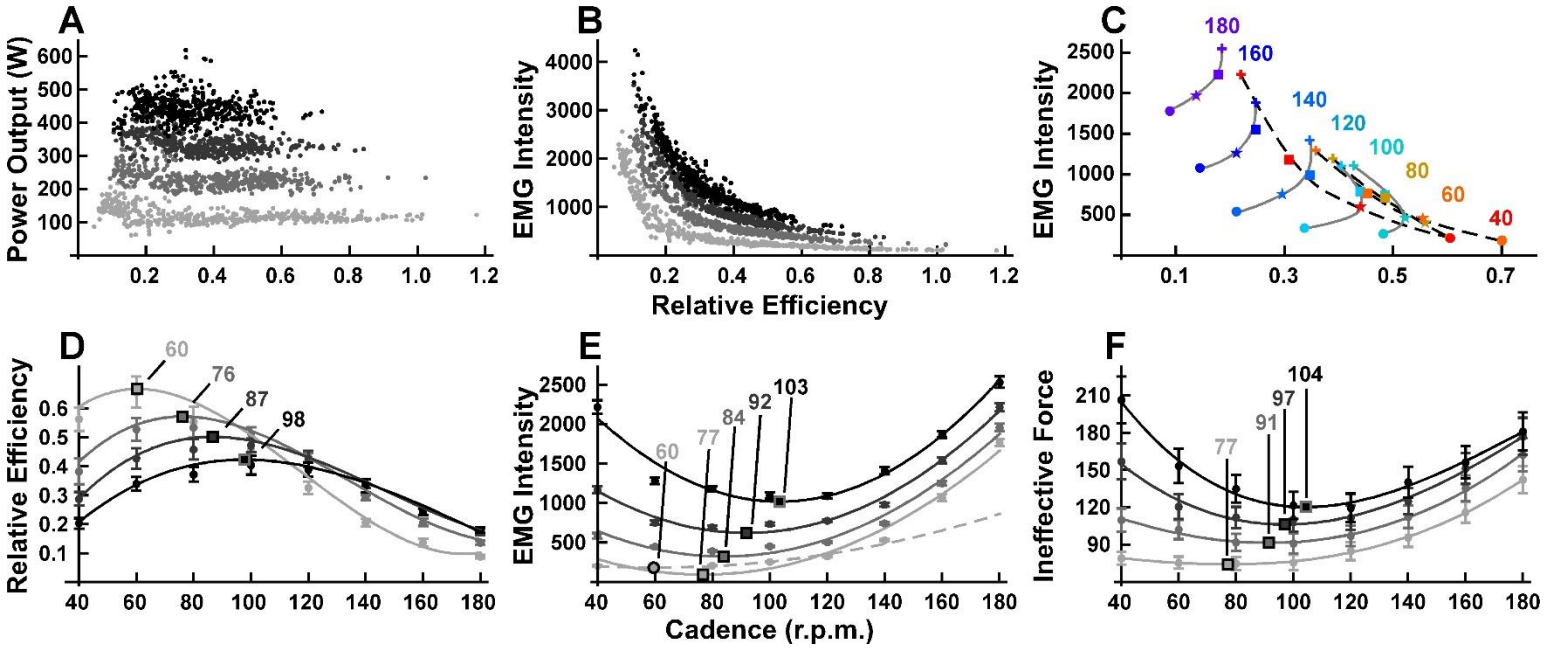
A
Power Output (W)
600
500
400
300
200
100
0.2
0.4
0.6
0.8
1.0
1.2
B
EMG Intensity
4000
3000
2000
1000
Relative Efficiency
C
EMG Intensity
2500
2000
1500
1000
500
180
160
140
120
100
80
60
40
0.1
0.3
0.5
0.7
D
Relative Efficiency
0.6
0.5
0.4
0.3
0.2
0.1
60
76
87
98
40
60
80
100
120
140
160
180
E
EMG Intensity
2500
2000
1500
1000
500
60
77
84
92
103
Cadence (r.p.m.)
F
Ineffective Force
210
180
150
120
90
77
91
97
104

Figure 4-1. The relations between total EMG intensity, power output and relative efficiency.

(A) Relative efficiency at each power output where each point represents a pedal cycle. (B) Relationship between relative efficiency and total EMG intensity across all ten muscles where (C) shows mean values for each cadence-power output combination. Power outputs are represented by symbols (cirlce, 100 W; star, 200 W; square, 300 W and cross, 400 W) and cadences are represented by each color labeled (40 to 180 r.p.m.). Lines have been added to give a visual representation of the relationships across power outputs for each cadence and are solid grey (100 to 180 r.p.m.) and dashed black (40 to 80 r.p.m.) to better identify the different trends. Relationships across cadences at each power output are shown for mean +/- S.E.M. relative efficiency (D), and total EMG intensity across all muscles (E), and mean ineffective pedal force per pedal cycle (F). Lines are best-fit polynomials and squares show the maximum (D) or minima (E and F) for these curves. The dashed line in (E) shows the best-fit polynomial at 100 W for 40 to 120 r.p.m. with its minimum shown by the square marker: this reduced range of cadences matches that used by MacIntosh and co-workers (2000). Power outputs are identified as light grey through black for 100 through 400 W, respectively.

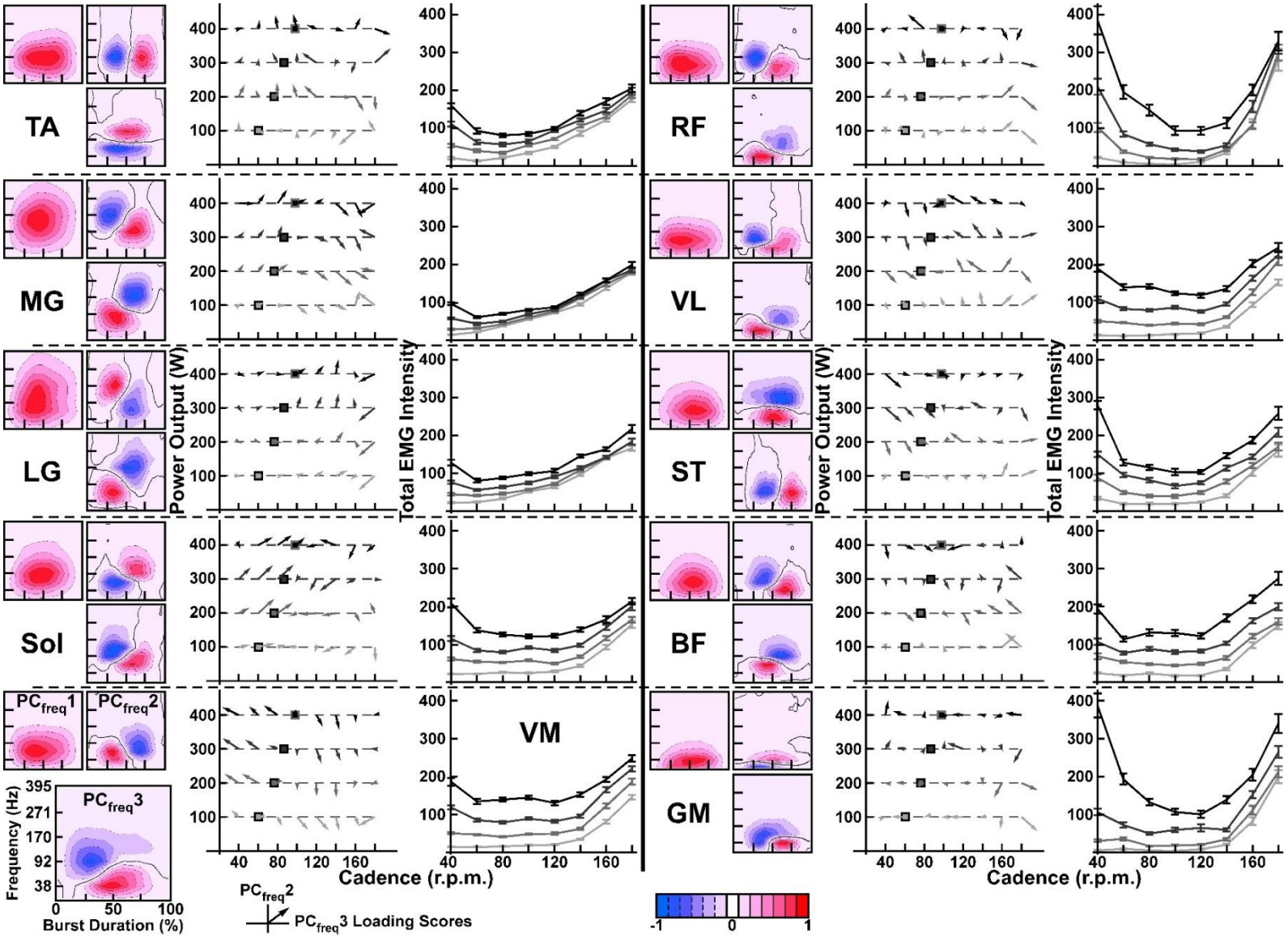
TA
MG
LG
Sol
VM
RF
VL
ST
BF
GM
PC$_{freq}$1
PC$_{freq}$2
PC$_{freq}$3
Frequency (Hz)
395
271
170
92
38
0
50
100
Burst Duration (%)
Power Output (W)
Total EMG Intensity
400
300
200
100
40
80
120
160
Cadence (r.p.m.)
PC$_{freq}$2
PC$_{freq}$3 Loading Scores
-1
0
1

Figure 4-2. Principal component representation of the fluctuations in EMG intensity through time-frequency space for the bursts of muscle excitation and muscle specific total EMG intensities.

Principal component representations of the time-varying frequency (PC_{freq}) of the muscle burst (contour plots; $PC_{freq}1$ top left, $PC_{freq}2$ top right and $PC_{freq}3$ bottom right for each muscle). Vectors represent the relationship between $PC_{freq}2$ (vertical) and $PC_{freq}3$ (horizontal) loading scores at each cadence-power output condition and squares show cadences for maximum relative efficiency at each power output as determined in Figure 4.1. Line plots show mean +/- S.E.M. EMG intensity for each muscle at each cadence-power output condition, and are shown with the same grey scale as in Figure 4.1.

The muscle coordination patterns for each condition can be seen in Figure 4.3. The first two PC_{mus}'s that quantify the coordination (Figure 4.4) explained over 66% of the variability in coordination patterns and the first ten explained over 82%. Loading scores for the first PC_{mus} ($PC_{mus}1$) were significantly correlated with the sum of the total EMG intensities across all ten leg muscles ($r = 0.99$). Muscle coordination (as evaluated through the PC_{mus} loading scores) had a significant effect on relative efficiency, with nine of the first ten PC_{mus}'s having an effect, while cadence and power output had significant influences on muscle coordination (Figure 4.4) and relative efficiency (Figure 4.1D). Muscle coordination and relative efficiency were also significantly affected by the interaction of cadence and power output. The predominant muscles featured in $PC_{mus}2$ to $PC_{mus}5$ were RF and GM where $PC_{mus}2$ and $PC_{mus}3$ highlighted a balance between RF and GM and all other muscles, $PC_{mus}4$ represented the balance between RF and GM and $PC_{mus}5$ showed a shift in timing of most muscles opposite to that of RF (Figure 4.4). Visualizations of the primary muscle coordination patterns for maximum relative efficiency were established through reconstructions of the EMG intensities using a reduced number of PC_{mus}'s. The cadence at which relative efficiency was maximized was 60, 76, 86 and 97 r.p.m. at 100, 200, 300 and 400 W, respectively (Figure 4.1D), which displayed progressive muscle excitation from the knee (VM and VL together) to the hip (GM) to the ankle (SOL) and finally to BF through the down stroke of the pedal cycle. These muscles also showed the highest levels of relative muscle excitation for these high relative efficiency conditions when compared to the other muscles. Conditions associated with decreased relative efficiency had the highest relative muscle excitation for RF and GM at high power outputs as well as TA, MG, LG, RF and ST across all power outputs with low relative excitation for VM and VL.

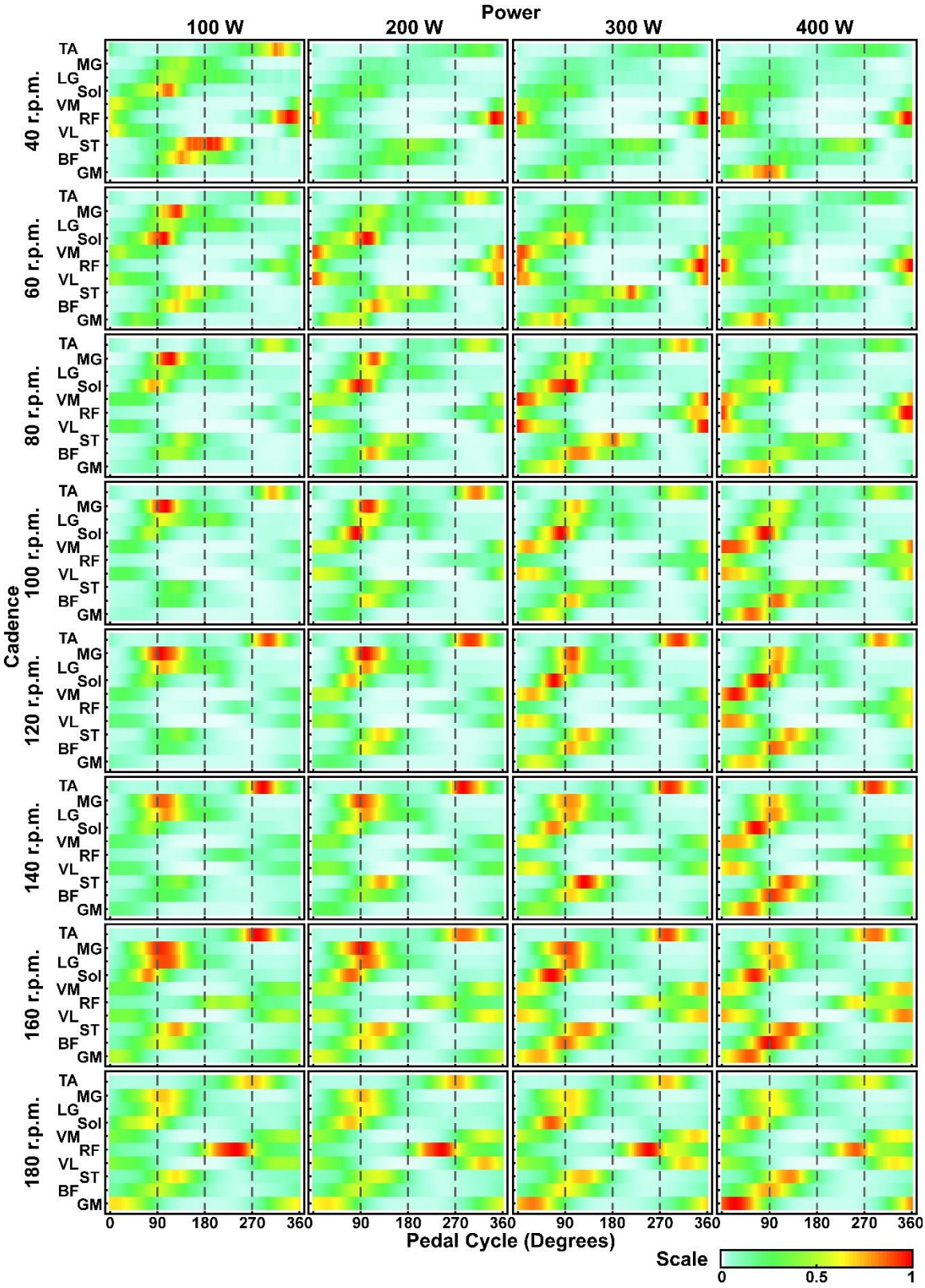
Power
100 W
200 W
300 W
400 W
Cadence
40 r.p.m.
60 r.p.m.
80 r.p.m.
100 r.p.m.
120 r.p.m.
140 r.p.m.
160 r.p.m.
180 r.p.m.
TA
MG
LG
Sol
VM
RF
VL
ST
BF
GM
0
90
180
270
360
Pedal Cycle (Degrees)
Scale
0
0.5
1

Figure 4-3. Muscle coordination patterns for each cadence-power output combination.

Mean EMG intensity pattern for each cadence (rows) and power output (columns) combination normalized to the maximum for each condition.

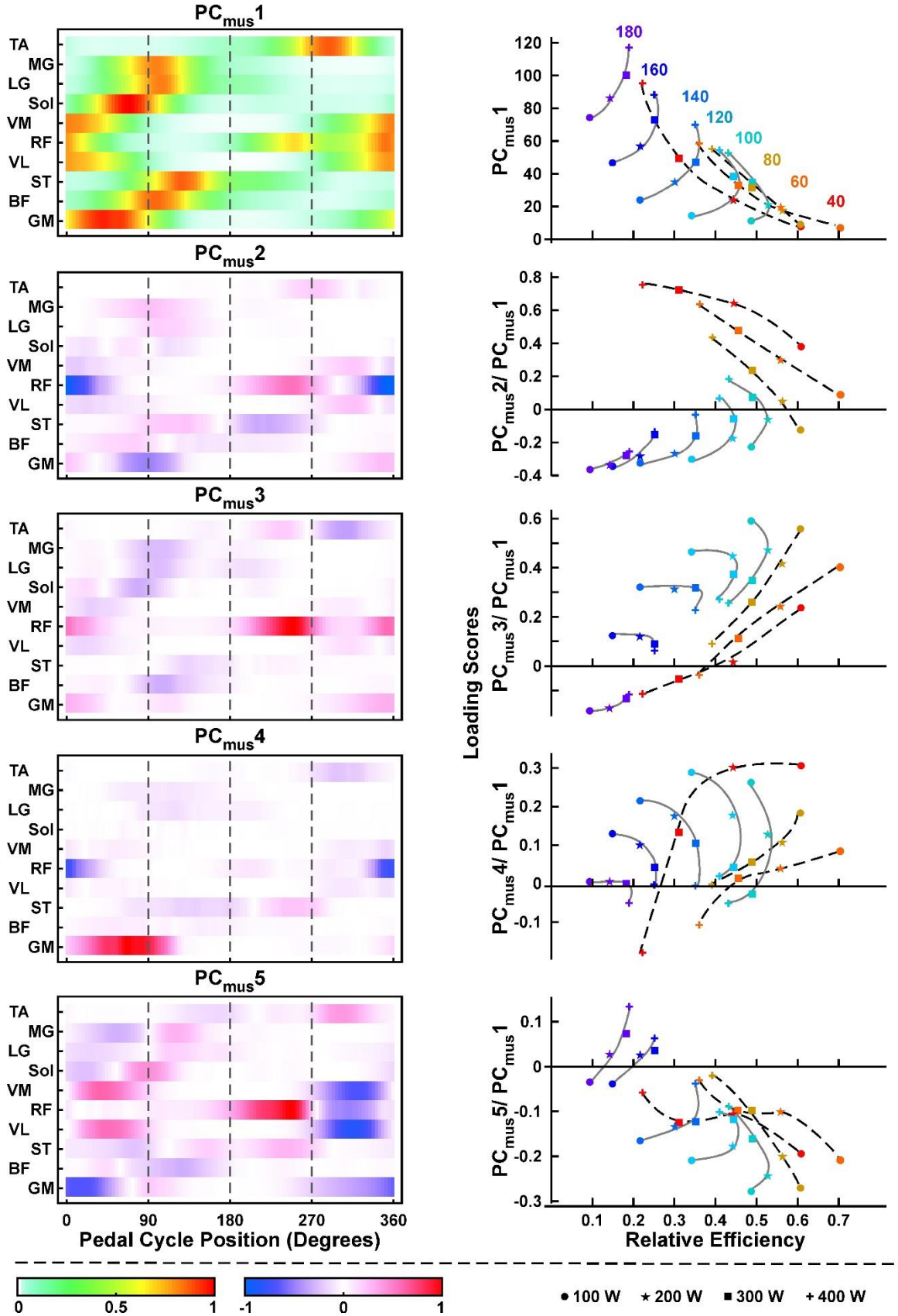
PC$_{mus}$1
PC$_{mus}$2
PC$_{mus}$3
PC$_{mus}$4
PC$_{mus}$5
TA
MG
LG
Sol
VM
RF
VL
ST
BF
GM
0
90
180
270
360
Pedal Cycle Position (Degrees)
180
160
140
120
100
80
60
40
PC$_{mus}$1
PC$_{mus}$2/ PC$_{mus}$1
PC$_{mus}$3/ PC$_{mus}$1
PC$_{mus}$4/ PC$_{mus}$1
PC$_{mus}$5/ PC$_{mus}$1
Loading Scores
0.1
0.2
0.3
0.4
0.5
0.6
0.7
Relative Efficiency
0
0.5
1
-1
0
1
100 W
200 W
300 W
400 W

Figure 4-4. Principal component representation of the muscle coordination. Visual representations of the first five muscle coordination principal components (PC_{mus}) and the relationship between mean PC_{mus} loading scores (vertical axis) and relative efficiency (horizontal axis) for each cadence-power output condition. Power outputs are represented by symbols (circle, 100 W; star, 200 W; square, 300 W and cross, 400 W) and cadences are represented by each color labeled (40 to 180 r.p.m.) in $PC_{mus}1$. Lines have been added to give a visual representation of the relationships across power outputs for each cadence and are solid grey (100 to 180 r.p.m.) and dashed black (40 to 80 r.p.m.) to better identify the different trends.

The first PC_{freq} ($PC_{freq}1$) of the time-varying frequency spectra explained approximately 60% of the time-frequency spectra and was similar to the mean frequency spectrum for each muscle. The loading scores for $PC_{freq}1$ were significantly correlated with each muscle's total EMG intensity and displayed similar relationships with cadence and power output as total EMG intensity with minimum loading scores occurring at increasing cadences with increases in power outputs (Figure 4.1E). The first ten PC_{freq}s ($PC_{freq}1$ to $PC_{freq}10$) explained approximately 81-95% of the time-varying frequency spectra, depending on the muscle where $PC_{freq}2$ and $PC_{freq}3$ displayed increases and decreases in high and low frequencies and/or timing shifts of the frequency relative to the muscle burst duration (Figure 4.2). Vector plots showing mean loading scores of $PC_{freq}2$ and $PC_{freq}3$ projected onto plots of maximum relative efficiency at each condition highlight the frequency shifts of each muscle relative to cadence and power output (Figure 4.2). Sol, VM and VL displayed frequency shifts in $PC_{freq}2$ and $PC_{freq}3$ that corresponded to changes in relative efficiency and total EMG intensity across all muscles. Notably, $PC_{freq}1$ of these muscles explained more of the time-frequency spectra for each muscle burst than any other muscle except GM. Most muscles exhibited pronounced changes in EMG frequency at the highest cadences and in some cases at 40 r.p.m..

4.3.2. Relative efficiency

Relative efficiency (the ratio of power output to total EMG intensity across all muscles: Blake and Wakeling, 2013; Wakeling et al., 2011) was maximized at increasing cadences for increasing power outputs from 60 r.p.m. at 100 W to 98 r.p.m. at 400 W (Figure 4.1D). Relative efficiency increased while total EMG intensity decreased at each power output (Figures 4.1B, 4.1D & 4.1E) with total EMG intensity displaying more pronounced parabolic relationships with cadence as power output increased (Figure 4.1E). Cadences for maximum relative efficiency (Figure 4.1D) coincided with cadences

for minimum EMG intensity (Figure 4.1E) determined from the best-fit polynomials of the relationships. For example, at 400 W relative efficiency reached a maximum at approximately 98 r.p.m. while total EMG intensity displayed a parabolic relationship with minimum values at approximately 103 r.p.m.. The relationships between cadence, power output and relative efficiency can be visualized in the Figure 4.1D where from 40 to 80 r.p.m. relative efficiency decreases with each increase in power output, whereas from 100 to 180 r.p.m. it displays non-linear relationships with maximum relative efficiency occurring at higher power outputs as cadence increases. There was no significant difference in relative efficiency between 60 and 100 r.p.m. at 200 W, 60 and 120 r.p.m. at 300 W and 80 and 120 r.p.m. at 400 W.

4.3.3. Phase Shifts

Significant systematic phase shifts of the EMG intensity to be earlier in the pedal cycle were found with increasing cadences for all muscles, yet not across all power outputs (Figure 4.5). Phase shifts occurred in a limited cadence range for some muscles. For example, phase shifts earlier for ST occurred primarily between 40 and 120 r.p.m. at all power outputs, while for TA, VM, VL, Sol and MG phase shifts primarily occurred from 100 to 180 r.p.m.. The largest phase shifts across the full range of cadences could be found in RF (maximum ~100 degrees), ST and GM (both maxima ~70 degrees) with many muscles displaying shifts of approximately 40 degrees (TA, MG, VM, VL and BF). No significant phase shift was found for the LG at 200 to 400 W, with a relatively small systematic shift at 100 W of approximately 27 degrees. Relatively small shifts were also found in Sol of approximately 20-30 degrees. The phase shifts of the EMG intensity varied with power output in muscle-specific and cadence dependent manner with the phase sometimes increasing and sometimes decreasing with power, and this is displayed in Figure 4.5.

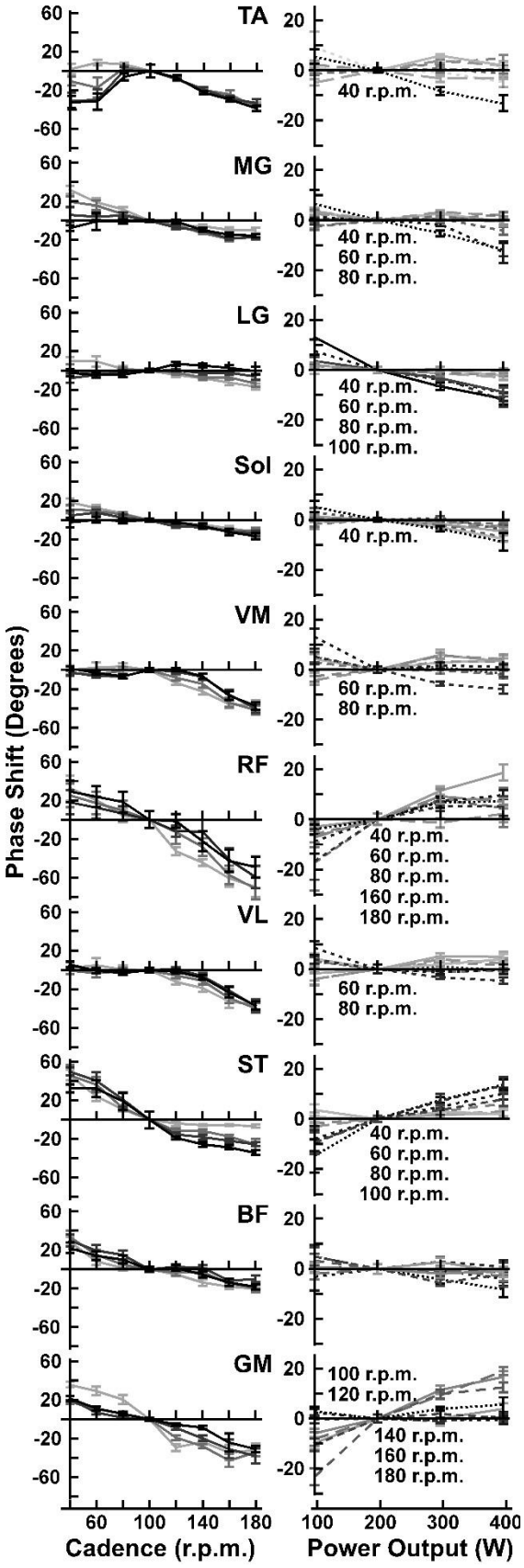
TA
MG
LG
Sol
VM
RF
VL
ST
BF
GM
Phase Shift (Degrees)
60
20
-20
-60
0
40 r.p.m.
60 r.p.m.
80 r.p.m.
100 r.p.m.
120 r.p.m.
140 r.p.m.
160 r.p.m.
180 r.p.m.
100
200
300
400
Cadence (r.p.m.)
Power Output (W)

Figure 4-5. Relative phase shifts of the total EMG intensity within the pedal cycle.

Phase shifts are shown across cadence values at each power output (first column) and across power outputs at each cadence (second column). Cadences listed in each plot in the second column indicate a significant effect of power output on the phase shift for that cadence. Power outputs in the first column are identified with the same grey scale as in Figure 4.1 as light grey through black for 100 through 400 W, respectively. Cadences are distinguished by dashing, as shown in Figure 4.7.

4.3.4. Muscle Burst Duration

All muscles displayed a significant systematic decrease in muscle burst duration that plateaued at the highest cadences (Figure 4.6). There was no significant difference in muscle burst duration between 120 and 180 r.p.m. for TA (except 100 W), Sol, VM, RF, VL, ST, BF and GM (except 100 W) and between 140 and 180 r.p.m. for MG and LG. There was a significant effect of power output on burst duration for TA at 80 and 100 r.p.m., MG at 40 and 60 r.p.m. and for BF at 60 r.p.m.. Significant increases in the duty cycles were found above 120 r.p.m. for TA, Sol, VM, VL, ST (above 140 r.p.m.), BF and GM (Figure 4.6). No significant difference in duty cycle between cadences from 40 to 120 r.p.m. were found for TA (at 200-300 W), VM, VL, ST, BF (40 to 80 r.p.m. at 100 W) and GM (except 100 W). There was no significant difference in duty cycle between all cadences for LG, a significant increase in duty cycle across all cadences for RF and a significant decrease in duty cycle from 40 to 100 r.p.m. at 200-400 W for Sol.

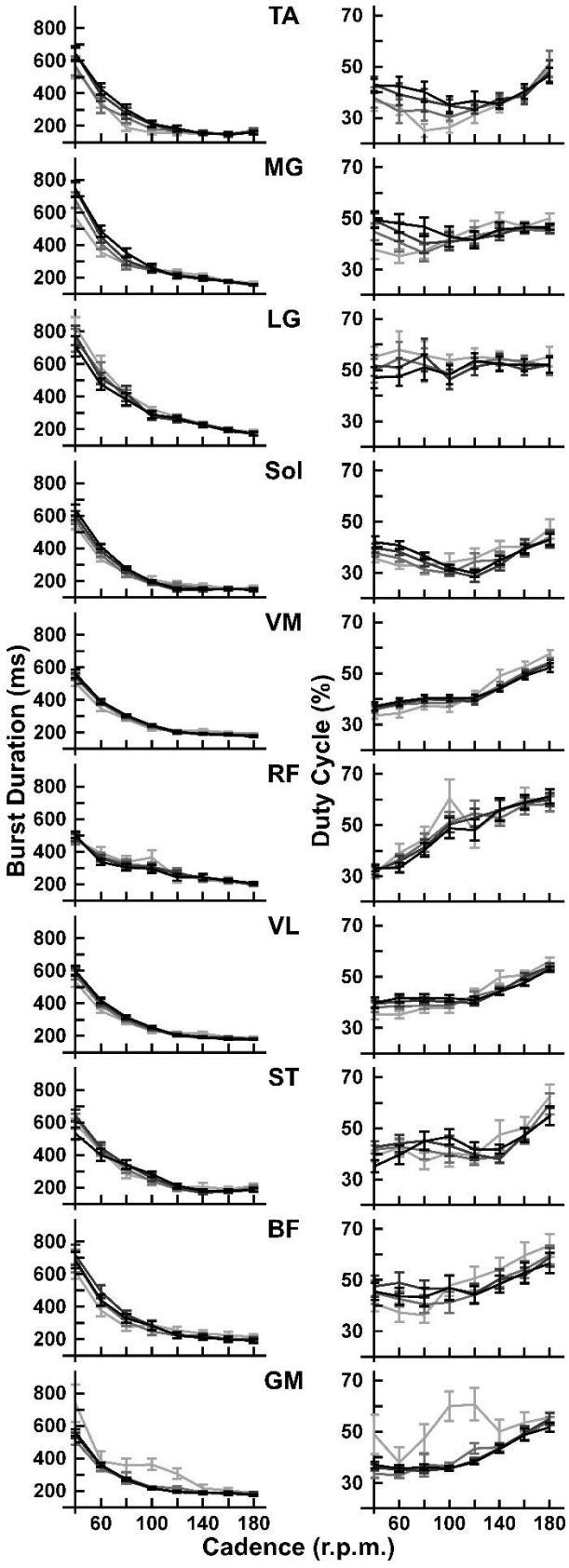
TA
MG
LG
Sol
VM
RF
VL
ST
BF
GM
Burst Duration (ms)
Duty Cycle (%)
Cadence (r.p.m.)
800
600
400
200
70
50
30
60
100
140
180

Figure 4-6. Muscle burst durations and duty cycles.
Mean +/- S.E.M. muscle burst durations (first column) and duty cycle (second column) across cadences for each power output. The duty cycle represents the muscle burst duration as a percentage of the complete pedal cycle. Power outputs are identified with the same grey scale as in Figure 4.1 as light grey through black for 100 through 400 W, respectively.

4.3.5. Pedal Forces

Both the peak maximum and peak minimum effective forces per pedal cycle displayed an inverse relationship with cadence across all power outputs with the differences between cadences decreasing at the highest cadences (Figure 4.7). Mean effective force per pedal cycle showed a decreasing relationship with cadence, whereas maximum and mean ineffective forces per pedal cycle displayed parabolic relationships with cadence with minimum values occurring at increased cadences for increased power outputs (Figure 4.7). All pedal forces systematically shifted later in the pedal cycle as cadence increased with the largest shifts visible in the resultant pedal force (Figure 4.7).

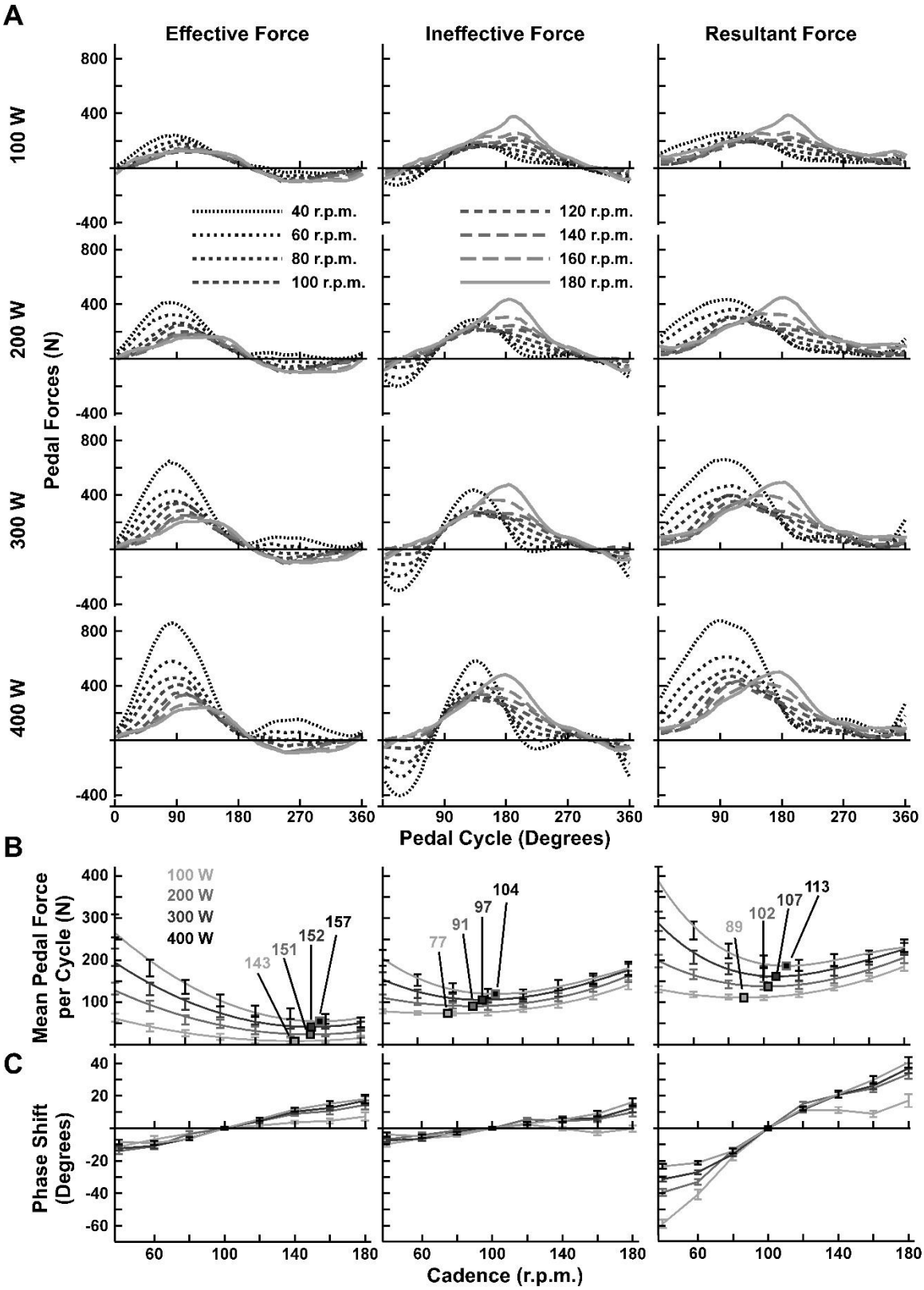
A
Effective Force
Ineffective Force
Resultant Force
100 W
200 W
300 W
400 W
Pedal Forces (N)
40 r.p.m.
60 r.p.m.
80 r.p.m.
100 r.p.m.
120 r.p.m.
140 r.p.m.
160 r.p.m.
180 r.p.m.
Pedal Cycle (Degrees)
B
Mean Pedal Force per Cycle (N)
100 W
200 W
300 W
400 W
143
151
152
157
77
91
97
104
89
102
107
113
C
Phase Shift (Degrees)
Cadence (r.p.m.)

Figure 4-7. Pedal forces.
(A) Mean resultant (first column), effective (second column) and ineffective (third column) pedal forces for each power output and cadence. (B) Mean +/- S.E.M. pedal force per pedal cycle at each cadence. Best-fit polynomials have been fit to each power output with minima shown by square symbols. (C) Phase shift of each pedal force across cadences for each power output. Power outputs in (B & C) are identified with the same grey scale as in Figure 4.1 as light grey through black for 100 through 400 W, respectively. Cadences in (A) are identified in the second row.

4.4. Discussion

This study investigated the influence on relative mechanical efficiency of cycle frequency, workload and muscle coordination across a wide range of mechanical demands. One of the primary contributions of this research is that it unifies the seemingly inconsistent previous findings, with respect to muscle excitation responses to changes in cycle frequency, by revealing an interactive effect of cycle frequency and workload on muscle excitation. Maximum relative efficiency was evident in (1) the mechanical output since minimum ineffective pedal forces occurred at similar increasing cadences for increasing power outputs, (2) the muscle coordination with progressive muscle excitation through the uniarticulate knee, hip and ankle muscles during the down stroke, and (3) changes in the timing and recruitment of different muscle fibre types in VM, VL and Sol. In contrast, elevated muscle excitation and reduced relative efficiency were dependent on muscle coordination at the top and bottom of the pedal cycle and dominated by excitation of bi-articulate muscles and TA and GM and larger duty cycles for many muscles.

Power output was also limited beyond a cycle frequency of 120-140 r.p.m. where there were plateauing muscle burst durations, longer duty cycles and disproportionate increases in EMG intensity for most muscles. These factors represented a constraint of muscle excitation, increasing metabolic costs and rapidly decreasing relative mechanical efficiency. The changes in muscle burst duration, duty cycle and EMG intensity suggest a limitation of the activation-deactivation capabilities of the muscle fibres at the highest cycle frequencies.

4.4.1. Muscle Coordination influence on Relative efficiency – Mechanical Demands

Relative efficiency was significantly affected by muscle excitation, muscle coordination and the mechanical demands of the cycling task. Increased relative efficiency at constant power output and cadence has been shown to result from a decrease in muscle excitation (EMG intensity) as a consequence of altered muscle coordination (Blake et al., 2012). The current findings add that the relationships between relative efficiency and both EMG intensity (Figure 4.1C) and muscle coordination (Figure 4.4) are cadence specific, with power output and cadence having an interactive influence. The interactive influence between power output and cadence helps explain how increased relative efficiencies result from changes in muscle coordination due to reduced muscle excitation and also unifies the seemingly inconsistent previous findings related to changes in EMG with cadence and power output. For example, Sarre and co-workers (2003) found RF EMG decreased with increased cadence and was higher at 60 r.p.m. than any other cadence tested (up to approximately 115 r.p.m.) at 297 and 371 W. In contrast, Ericson (1985) and Neptune (1997) determined that RF EMG was uninfluenced between 40 and 100 r.p.m. at 120 W and between 45 and 120 r.p.m. at 250 W, respectively. In the current results RF intensity displayed a parabolic relationship with cadence at high power outputs, similar to MacIntosh et al. (2000) and Marsh and Martin (1995), with the curvature decreased to an exponential relationship at 100 W (Figure 4.2). Therefore, RF intensity was significantly higher at 60 r.p.m. than 100 and 120 r.p.m. at 400 W and uninfluenced between 40 and 120 r.p.m. at 100 W supporting these previous findings (Ericson et al., 1985; Neptune et al., 1997; Sarre et al., 2003). Similarly, the EMG intensity of all muscles displayed exponential and/or parabolic relationships with cadence depending on the workload (Figure 4.2), helping explain other differences previously found and highlighting the need to investigate a large array of conditions to fully understand muscle excitation and muscle coordination responses to altered mechanical demands.

These results support evidence that efficiency is maximized (Böning et al., 1984; Coast and Welch, 1985; Foss and Hallén, 2004; Hagberg et al., 1981; Seabury et al., 1977) and muscle excitation is minimized (MacIntosh et al., 2000) at increasing cadences for increasing power outputs during cycling and that the influence of cadence on efficiency decreases at higher power outputs (Figure 4.1D; Chavarren and Calbet, 1999; Di

Prampero, 2000). Maximum relative efficiency occurred at 60, 76, 86 and 97 r.p.m. at 100, 200, 300 and 400 W, respectively (Figure 4.1D), which is similar to the values of minimum muscle excitation found by MacIntosh and co-workers (2000). Efficiency in cycling has been shown to be dependent primarily on workload (Ettema and Loras, 2009), which is supported here at lower cadences (less than 100 r.p.m.), but the dependence was decreased at high cadences (Figure 4.1D). Indeed, there was little difference in relative efficiency between all power outputs at 100 r.p.m. and between 300 and 400 W at the highest cadences such that a change in power output resulted in a proportionally similar change in total EMG intensity. The greatest difference in relative efficiency values across all power outputs occurred at 40 and 60 r.p.m. implying that increasing workload at low cadences required a larger increase in muscle excitation than an equal change at other cadences (Figure 4.1E). One explanation for the increased muscle excitation at low cadences is that more faster muscle fibres would need to be recruited to generate increased power (Ahlquist et al., 1992), however such fibres are very inefficient at low shortening velocities.

4.4.2. Muscle Coordination influence on Relative efficiency – Mechanical Output

Evidence from both the muscle coordination and the resulting mechanical output, seen in the pedal forces, indicates that the top and bottom of the pedal cycle are critical to efficiently completing the cycling action (Blake et al., 2012; Dorel et al., 2010; Leirdal and Ettema, 2011), despite the effective force being low at these times (Figure 4.7; Patterson et al., 1983; Sanderson, 1991). The importance of different sectors of the pedal cycle, other than the down stroke, to effectively complete the pedaling action has been shown during submaximal (Blake et al., 2012; Hug et al., 2008; Korff et al., 2007; Leirdal and Ettema, 2011) and maximal sprint cycling (Dorel et al., 2010; Martin and Brown, 2009; Samozino et al., 2007) and this study adds that the top and bottom are critical for efficient cycling. RF and TA were the primary muscles active at the top and MG, LG, ST and BF were the primary muscles active at the bottom of the pedal cycle, respectively (Figure 4.3), and all had a significant effect on relative efficiency (Figure 4.4). These muscles (except TA) are bi-articulate muscles, whereas the traditionally classified power producing muscles (VM, VL and GM) and Sol are all single joint muscles, thus supporting the notion

that the bi-articulate muscles are important for the transfer of force between joints and the orientation of the forces on the pedals (Raasch et al., 1997; van Ingen Schenau et al., 1992). The ineffective pedal force displayed peak amplitudes at the top and/or bottom of the crank rotation (Figure 4.7), again providing evidence of the constraints and importance of these regions of the pedal cycle. The ineffective force may provide a better indication of the relative efficiency-cadence-workload relationships than the effective or resultant forces since there was little difference in effective force at high cadences for high workloads, making it difficult to ascertain a minimum, and the resultant force is dependent on the effective force (Figure 4.7).

Across all power outputs the muscle coordination patterns characteristic of maximum relative efficiency showed synchronized or coordinated timing and progressive excitation, primarily during the down stroke, from muscles spanning the knee (VM and VL together) to the hip (GM) to the ankle (SOL) and finally to BF. In contrast, inefficient cycling was dominated by excitation of RF and GM at high power outputs, TA, MG, LG, RF and ST across most power outputs, shrinking relative levels of excitation for VM and VL and larger duty cycles for many muscles. Again, the muscles active at the top and bottom of the pedal cycle determined the balance between efficient and inefficient cycling and, while not able to conclusively ascertain, it may be speculated that the synchronized timing and progressive excitation of muscles during the down stroke may be the result of effective transitions at the top and bottom of the pedal cycle.

The parabolic relationship between pedal forces and cadence (Figure 4.7) has been attributed to the competing requirements for decreasing muscular and increasing non-muscular components of the pedal forces with cadence, as determined from pedal force decomposition (Kautz and Hull, 1993). At cadences beyond 90 r.p.m. the increases in pedal forces have been attributed to non-muscular components (Kautz and Hull, 1993; Neptune and Herzog, 1999) and in particular the inertial component or centripetal-like force keeping the foot and leg following a constrained path (Kautz and Hull, 1993). To accommodate increased workloads at each cadence the muscular component would be higher, whereas the non-muscular components (inertial and weight) should show a consistent cadence relationship independent of workload since the mass of the foot and pedal, length of the crank arm and the velocity remain constant at each cadence.

Therefore, it would be expected that minimum resultant and ineffective pedal forces occurred at increasing cadences for increasing power outputs, as seen in Figure 4.7, because the intersection of the decreasing muscular and increasing non-muscular components would depend primarily on the muscular component. The importance of the muscular component highlights the significance of muscle activation and coordination for efficient and effective cycling action.

The deterioration in muscle coordination and the alterations in mechanical output at the top and bottom of the pedal cycle seen at the highest cadences may be one explanation why maximum power output occurs around 120 r.p.m. (Beelen and Sargeant, 1991; Dorel et al., 2010; Hautier et al., 1996; Samozino et al., 2007; Sargeant et al., 1981) despite the fact that most muscles would not produce maximum power at this cycle frequency (Van Soest and Casius, 2000; Wakeling et al., 2010).

4.4.3. Muscle Excitation Timing – Limits to performance

Muscle excitation timing and burst duration were limiting factors of performance of the cyclical limb movement at high cadences. Disruptions in limb and muscle coordination occurred at consistent cadence thresholds of approximately 120-140 r.p.m. confirming that it was necessary to use an extreme range of cadences to investigate the limitations to produce effective and efficient movements. Altered muscle coordination above 120 to 140 r.p.m. was represented in the PC_{mus}'s where there was a reduced range of loading scores across power outputs (Figure 4.4). A smaller range of loading scores signifies a reduction in relative variability of the muscle coordination patterns at the highest cadences, which may represent a muscle coordination limit to produce these rapid movements. Muscle coordination was also affected by the plateau in muscle burst duration for all muscles beyond 120-140 r.p.m. (Figure 4.6), similar to previous findings for MG (Blake and Wakeling, 2014). The plateau in muscle burst duration resulted in a larger duty cycle at high cadences since muscle excitation occurred over a greater proportion of the pedal cycle (Figure 4.6). Longer muscle burst durations also limited limb movement relative efficiency as total EMG intensity increased disproportionately above 120-140 r.p.m. (Figure 4.1E) indicating a greater metabolic cost and rapidly decreasing relative mechanical efficiency (Figure 4.1D).

Evidence suggests that larger duty cycles are a limitation of the activation-deactivation dynamics of muscle resulting in increased negative muscular work and unnecessary co-contraction of antagonistic muscle pairs (Josephson, 1999; Neptune and Herzog, 1999; Neptune and Kautz, 2001; Van Soest and Casius, 2000), and this is likely to be the case for duty cycles over 50% (Figure 4.6). Activation-deactivation rates increase with increased velocities (Askew and Marsh, 1998), but the extreme cycle frequencies used in this study would push the limits of the activation-deactivation capabilities. Previously, we speculated (Blake and Wakeling, 2014) that the activation-deactivation limits may have been reached resulting in minimum excitation durations being approached at the highest cadences in these mixed fibre muscles. Reaching activation-deactivation and excitation duration limits would be particularly impactful during the transitions between extension and flexion of the hip, knee and ankle at the top and bottom of the pedal cycle. The consequence of activation-deactivation and excitation duration limits at the extension-flexion transitions is that deactivation would need to occur over a shorter portion of the pedal cycle in order to apply force long enough for the task and not induce large amounts of negative muscular work.

The muscles did not apply force at the same location of the pedal cycle as the mechanical demands changed, effectively altering their mechanical contribution to the performance of the limb movement. For example, VM and VL shifted their excitation earlier in the pedal cycle by approximately 40 degrees, most of which occurred above 120-140 r.p.m. (Figure 4.5). VM and VL are the major muscles responsible for the effective pedal forces during the down stroke (Raasch et al., 1997), yet the shift in muscle excitation timing did not result in the timing of the effective pedal force being maintained at a constant position since the effective pedal force shifted progressively later in the pedal cycle by approximately 30 degrees (Figure 4.7). The altered mechanical contribution of VM and VL may be attributed to an activation-deactivation limitation since the duty cycle for these muscles reached approximately 55% at 180 r.p.m. (Figure 4.6) such that they were active for more than half of the pedal cycle, inevitably contributing to negative muscular work. Similarly, most muscles displayed systematic phase shifts of muscle excitation relative to the pedal cycle (Figure 4.5) that were different for each muscle and were cadence and workload dependent explaining differences previously found for the timing of EMG for different muscles, cadences and workloads (Jorge and Hull, 1986; Sarre and Lepers,

2007). The differences in phase shifts across cadences and power outputs (Figure 4.5) for different muscles that share similar functions, such as ST and BF, highlights the complexity of muscle control for this movement task.

The time-frequency properties of the EMG intensity during the bursts of muscle excitation were classified by their principal components, and general patterns of the PC_{freq} weights were seen for the first three principal components across all the muscles (Figure 4.2). $PC_{freq}2$ and $PC_{freq}3$ account for the time-varying intensity spectra as each burst of muscle excitation progresses, and the vectors describing their loading scores (Figure 4.2) showed characteristic directions that changed at the cadence of maximum relative efficiency. Thus the relative efficiency of limb movement was related to the time varying frequency spectra of the EMG intensities. The frequency components of the EMG intensity spectra can be related to the type of motor units recruited (von Tscharner, 2000; Wakeling, 2009; Wakeling and Horn, 2009; Wakeling and Rozitis, 2004), although this has been controversial (Farina, 2008; von Tscharner and Nigg, 2008). The shifts in EMG frequency may result from the activation-deactivation limitations at the highest cadences, mentioned previously (Figure 4.6) and may reflect a shift in muscle fibre recruitment such that these muscles are still able to contribute to power production, while attempting to minimize negative muscular work (Figure 4.7: Sarre and Lepers, 2007).

4.5. Conclusion

This study investigated the influence of mechanical demands on muscle coordination during human limb movement, and the subsequent relationship between muscle coordination and movement performance parameters, relative mechanical efficiency and power output. Relative mechanical efficiency was maximized at increasing cadences for increasing power outputs, which corresponded to muscle coordination and altered the muscle fibre type recruitment that minimized the total muscle excitation across all muscles. In addition, mechanical power output was limited beyond a critical cycle frequency of 120-140 r.p.m., which was related to a breakdown in muscle coordination. The breakdown in muscle coordination was demonstrated by limits to minimum muscle burst duration, longer duty cycles and disproportionate increases in muscle excitation for most muscles, which suggests a limitation of the activation-deactivation capabilities of the

muscles, resulting in increasing metabolic costs and rapidly decreasing relative mechanical efficiency.

Chapter 5.

Biofeedback-Driven Muscle Coordination.

5.1. Introduction

Muscles often work in groups to produce movement. Within these groups, multiple muscles cross the same joint and can be recruited in numerous combinations and proportions making it possible to perform a range of smooth controlled limb movements. Differences in the way muscle recruitment is coordinated (muscle coordination) are reflected in outcome variables such as limb kinematics, energy consumption and mechanical power (Wakeling et al., 2010). Muscle coordination is therefore an important factor when attempting to manipulate limb movement, such as during rehabilitation and sport performance, yet it is unknown if muscle coordination can be purposefully manipulated.

Manipulation of muscle excitation using real-time sensory feedback (biofeedback) has been successfully used in areas such as post stroke rehabilitation (Moreland et al., 1998), headache disorders (Nestoriuc et al., 2008) and re-education of pelvic floor musculature (Koh et al., 2008). These manipulation methods predominantly focus on the spatiotemporal (amplitude and timing) properties of excitation in single muscles. Although individual muscles are important, it is the spatiotemporal properties of the coordination between multiple muscles that determines the limb movements and mechanics. In this regard, manipulation of a single muscle is unrealistic as other muscles and the coordination amongst muscles will also be affected. Therefore, the goal of this proof of concept methodological research was to develop a sensory feedback tool to evaluate and purposefully modify the coordination between muscles in real-time. To attain this goal we aimed to accomplish two objectives, (1) develop a system able to record, evaluate and distinguish differences in muscle coordination in real-time and (2) facilitate the purposeful manipulation of muscle coordination by providing real-time feedback based on differences in muscle coordination.

Principal component analysis (PCA) has been an increasingly utilized method for both muscle coordination (Blake and Wakeling, 2012; Blake et al., 2012; Enders et al., 2014; Wakeling and Horn, 2009; Wakeling et al., 2010) and movement analysis (Astephen et al., 2008; Dillmann et al., 2014; Dona et al., 2009; Federolf et al., 2013; Federolf et al., 2014; Muniz and Nadal, 2009; Troje, 2002; Young and Reinkensmeyer, 2014). It is predominantly employed as a data reduction tool for large multivariate data sets in order to extract the predominant features. This makes PCA particularly attractive for muscle coordination and movement analysis during repetitive, cyclical actions since it can identify the common underlying features. For example, PCA has been used to distinguish gender using muscle excitation (von Tscharner and Goepfert, 2003), distinguish gender and age through differences in gait kinematics (Troje, 2002), identify key movement patterns of successful race walking (Dona et al., 2009), diving technique (Young and Reinkensmeyer, 2014) and alpine ski racing technique (Federolf et al., 2014) as well as muscle coordination patterns for relative efficiency (Blake and Wakeling, 2012; Blake et al., 2012) and power production (Wakeling et al., 2010) during cycling. Therefore, PCA should be sufficiently sensitive to include in a biofeedback system to distinguish muscle coordination patterns used in different techniques during cyclic movements, such as walking and cycling, as well as muscle coordination patterns used to reach specific outcome goals, such as greater mechanical efficiency.

5.2. Methods

As mentioned in previous chapters, cycling on a stationary ergometer is an appropriate mode to investigate the manipulation of muscle coordination as it provides constrained limb movement and workload and crank velocity can be uncoupled during cycling (Wakeling and Horn, 2009; Wakeling et al., 2006). Thus cycling is a good model to account for the effects of workload and cadence on muscle excitation and muscle coordination. Therefore in this proof of concept study the biofeedback system was designed and constructed to evaluate muscle coordination patterns while cycling. In addition, the subjects selected had a background in cycling specific training so that they could adapt to different pedaling techniques and maintain a constant cadence and workload for the full duration of the test.

The biofeedback system was developed in LabView (National Instruments, Austin, TX) and two features of it were tested: (1) the sensitivity and ability of the system to correctly identify differences in muscle coordination in real-time and (2) the efficacy of the system for manipulating muscle coordination.

5.2.1. Electromyography

Muscle excitation was monitored continuously from 10 leg muscles (tibialis anterior (TA), medial gastrocnemius (MG), lateral gastrocnemius (LG), soleus (Sol), vastus medialis (VM), rectus femoris (RF), vastus lateralis (VL), semitendinosus (ST), biceps femoris (BF) and gluteus maximus (GM)) using surface electromyography (EMG). The skin was prepared with the removal of hair and dead skin and subsequently cleaned using isopropyl wipes. The EMG signals were monitored through bipolar electrodes (Ag/AgCl surface electrodes with 10 mm diameter and 21 mm spacing: Norotrode; Myotronics, Kent, WA) fixed to the skin. The EMG signals were amplified close to the electrode site (gain 1000), band-pass filtered (bandwidth 10-500 Hz: Biovision, Wehrheim, Germany) and recorded at 2000 Hz (16-bit analog to digital converter: USB-6210; National Instruments, Austin, TX).

5.2.2. System Sensitivity – General Overview

The sensitivity of the biofeedback system to correctly identify specific muscle coordination patterns was tested first. A subject-specific muscle coordination reference space was established using four pedaling techniques focused on different aspects of the pedal cycle: (1) *Regular* - regular cycling, (2) *Down* - pushing down on the pedal during the downstroke, (3) *Bottom* - applying force perpendicular to the crank arm at the bottom of the pedal cycle and (4) *Early* - applying force down on the pedal as early as possible during the down stroke. A reduced muscle coordination subspace was then determined that best represented the differences in muscle coordination patterns of the four different pedaling techniques. Finally, while cycling, the muscle coordination pattern for each new pedal cycle was processed and categorized into one of the four techniques based on its similarity to the reference muscle coordination space. The sensitivity was calculated as the percentage of pedal cycles correctly identified by the system.

5.2.3. System Sensitivity - Technical details

After a 10 minute warm-up, the subject cycled at a fixed, self-selected resistance and cadence, which they felt confident they could maintain continuously for a minimum of 40 minutes, for 200 pedal cycles per pedaling technique. The subject was then asked to perform the four pedaling techniques in random order.

The EMG signals for each muscle were processed cycle-by-cycle by subtracting the mean, applying a 4^{th} order Butterworth band-pass filter (11-430 Hz), squaring the signal, applying a 2^{nd} order Butterworth low-pass filter (10 Hz) then interpolating to 50 points per muscle. This process was applied to attain a smooth trace of muscle excitation for each muscle for each cycle similar to the total EMG intensities previously calculated using wavelet techniques (Blake et al., 2012; von Tscharner, 2000; Wakeling and Horn, 2009). Initially the system incorporated wavelets to replicate these previous studies, but the process described above provides similar results with substantial improvements in computational efficiency. The muscle coordination pattern for each cycle was therefore composed of the 500 points of processed EMG (50 points per muscle * 10 muscles).

PCA was used to identify the primary muscle coordination patterns as has previously been described (Blake and Wakeling, 2012; Blake et al., 2012; Wakeling and Horn, 2009). Briefly, eigenvectors and their corresponding eigenvalues were calculated from the covariance of the matrix constructed of 500 processed EMG points per cycle by 800 cycles (200 cycles per pedal technique). The eigenvectors represent principal component (PC) weightings and the corresponding eigenvalues indicate the amount of muscle coordination variability represented by that eigenvector. The product of the transpose of the matrix of eigenvectors (PC weightings) and the original matrix (500 EMG points x 800 cycles) determines the loading scores of each cycle on each PC. Therefore there was one loading score for each of the 800 cycles, for each PC, and the mean and standard error of the mean (S.E.M.) loading score per pedal technique was calculated for each of the first 10 PCs. If the mean ± S.E.M. loading score of any one pedal technique was distinct from all other technique's mean ± S.E.M. for a particular PC, the PC was selected and the group of PC's that fit this criteria collectively formed a subspace used in the subsequent analysis.

After a 10-minute break the subject cycled at the same resistance and cadence for one minute at each pedal technique in random order five times (20 minutes total) in a randomized block design such that all techniques were completed in each block. EMG signals from each muscle for each cycle were processed in the same manner as described above and added to the reference set of muscle coordination patterns. PCA was completed on this new data set (500 EMG points x 801 cycles) and a new set of eigenvectors were determined, which were subsequently transformed back onto the reference eigenvectors with the same transformation applied to the loading scores, including the current cycle. This methodology is similar to the calculation of an EMG normalcy score used to quantify muscle dysfunction in children with cerebral palsy (Wakeling et al., 2007). An example of the PCA determination and subsequent transformation is shown in Figure 5.1. The loading scores for each PC were further processed by subtracting the mean and dividing by the standard deviation of the loading scores for that PC so that each PC was weighted equally in the subsequent analysis.

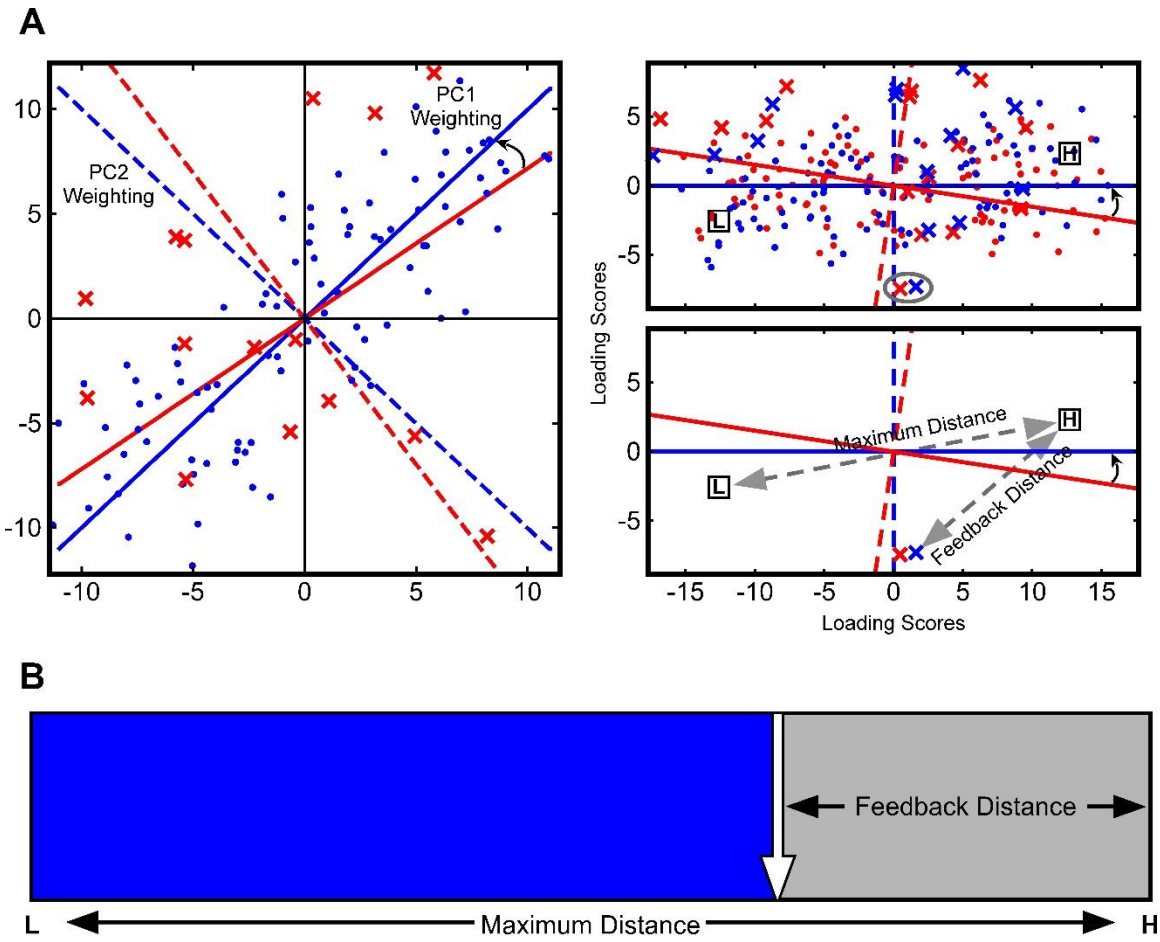

Figure 5-1. A two-dimensional example of the PCA determination, transformation and feedback.

(A) Blue data points represent the reference set with the corresponding PC weightings (top left) for PC1 (blue solid line) and PC2 (blue dashed line). When new data points are added (X) to the reference, for example a new pedal cycle, new PC weightings are determined (red lines). Each data point has a corresponding loading score for each PC (top right). When the new data points are added (red X), and new PCs determined (red lines), all data points are represented relative to the new PCs (red data). The loading scores can then be transformed into the reference space (blue lines and blue data points). The mean high (H) and low (L) relative efficiency data points are shown and the distance between these points is labeled the maximum distance (bottom right). Visualization of the *Feedback Distance* calculated for each pedal cycle can be seen in the bottom right where the distance is determined to H, after it has been transformed into the reference (blue). (B) The feedback shown to the participant is in the form of a sliding bar where the *Feedback Distance* is relative to the maximum distance. *Feedback Distance* is shown in grey as the goal is to move the slider to the right, thus decreasing the distance to H.

Each pedal cycle had a loading score for each of the PCs, and this included the current cycle. The distance of the current cycles' loading scores to the mean loading scores for each pedal technique were calculated only for the PCs retained (as described above) by taking the square root of the sum of square differences between the mean

loading score and the current cycle loading score (for example see Figure 5.1). The total distance of the current cycle to each pedal technique was subsequently calculated as the sum of the individual distances calculated for each of the retained PCs (Figure 5.1). The pedal technique with the smallest distance to the current cycle was assumed to be the actual pedal technique. The sensitivity of the system to identify the muscle coordination patterns used in each pedal technique was determined as the percentage of correctly labeled cycles across the entire trial.

5.2.4. Muscle Coordination Manipulation – General Overview

The ability of the biofeedback system to facilitate the manipulation of muscle coordination was tested in a different and separate test. As with the sensitivity testing, a subject specific muscle coordination reference space was established and a subspace was extracted using PCA. The reference subspace was based on muscle coordination patterns generating high and low relative mechanical efficiencies. During a steady-state cycling trial, the muscle coordination pattern for each new pedal cycle was processed and compared to the muscle coordination patterns eliciting high and low relative mechanical efficiencies. Visual feedback was presented to the subject cycle-by-cycle based on the muscle coordination comparison and the overall ability of the system to elicit purposeful changes in muscle coordination was evaluated over time (Figure 5.1B).

5.2.5. Muscle Coordination Manipulation - Technical details

This test was completed by four subjects where the third and fourth subjects completed a modified protocol from the first two subjects. For the test, after a 10 minute warm-up, all subjects selected a resistance and cadence to be used for the duration of the test that they felt confident they could maintain continuously for a minimum of 40 minutes. The third and fourth subjects then completed 10 minutes of continuous cycling followed by 10 minutes of rest before completing the same protocol as the first two subjects. All subjects then completed a total of 1000 pedal cycles using five different pedaling techniques in a randomized block design (100 cycles for each technique randomized into two blocks). Four of the techniques were the same as in 5.2.2. above (*Regular*, *Down*, *Bottom* and *Early*) with the fifth technique focused on *Smooth* crank rotation.

The EMG signals for each muscle were processed cycle-by-cycle in the same manner described above to attain 50 EMG points per muscle per cycle. The total amount of EMG per cycle was calculated as the sum of the 500 processed EMG points (50 per muscle). Relative mechanical efficiency was then calculated cycle-by-cycle as the ratio of mechanical power output measured at the pedals (Powerforce, Radlabor, Freiburg, Germany) to total EMG (Blake and Wakeling, 2013; Wakeling et al., 2011). The relative mechanical efficiency was calculated using the mechanical power output of only the right leg since subjects quickly learned that they could cycle predominantly with the left leg to maintain power and reduce total EMG (measured from the right leg), thereby increasing the apparent relative efficiency, during pilot testing. PCA was applied to the matrix composed of 500 EMG points per cycle for those 1000 cycles to determine the PC weightings and loading scores with one loading score for each cycle for each PC. The pedal cycles with the highest and lowest five percent relative mechanical efficiencies (50 cycles for each group) were extracted and the mean ± S.E.M. loading scores for the high and low relative efficiency groups were determined for the first 10 PCs. The PCs displaying distinct mean ± S.E.M. between the high and low relative efficiency groups were selected for use in the subsequent testing and analysis.

After a 10 minute break the subjects cycled for 10 minutes at the same cadence and resistance, and therefore power output, at each of two feedback conditions presented in random order with a minimum 5 minutes rest between. The EMG signals were again processed cycle-by-cycle as described above, added to the reference muscle coordination patterns and PCA was completed on the new data set (500 EMG points x 1001 cycles) to obtain a new set of eigenvectors and loading scores. A transformation was then applied to the new eigenvectors and loading scores to transform them back onto the reference space. The distance of the loading score for the current cycle to the mean loading score of the high relative efficiency cycles was calculated for each of the selected PCs and the sum of these distances was deemed the distance from the high relative efficiency muscle coordination patterns. The PCA, transformation and distance calculations are similar to those used to quantify muscle dysfunction in children with cerebral palsy (Wakeling et al., 2007) and a visual example using two PCs can be found in Figure 5.1. As with the sensitivity testing, the loading scores for each PC were processed by subtracting the mean and dividing by the standard deviation of the loading scores for that PC and the distance

was calculated as the square root of the sum of square difference between the mean high relative efficiency loading score and the loading score for the current cycle. *Feedback Distance* (Figure 5.1) was calculated as the sum of the distances of each PC.

Visual feedback was given to the subject based on two different sources. (1) The total distance across all selected PCs of the loading scores for the current cycle to the mean high relative efficiency loading scores (*Feedback Distance*). This *Feedback Distance* was expressed as a percentage of the distance between the mean low relative efficiency loading scores and the mean high relative efficiency loading scores (Figure 5.1). (2) Random feedback by selecting a normally distributed number between 1 and 100. The subjects were not informed that the feedback was different for the two trials and both visual feedback screens looked the same, as a sliding bar with no units (Figure 5.1). The subjects were all given the same instruction that "the system is evaluating and providing feedback on your cycling technique and that the goal of the task is to move the sliding bar to the right as much as possible".

5.2.6. Statistics

During each form of feedback the *Feedback Distance* (total distance of the loading scores for the current cycle to the mean loading scores for the high relative efficiency cycles) was calculated and used to evaluate the efficacy of the system to facilitate the purposeful manipulation of muscle coordination. In addition, the 10 minute continuous cycling completed after the warm-up by the third and fourth subjects was post processed through the biofeedback system pedal cycle-by-pedal cycle to calculate the *Feedback Distance* using the same reference space used during the feedback trials.

The ability of the system to elicit purposeful changes in muscle coordination was assessed using the Mann Kendall non-parametric test statistic to evaluate if a significant decreasing trend existed for *Feedback Distance* for each source of feedback. In addition, a one-tailed t-test was used to evaluate if there was a significant decrease in *Feedback Distance* between the first and the last minute of each trial. Statistical significance was assessed at $P < 0.05$.

It was apparent that the first two subjects were able to reach and maintain a minimum *Feedback Distance* for approximately 2-3 minutes during the biofeedback trial (Figure 5.2). Therefore, the two minute block with the lowest mean *Feedback Distance* was extracted from the biofeedback trial for the third and fourth subjects. From these two minute blocks the percentage of pedal cycles with *Feedback Distances* within 10% of the mean high relative efficiency loading scores were determined. This percentage was then compared to the percentage of pedal cycles with *Feedback Distances* within 10% of the mean high relative efficiency loading scores for the 10 minute continuous cycle completed at the beginning of the test by the third and fourth subjects.

5.3. Results

5.3.1. System Sensitivity

The biofeedback system was able to correctly identify the intended pedaling technique in approximately 83% of the cycles (correct identification during each pedaling technique was 83.67% *Regular*, 86.36% *Down*, 87.44% *Early* and 75.43% *Bottom*) and was able to process and give feedback in real-time for all cycles. The percentage of correctly identified techniques increased to 90% (89.55% *Regular*, 93.50% *Down*, 95.90% *Early* and 82.50% *Bottom*) when the first five cycles after a technique transition were removed.

5.3.2. Muscle Coordination Manipulation

All subjects showed significant decreasing trends in *Feedback Distance* across the entire trial when biofeedback of the muscle coordination was provided ($p < 0.0001$ for three subjects and $p = 0.0369$ for one subject), while three subjects showed no significant decreasing trend with random feedback with one subject did show a decreasing trend ($p = 0.0095$). In addition, there was a significant decrease in *Feedback Distance* from the first to the last minute of the trials with biofeedback for all subjects ($p < 0.0001$) and no significant decrease with random feedback (subject 1, $p = 0.6247$; subject 2, $p = 0.9635$; subject 3, $p = 0.7177$; subject 4, $p = 0.1057$).

Subjects 3 and 4 had 4.37% and 5.02%, respectively, of all pedal cycles within 10% of the mean high relative efficiency loading scores when cycling for 10 minutes continuous. During the biofeedback trial subjects 3 and 4 had 6.35% and 17.50%, respectively, of the pedal cycles during the two minute block with minimum mean *Feedback Distance* within 10% of the mean high relative efficiency loading scores.

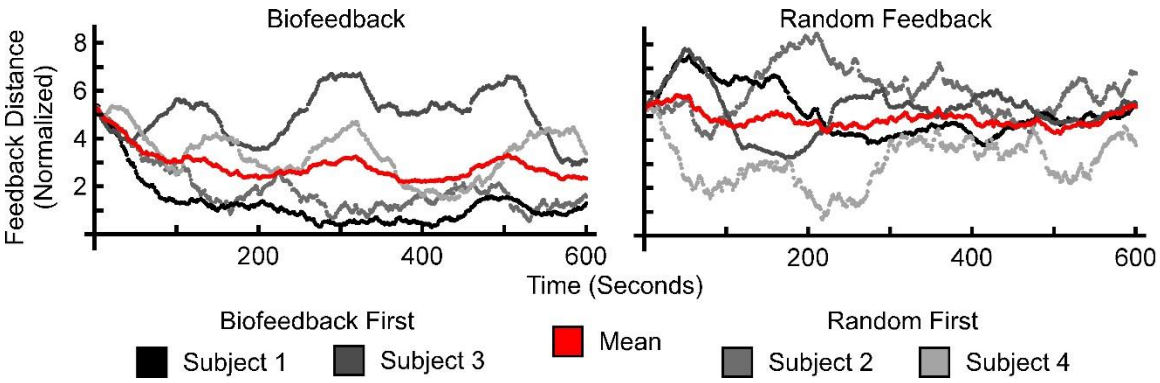

Figure 5-2. Distance of the muscle coordination for each pedal cycle to the high relative efficiency muscle coordination patterns over the duration of the trial.

A 60 second moving average showing *Feedback Distance* for each subject during the biofeedback (left) and random feedback (right) trials. Subjects 1 and 3 completed the biofeedback trial first and subjects 2 and 4 completed the random feedback trial first. Values have been normalized so that all trials start at the same point in order to highlight the trend over the duration of trials.

For all subjects the difference between the muscle coordination patterns eliciting high and low relative efficiencies were primarily reliant on excitation in TA, VM, RF and VL (Figure 5.3). The first two subjects showed increased excitation in TA with increased relative efficiency and timing shifts in VM, RF and VL to earlier in the pedal cycle to reduce excitation of these muscles in the second half of the down stroke of the pedal cycle. The third subject showed an increase in RF and decrease in VL and VM excitation with increased relative efficiency, while the fourth subject showed an increase in TA during the upstroke and a decrease in most other muscles during the downstroke with increased relative efficiency.

The pedaling technique compositions of the high and low relative efficiency reference sets for all subjects were distributed amongst all of the pedaling techniques (Figure 5.3). For example, the high relative efficiency reference set for the first subject was composed of 58.33% *Smooth*, 25.00% *Regular*, 10.42% *Bottom* and 6.25% *Early* focused,

while the high relative efficiency reference set for the second subject was composed of 35.42% *Bottom*, 31.25% *Down*, 18.75% *Early*, 12.50% *Regular* and 2.08% *Smooth* (Figure 5.3).

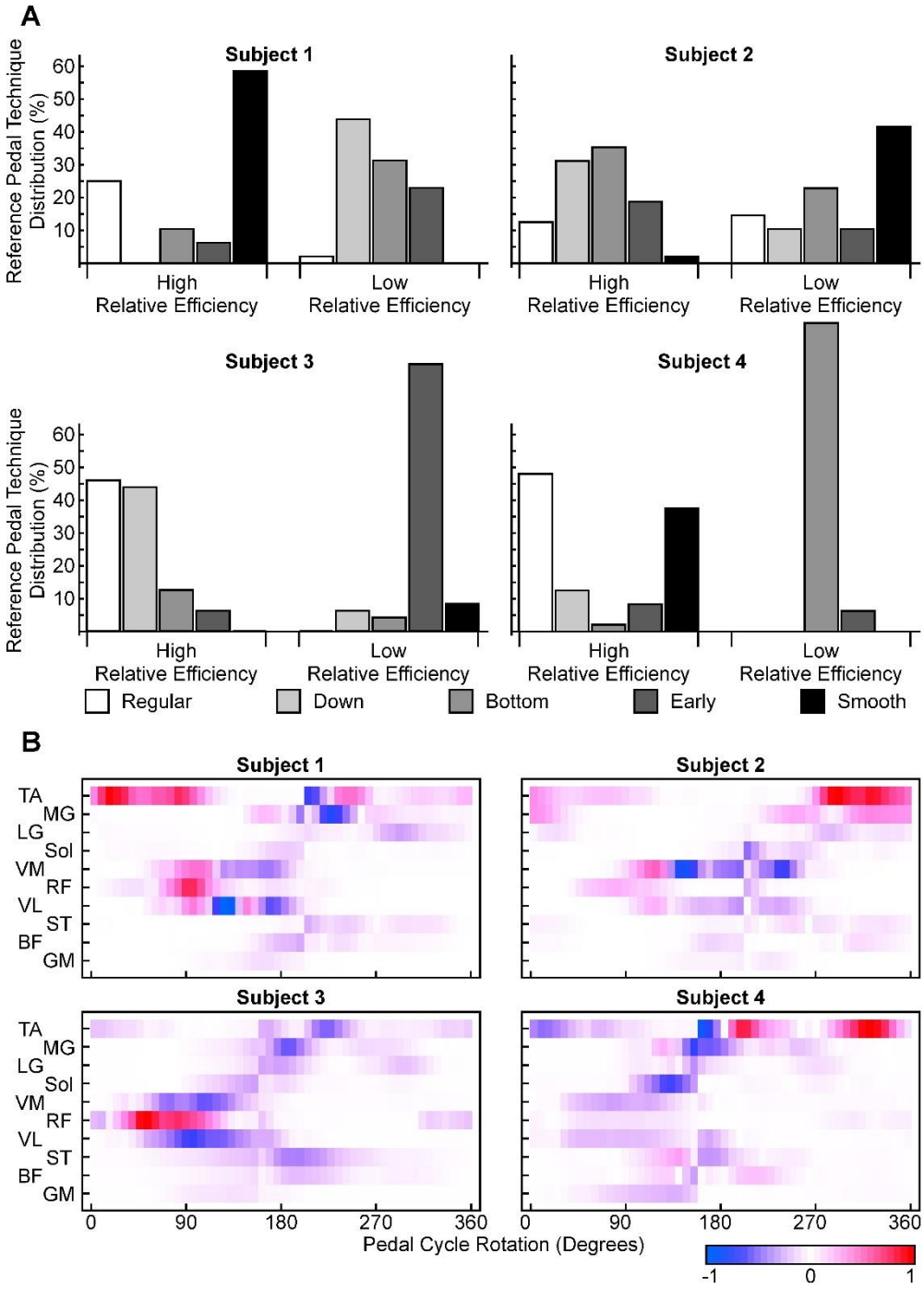
A
Subject 1
Subject 2
Subject 3
Subject 4
Reference Pedal Technique Distribution (%)
60
50
40
30
20
10
High Relative Efficiency
Low Relative Efficiency
Regular
Down
Bottom
Early
Smooth
B
TA
MG
LG
Sol
VM
RF
VL
ST
BF
GM
0
90
180
270
360
Pedal Cycle Rotation (Degrees)
-1
0
1

Figure 5-3. High and low relative efficiency pedaling technique distributions and corresponding muscle coordination patterns for each subject.

(A) Relative distribution of pedaling techniques (*Regular* - regular cycling, *Down* - pushing down on the pedal during the down stroke, *Bottom* - applying force perpendicular to the crank arm at the bottom of the pedal cycle, *Early* - applying force down on the pedal as early as possible during the down stroke and *Smooth* - smooth crank rotation for the pedal cycle) for the high and low relative efficiency references for each subject. (B) PCA reconstructions of the muscle coordination patterns for the high relative efficiency references for each subject (muscle excitation across one pedal cycle rotation for the ten muscles, tibialis anterior (TA), medial gastrocnemius (MG), lateral gastrocnemius (LG), soleus (Sol), vastus medialis (VM), rectus femoris (RF), vastus lateralis (VL), semitendinosus (ST), biceps femoris (BF) and gluteus maximus (GM)). Each muscle coordination pattern was calculated as the sum of the products of each PCs weighting (eigenvector) and the mean loading scores for the high and low relative efficiency cycles for those PCs used in the analysis (see methods), except PC1. PC1 was excluded as it was similar to the mean coordination pattern for each group of pedal cycles (high and low) and thus the other PCs highlight the muscle coordination changes relative to PC1.

5.4. Discussion

The results support the objectives of this proof of concept study showing that the biofeedback system was able to: (1) record, evaluate and distinguish differences in muscle coordination in real-time and (2) facilitate the purposeful manipulation of muscle coordination using real-time biofeedback.

5.4.1. Development Challenges

The development of a system sensitive enough to detect changes in muscle coordination in subjects with a background in cycling training presented a challenge as there is less variability in trained versus novice cyclists (Chapman et al., 2008). The sensitivity of PCA to distinguish the primary changes in muscle coordination using a reference frame constructed from a pool of cyclists, as was originally intended, was not appropriate since it only identified that the coordination was different from the reference. In other words the sensitivity of PCA was adequate to identify that the cyclist was different from the reference cyclists, but not sufficient to identify differences with respect to a specific outcome, since there is more variability in EMG between subjects than within the same subject (Dorel et al., 2008). Therefore, PCA was only a suitably sensitive tool to divide the data based on the variability and relate that variability to differences in the intended outcome, relative mechanical efficiency or pedal technique, when using a subject specific reference that better reflected the muscle coordination of the individual.

Successful implementation of the biofeedback system to meet the first objective of processing and evaluating muscle coordination in real-time was limited by computational efficiencies. The system was able to process and evaluate muscle coordination on a cycle-by-cycle basis when the EMG signals were processed without, and not with, wavelet techniques. The EMG was originally processed into intensities using wavelet techniques (Blake and Wakeling, 2012; Blake et al., 2012; Wakeling and Horn, 2009; Wakeling et al., 2006) and PCA was used to extract the primary muscle coordination patterns (Blake and Wakeling, 2012; Blake et al., 2012; Wakeling and Horn, 2009) in order to be consistent with the methodologies used in previous studies. Processing EMG using wavelets and PCA required computationally intensive transformations on 10 sets of data, sampled at 2000 Hz, at approximately 1-2 Hz when pedaling at 60-120 r.p.m.. Preliminary testing indicated this was not possible with the computer used (Windows 7, quad core processor at 3.20GHz with 8GB RAM) and more computationally efficient methods were needed. To process the EMG in a computationally efficient manner, and simulate the wavelet techniques, the EMG signals were: band-pass filtered, using the same bandwidth as the wavelets; squared, since EMG intensity is similar to the power of the signal; and low pass filtered to obtain a smooth envelope of the signal similar to an intensity trace. Provided the reference set was not too large, using the smoothed envelope to represent muscle excitation in combination with PCA proved to be an adequate solution to process the data in real-time, cycle-by-cycle. It is possible that the exact nature of EMG processing can be revisited with a faster computer processor and/or using a more computationally efficient computer coding environment.

Additional computational time constraints were encountered when using PCA with a reference frame that was too large. PCA was applied each pedal cycle to calculate new eigenvectors, eigenvalues and loading scores, which were subsequently transformed back into the reference frame (for example see Figure 5.1). PCA was therefore applied to the entire reference each pedal cycle. Preliminary testing showed that PCA computations were consistently completed in real-time using a reference frame of 1000 pedal cycles, even at cadences exceeding 120 r.p.m., while larger references frames did not and therefore 1000 cycles was selected and successfully used.

5.4.2. System Sensitivity

Several testing sessions were necessary to overcome the challenges encountered during the development stages (mentioned above). Once the system was successfully able to process the data in real-time and correctly identify more than 80% of the pedal cycles we progressed to testing the system's ability to manipulate muscle coordination. Therefore, only one subject was fully tested, and reported here, for the system sensitivity with the understanding that if the biofeedback testing was unsuccessful, the system sensitivity would be revisited.

The biofeedback system was sensitive enough to correctly identify the pedaling technique based on the muscle coordination patterns in approximately 83% of the pedal cycles. The sensitivity assumes that the correct pedaling technique was known, but in this study it was not possible to be certain the subject applied the same technique each cycle. For example, when transitioning to a new technique the system correctly identified the pedaling technique in 80% of the cycles, as determined from the first five cycles after the pedal technique was changed. The sensitivity of the system improved to 90% when these five cycles were excluded and shows that the subject needed time to transition from one technique to the next and highlights the sensitivity error when assuming the technique is known.

5.4.3. Muscle Coordination Manipulation

The results also support the second objective to facilitate the purposeful manipulation of muscle coordination using real-time biofeedback. There was a statistically significant trend towards improved muscle coordination patterning using PCA based feedback that was not present in the random feedback condition. The general trend was assessed using the Mann Kendall statistic as there was considerable cycle-to-cycle variability in muscle coordination, assessed through the loading score distances, as the subjects responded to the different forms of feedback (Figure 5.2).

In movement there is variability that adds noise to attributes such as the kinematics (Vereijken et al., 1997; Wilson et al., 2008) and muscle coordination (Chapman et al., 2008; Dorel et al., 2008), even in the most skilled subjects (Bartlett et al., 2007). Variability

is important in movement (Fetters, 2010; Preatoni et al., 2013; Van Emmerik et al., 2005), yet it can disguise underlying features that are important for successful movement patterns (Preatoni et al., 2013). It was therefore critical to find a means to extract both the sources of variability that contribute to the movement outcome and the underlying features of successful movement. The variability within the muscle coordination patterns was extracted and partitioned using PCA as this has been successfully used for muscle coordination (Blake and Wakeling, 2012; Blake et al., 2012; Enders et al., 2014; Wakeling and Horn, 2009; Wakeling et al., 2010) and movement analysis (Astephen et al., 2008; Dillmann et al., 2014; Dona et al., 2009; Federolf et al., 2013; Federolf et al., 2014; Muniz and Nadal, 2009; Troje, 2002; Young and Reinkensmeyer, 2014). The variability of the muscle coordination patterns that contribute to overall relative mechanical efficiency of limb movement were also successfully identified using PCA. Using the variability of muscle coordination that contributed to relative mechanical efficiency, the manipulation of muscle coordination towards the coordination identified as eliciting higher relative efficiencies occurred (Figure 5.2), thus showing that PCA was a good tool for this objective.

The subjects were not given any information regarding the specific performance or features of muscle coordination variability that contributed to the higher relative mechanical efficiency reference set, or their cycle-by-cycle muscle coordination, as the feedback source was blinded and the biofeedback was a general singular value. Specific performance feedback of the muscle coordination would likely be inadequately conveyed cycle-by-cycle given the high cycle frequencies used during the trials (~1.5 Hz). Without specific muscle coordination information the biofeedback system still showed a systematic and purposeful change in muscle coordination (Figure 5.2). Therefore it is reasonable to suggest that muscle coordination can be purposefully altered using biofeedback from EMG without explicit instruction about the individual muscle excitation or the muscle coordination. The use of a singular value for the biofeedback was therefore justified, since it produced significant changes in muscle coordination, and suggests that using the biofeedback system as a training tool to purposefully elicit changes in muscle coordination is a reasonable prospect and direction for future studies.

It is unclear how much time is needed to elicit changes in muscle coordination using biofeedback from EMG. The rate of change of the muscle coordination appears to

have started to plateau at approximately 180 seconds for the first two subjects (approximately 279 and 240 pedal cycles for subject 1 and subject 2, respectively, given the average cadences of 93 and 80 r.p.m.), while the third and fourth subjects needed more than 400 seconds (Figure 5.2). It is unknown if the changes in muscle coordination would appear earlier in subsequent trials from a learning effect, but this would be a desirable outcome such that the biofeedback system could elicit changes in muscle coordination more rapidly over repeated trials. Reductions in the time taken to see changes in muscle coordination is therefore another area of interest for future experiments.

One potential limitation of the biofeedback system would be if the reference set was composed entirely or predominantly of one pedaling technique, especially if it was regular cycling. The biofeedback system would then be manipulating the subject towards that one pedaling technique, which could be accomplished without the use of the biofeedback system. In this study the first two subjects did not have a reference dominated by regular cycling thus implying that the muscle coordination used during regular cycling was not the most efficient technique. Both subjects' reference sets were composed of a mixture of pedaling techniques (Figure 5.3) such that the biofeedback system was manipulating the subjects towards the common features of these techniques that relate to increased relative mechanical efficiency. We therefore conducted tests on two more subjects (subjects 3 and 4) to compare the proportion of pedal cycles that were close to the desired muscle coordination during regular cycling to the proportion achieved during the biofeedback trial. Both subjects showed in increase in the proportion of cycles near the desired muscle coordination thus showing that cycling with the biofeedback system was more effective at changing muscle coordination towards the desired coordination pattern than simply cycling regularly. In addition, the mixed nature of the reference sets provides support for the use of different pedaling techniques to create the reference as they provided the necessary variability in muscle coordination related to relative mechanical efficiency that would not be found using just regular cycling.

Trial order presents a limitation to the interpretation of the results. The second and third subjects completed the random feedback trial first and showed no consistent change in *Feedback Distance*, and therefore no consistent change in muscle coordination. In

contrast the first and fourth subjects completed the random feedback trial second and displayed some carryover learning effects from the biofeedback trial. At the beginning of the random feedback trial the *Feedback Distances* were similar to the distances observed at the end of the biofeedback trial. Also, during the first portion of the random feedback trials both subjects verbally expressed that they tried to change their cycling technique, did not get the response anticipated and subsequently altered their cycling towards the successful cycling reached during the biofeedback trial. The alteration in cycling technique can be visualized in the *Feedback Distance* over time where there was a systematic decrease after approximately 250 and 75 seconds for subjects 1 and 4, respectively (Figure 5.2).

5.5. Conclusion

This proof of concept methodological study delivers the tools and methodology for a biofeedback system able to purposefully manipulating muscle coordination in real-time during movement. The purposeful manipulation of muscle coordination is in contrast to previous methodologies that have focused on the manipulation of single muscle and thus offers an alternative to help ensure the changes in muscle excitation are appropriate to reach the desired movement outcome. Therefore this study provides a valuable tool for future studies to investigate the motor learning and retention capabilities of biofeedback manipulation with applications in areas focused on the manipulation of muscle excitation.

Chapter 6. Discussion

This research delivers a tool and methodology capable of purposefully manipulating muscle coordination in real-time during movement. Previous research and methodologies have focused on the manipulation of excitation in a single muscle (Koh et al., 2008; Moreland et al., 1998; Nestoriuc et al., 2008) with no regard for the consequence that changing one muscle will have an effect on other muscles involved in the movement. In this regard, the manipulation of muscle coordination, amongst a group of muscles participating in a movement, provides an alternative method to help ensure the changes are appropriate to reach the desired movement outcome. Therefore this research provides a valuable tool and methodology with future applications in areas focused on the manipulation of muscle excitation to reach a desired outcome such as rehabilitation and sport performance.

To attain the goal of purposefully changing muscle coordination it was necessary to complete several intermediary stages that link the current muscle coordination to the desired muscle coordination. Therefore, to purposefully change muscle coordination it was important to determine the desired movement outcome, the current and desired end state of the muscle coordination and the factors that influence the relationship between the desired movement outcome and muscle coordination. In addition to the successful development of the biofeedback system, there are a few major findings from this research.

(1) In chapter 2 we showed that muscle excitation of a large number of muscles provides a good estimate of changes in metabolic power during dynamic activities (Blake and Wakeling, 2013). Muscle excitation thus provides a method to monitor the impact of different muscle coordination strategies on metabolic power, and therefore the relative mechanical efficiency, making it a suitable movement outcome for the biofeedback system.

(2) In chapters 3 and 4 we found that muscle and muscle fibre recruitment respond to changes in the mechanical demands of the movement (Blake and Wakeling, 2014; Blake and Wakeling, 2015) resulting in altered muscle coordination. The changes in muscle coordination that minimize muscle excitation during movement occurred at similar

increasing cycle frequencies (cadences) for increasing power outputs that maximize relative mechanical efficiencies (Blake and Wakeling, 2015). Thus the manipulation of muscle coordination facilitated by the biofeedback system will be influenced by the imposed mechanical demands and make the biofeedback manipulation more physiologically meaningful, and yet more difficult to attain, when the mechanical demands are constant at values typically used by cyclists.

(3) In chapters 3 and 4 we showed that muscle coordination deteriorates when a critical cadence is exceeded, resulting in increasing metabolic costs and decreasing relative mechanical efficiency, as demonstrated by limits to minimum muscle burst duration, longer duty cycles, disproportionate increases in muscle excitation and altered slow muscle fibre contributions (Blake and Wakeling, 2014; Blake and Wakeling, 2015). Purposeful changes in muscle coordination may therefore be most difficult above a critical cadence as there may be less control of muscle coordination.

(4) In chapter 3 we found evidence that one strategy used to meet the extreme demands imposed by high cycle frequencies was preferential recruitment of fast muscle fibres. The preferential recruitment of fast muscle fibres was manifested through early derecruitment of slow muscle fibres at the end of muscle excitation, as determined from a reduction of low-frequency content of the EMG signal at the highest cycle frequencies (Blake and Wakeling, 2014). This study provides further evidence of modifications of muscle fibre recruitment strategies to meet the mechanical demands of movement and indicates that purposefully changing muscle coordination may be most difficult at extremely high cycle frequencies.

6.1. Establishing a Biofeedback Outcome

Mechanical efficiency, the ability to utilize metabolic power to produce mechanical power, is a desirable outcome of many movement tasks, yet an instantaneous determination of efficiency during dynamic movements is not yet possible. Mechanical power output can be monitored continuously during a cycling task with the development of instrumented pedals and crank systems, whereas the temporal resolution of metabolic power is limited to the respiration rate when using gas exchange measures. Without a

higher temporal resolution measurement of metabolic power it is not possible to determine what changes in muscle coordination result in increased efficiencies since pedal and gait cycles can occur at much higher frequencies than the respiration rate during these dynamic tasks.

Metabolic rates have been shown to increase as much as 21 times above resting levels in trained cyclists (Astrand and Rodahl, 1986), which can primarily be attributed to the demands of the active muscles since the energy utilized by the working muscles reflects the changes in pulmonary oxygen uptake (Poole et al., 1992). Therefore, information about changes in metabolic power must be contained in the EMG signal, since EMG can monitor muscle excitation of the active muscles and can change considerably during such dynamic movement tasks. Establishing a scientifically meaningful relationship between metabolic power and EMG was therefore one of the primary aims of this research such that EMG could be used as a proxy for metabolic power in the calculation of relative mechanical efficiency. Estimating changes in metabolic power and relative mechanical efficiency using EMG is desirable as it provides a means to evaluate the metabolic impact of different muscle coordination strategies, which is especially valuable for a biofeedback system that aims to purposefully manipulate muscle coordination in real-time based on relative mechanical efficiency.

The results from chapter 2 present evidence that muscle excitation monitored using EMG does indeed provide good estimates of changes in metabolic power during dynamic activities, at a higher temporal resolution than has previously been established (Wakeling et al., 2011), while also including non-steady-state conditions. Muscle excitation monitored through EMG, therefore, provides a good alternative to gas exchange measures, at a higher temporal resolution, to evaluate changes in metabolic power (Blake and Wakeling, 2013). The determination of an instantaneous measure of metabolic power remains elusive, but the results suggest that cycle-by-cycle EMG intensity with a time resolution of approximately 0.70 seconds would offer a reasonable estimate of the $\dot{V}O_2$ kinetics and therefore the metabolic power. Estimating changes in metabolic power using muscle excitation is not only important for the biofeedback system, but is also a valuable tool for studies employing EMG during movement.

6.2. Establishing a Biofeedback Reference Frame

To manipulate muscle coordination it was essential to know both the current and desired end states of muscle coordination as well as the factors that influence the changes in muscle coordination. Evidence from chapter 4 showed that the primary factors that affected muscle coordination were the imposed mechanical demands and those demands in turn affected desired movement outcomes such as relative mechanical efficiency and power output (Blake and Wakeling, 2015). In this regard, the research findings in chapters 3 and 4 provide valuable insights into the muscle coordination responses, in particular the muscle excitation and muscle fibre recruitment, to changing mechanical demands and the subsequent impact on relative mechanical efficiency and power output.

It might be hypothesized that muscle coordination patterns that maximize relative efficiency would share a common underlying pattern and be scaled based on the mechanical demands of the movement, yet chapter 4 provides evidence that the muscle coordination that maximizes relative efficiency differs with the mechanical demands (Blake and Wakeling, 2015). The differences in muscle coordination occurred because muscle excitation responses to alterations in mechanical demands differed for each muscle, as has also been shown for the muscle excitation responses to force or workload (Ericson, 1986; Hug and Dorel, 2009; Hug et al., 2004b; Lawrence and De Luca, 1983), and were dependent on an interactive effect of workload and cadence (MacIntosh et al., 2000). Therefore the relative amount of muscle excitation, amongst the active muscles, differed with the mechanical demands of the task. Also, the mechanical contribution of each muscle to the limb movement was effectively altered since the muscles did not apply force at the same location in the pedal cycle as the mechanical demands changed (Samozino et al., 2007). Therefore the results suggest that a simple way to change muscle coordination and shift the emphasis towards different muscles is to change the mechanical demands, but this strategy neglects a desirable outcome of increasing movement efficiency when the mechanical demands remain constant. Thus a more complex problem arises when attempting to manipulate muscle coordination to attain increased relative efficiencies when the mechanical demands remain fixed.

Despite alterations in muscle coordination as the mechanical demands changed, some commonalities were discerned in chapter 4 when exploring the muscle coordination patterns for increased relative mechanical efficiencies. Maximum relative efficiency occurred at increasing cadences for increasing power outputs (Böning et al., 1984; Coast and Welch, 1985; Foss and Hallén, 2004; Hagberg et al., 1981; Seabury et al., 1977) and these cadence-power combinations corresponded with minimum EMG intensity (Blake and Wakeling, 2015). Also, where maximum relative efficiency occurred there existed some consistencies in muscle coordination such as progressive muscle excitation through the uniarticulate knee, hip and ankle muscles during the down stroke (Blake and Wakeling, 2015; Blake et al., 2012) and changes in the timing and recruitment of different muscle fibre types in VM, VL and Sol (Blake and Wakeling, 2015). In contrast, reduced relative efficiency and elevated muscle excitation were dominated by excitation of bi-articulate muscles and TA and GM and larger duty cycles for many muscles. The cadence-power combinations where maximum relative efficiency occurred also corresponded with minimum ineffective pedal forces thus showing that relative efficiencies could be identified in the mechanical output of the movement. Finally, evidence from both the muscle coordination and the resulting pedal forces indicates that the top and bottom of the pedal cycle are critical to efficiently completing the cycling action (Blake et al., 2012; Leirdal and Ettema, 2011), despite the effective force being low at these times (Figure 4.7; Patterson et al., 1983; Sanderson, 1991).

Based on the common features of muscle coordination found in chapter 4 at high relative efficiencies, it was assumed that the successful application of the biofeedback system to facilitate the manipulation of muscle coordination towards greater relative efficiency would result in more cycles with progressive excitation through the uniarticulate knee, hip and ankle muscles during the down stroke as well as changes to the muscles acting at the top and bottom of the pedal cycle (Blake and Wakeling, 2015). In fact, the common features of muscle coordination, with respect to high relative efficiencies and established in chapter 5, used by the biofeedback system were focused on increased TA excitation and earlier VM, RF and VL excitation relative to the pedal cycle (Figure 5.3). The discrepancy of the common features of muscle coordination between chapters 4 and 5 highlights the difference between changing muscle coordination by changing the

mechanical demands and changing muscle coordination at constant mechanical demands, as was accomplished by the biofeedback system.

The muscle coordination patterns found in chapter 4 and muscle fibre recruitment found in chapter 3 at the highest cadences were not consistent with those found at lower and moderate cadences such that relative mechanical efficiency and power output were limited beyond a critical cadence of 120-140 r.p.m. The limitations of muscle coordination at these high cadences were underscored by a reduction in the variability of muscle coordination, plateauing muscle burst durations (Figure 4.6 & Figure 3.4), longer duty cycles (Figure 4.6 & Figure 3.4), disproportionate increases in EMG intensity for most muscles (Figure 4.2) and shifts in the frequency content of the EMG (Figure 4.2, Figure 3.1, Figure 3.3 & Figure 3.5). The reduction in variability of the muscle coordination patterns at the highest cadences indicates that fewer muscle coordination patterns were being utilized. The other limitations on muscle coordination relate directly to the muscle excitation and therefore represent a constraint of the activation-deactivation dynamics of muscle resulting in increased negative muscle work, unnecessary co-contraction of antagonistic muscle pairs (Josephson, 1999; Neptune and Herzog, 1999; Neptune and Kautz, 2001; Van Soest and Casius, 2000), increasing metabolic costs and rapidly decreasing relative mechanical efficiency (Figure 4.1D).

To compensate for the limitations on muscle coordination at such extreme high cadences, the findings in chapters 3 and 4 revealed a shift in the frequency content of the EMG signal from low to high (Figure 4.2 & Figure 3.1), similar to Wakeling and co-workers (2006), a shift in timing of the frequencies (Figures 3.1A, 3.3) as well as additional low frequency components at the highest cadence (Figures 3.3, 3.5). The results, therefore, indicate that the limitations of muscle coordination were at least partially overcome by the preferential recruitment of faster muscle fibres (Citterio and Agostoni, 1984; Gillespie et al., 1974; Gollnick et al., 1974; Grimby and Hannerz, 1977; Hodson-Tole and Wakeling, 2008a; Hoffer et al., 1981; Lee et al., 2013; Wakeling et al., 2006), which was identified as occurring through early derecruitment of the slowest muscle fibres, and greater muscle excitation, including slow muscle fibres, to achieve the highest cadence (Holt et al., 2014). With limited muscle coordination patterns being utilized and constraints on the activation-deactivation dynamics of the muscles, the possibilities to modify muscle and muscle fibre

recruitment for high frequency muscle contractions may be diminished. Therefore successful manipulation of muscle coordination for maximum efficiency at high cycle frequencies may be unrealistic. A similar argument could be made for muscle coordination being optimized for maximum power output where there are likely limited muscle coordination patterns available to accomplish the task.

6.3. Biofeedback Tool

The biofeedback system presented in chapter 5 represents the successful culmination of the research outlined in the preceding chapters and delivers proof of concept of a tool that facilitates the purposeful manipulation of muscle coordination in real-time during movement. Utilizing the findings from chapter 2, the biofeedback system employs EMG as a proxy for metabolic power in the calculation of relative mechanical efficiency, which allows the system to direct muscle coordination changes towards this physiologically relevant movement outcome. The findings from chapter 4 showed that relative efficiency is maximized at increasing cadences for increasing power outputs (Böning et al., 1984; Coast and Welch, 1985; Foss and Hallén, 2004; Hagberg et al., 1981; Seabury et al., 1977) and these cadence-power output combinations correspond to minimum muscle excitation. Thus muscle coordination can be manipulated to increase relative mechanical efficiency simply by inducing changes to the mechanical demands when the cadence-workload combination is not optimal. Muscle coordination cannot be manipulated to increase relative mechanical efficiency in this way when the cadence-workload is optimal, which is why a constant mechanical demand was the initial application used and tested by the biofeedback system. Finally, the results from chapters 3 and 4 reveal a critical cadence beyond which the biofeedback system may be ineffective due to muscle excitation and muscle coordination limitations that restrict the number of possible muscle coordination strategies.

The biofeedback system successfully employed PCA to extract the features of muscle coordination related to relative mechanical efficiencies and, based on these features, provide feedback to elicit changes in muscle coordination in real-time. Successful implementation by the biofeedback system of PCA is not entirely surprising given the growing use of PCA in different aspects of muscle and movement analysis

(Astephen et al., 2008; Blake and Wakeling, 2012; Blake et al., 2012; Dillmann et al., 2014; Dona et al., 2009; Enders et al., 2014; Federolf et al., 2013; Federolf et al., 2014; Muniz and Nadal, 2009; Troje, 2002; Wakeling and Horn, 2009; Wakeling et al., 2010; Young and Reinkensmeyer, 2014). Interestingly, the biofeedback system was able to use PCA to elicit these changes without supplying specific, detailed information about the important muscle coordination features to the subject. Therefore the biofeedback system was able to facilitate the manipulation of muscle coordination without the subject having explicit knowledge of the muscle coordination. The success of the biofeedback system without this explicit knowledge adds to the practicality of the system for use during the cycling movement since detailed feedback would be difficult to adequately process and interpreted by the subject in real-time at regular cycle frequencies (~1.5 Hz at cadences typical of professional endurance cyclists. (Foss and Hallén, 2004; Lucia et al., 2001; Sargeant, 1994)).

From a practical standpoint, with respect to cycling, there are limitations to the efficacy of the biofeedback system as stipulated. For example, changes in muscle coordination appear to occur over long periods of focused training, for example a cyclist over years of cycle training, as demonstrated by the different muscle coordination patterns between novice and elite cyclists (Chapman et al., 2009). Unfortunately, the changes in muscle coordination do not necessarily translate to differences in efficiency, measured through gas exchange, as there are no significant differences in efficiency between novice and elite cyclists (Moseley et al., 2004). With no translation between differences in muscle coordination and differences in efficiency, it is questionable whether efficiency is a defining factor that differentiates novice from elite cyclists and, therefore, whether efficiency is useful as an outcome measure for the biofeedback system. We have found evidence that muscle coordination is an important factor that affects relative mechanical efficiency, as estimated by the ratio of mechanical power to EMG intensity (Blake and Wakeling, 2012; Blake and Wakeling, 2015; Blake et al., 2012), and muscle coordination is less variable in trained versus novice cyclists (Chapman et al., 2008). With less variability in muscle coordination, the differences in relative efficiency may be attributed to an improved ability to maintain muscle coordination patterns that produce less total muscle excitation and thereby allow for prolonged cycling bouts at higher power outputs. Therefore alterations in muscle coordination that increase relative mechanical efficiency, estimated through

muscle excitation, and translate into physiologically relevant changes in cycling performance is an open question for future research.

Regardless of the chosen outcome variable used to direct the alterations in muscle coordination, the primary goal of this research was to develop and show proof of concept of a biofeedback tool that could evaluate and manipulate muscle coordination and this has been accomplished. Whatever the chosen outcome, accelerating the rate of change of muscle coordination is a desirable feature of the biofeedback system making it a valuable tool for future research and training applications. Future research applications will therefore delve into motor learning and retention aspects of the biofeedback system for changing muscle coordination with a goal of determining if the biofeedback system can elicit faster changes in muscle coordination that result in greater improvements in the chosen outcome with a lasting benefit.

In summary, this research delivers a tool and methodology capable of purposefully manipulating muscle coordination in real-time during movement. In particular, this research provides a valuable tool and methodology for future studies to investigate motor learning and retention capabilities of biofeedback manipulation with future applications in areas focused on the manipulation of muscle excitation to reach a desired movement outcome such as rehabilitation and sport performance.

References

Ahlquist, L. E., Bassett Jr, D. R., Sufit, R., Nagle, F. J. and Thomas, D. P. (1992). The effect of pedaling frequency on glycogen depletion rates in type I and type II quadriceps muscle fibers during submaximal cycling exercise. *Eur. J. Appl. Physiol.* **65**, 360–364.

Arnaud, S., Zattara-Hartmann, M. C., Tomei, C. and Jammes, Y. (1997). Correlation between muscle metabolism and changes in M-wave and surface electromyogram: dynamic constant load leg exercise in untrained subjects. *Muscle Nerve* **20**, 1197–1199.

Askew, G. N. and Marsh, R. L. (1998). Optimal shortening velocity (V/Vmax) of skeletal muscle during cyclical contractions: length-force effects and velocity-dependent activation and deactivation. *J. Exp. Biol.* **201**, 1527–1540.

Astephen, J. L., Deluzio, K. J., Caldwell, G. E., Dunbar, M. J. and Hubley-Kozey, C. L. (2008). Gait and neuromuscular pattern changes are associated with differences in knee osteoarthritis severity levels. *J. Biomech.* **41**, 868–876.

Astrand, P. O. and Rodahl, K. (1986). *Textbook of Work Physiology: Physiological Bases of Exercise*. 3rd edition. New York: McGraw-Hill, Inc.

Bartlett, R., Wheat, J. and Robins, M. (2007). Is movement variability important for sports biomechanists? *Sports Biomech.* **6**, 224–243.

Baum, B. S. and Li, L. (2003). Lower extremity muscle activities during cycling are influenced by load and frequency. *J. Electromyogr. Kinesiol.* **13**, 181–191.

Beelen, A. and Sargeant, A. J. (1991). Effect of fatigue on maximal power output at different contraction velocities in humans. *J. Appl. Physiol.* **71**, 2332–2337.

Bigland-Ritchie, B. and Woods, J. J. (1976). Integrated electromyogram and oxygen uptake during positive and negative work. *J. Physiol.* **260**, 267–277.

Blake, O. M. and Wakeling, J. M. (2012). Muscle coordination during an outdoor cycling time trial. *Med. Sci. Sports Exerc.* **44**, 939–948.

Blake, O. M. and Wakeling, J. M. (2013). Estimating changes in metabolic power from EMG. *SpringerPlus* **2**, 1–7.

Blake, O. M. and Wakeling, J. M. (2014). Early deactivation of slower muscle fibres at high movement frequencies. *J. Exp. Biol.* **217**, 3528–3534.

Blake, O. M. and Wakeling, J. M. (2015). Muscle Coordination Limits Efficiency and Power Output of Human Limb Movement under a Wide Range of Mechanical Demands. *J. Neurophysiol.* jn.00765.2015.

Blake, O. M., Champoux, Y. and Wakeling, J. M. (2012). Muscle Coordination Patterns for Efficient Cycling. *Med. Sci. Sports Exerc.* **44**, 926–938.

Böning, D., Gönen, Y. and Maassen, N. (1984). Relationship between work load, pedal frequency, and physical fitness. *Int. J. Sports Med.* **5**, 92–97.

Buchthal, F., Dahl, K. and Rosenfalck, P. (1973). Rise time of the spike potential in fast and slowly contracting muscle of man. *Acta Physiol. Scand.* **87**, 261–269.

Burden, A. (2010). How should we normalize electromyograms obtained from healthy participants? What we have learned from over 25years of research. *J. Electromyogr. Kinesiol.* **20**, 1023–1035.

Burke, R. E., Levine, D. N., Tsairis, P. and Zajac, F. E. (1973). Physiological types and histochemical profiles in motor units of the cat gastrocnemius. *J. Physiol.* **234**, 723–748.

Caiozzo, V. J. and Baldwin, K. M. (1997). Determinants of work produced by skeletal muscle: potential limitations of activation and relaxation. *Am. J. Physiol. - Cell Physiol.* **273**, C1049–C1056.

Chapman, A. R., Vicenzino, B., Blanch, P. and Hodges, P. W. (2008). Patterns of leg muscle recruitment vary between novice and highly trained cyclists. *J. Electromyogr. Kinesiol.* **18**, 359–371.

Chapman, A. R., Vicenzino, B., Blanch, P. and Hodges, P. W. (2009). Do differences in muscle recruitment between novice and elite cyclists reflect different movement patterns or less skilled muscle recruitment? *J. Sci. Med. Sport* **12**, 31–34.

Chavarren, J. and Calbet, J. A. L. (1999). Cycling efficiency and pedalling frequency in road cyclists. *Eur. J. Appl. Physiol.* **80**, 555–563.

Citterio, G. and Agostoni, E. (1984). Selective activation of quadriceps muscle fibers according to bicycling rate. *J. Appl. Physiol.* **57**, 371–379.

Close, R. I. and Luff, A. R. (1974). Dynamic properties of inferior rectus muscle of the rat. *J. Physiol.* **236**, 259–270.

Coast, J. R. and Welch, H. G. (1985). Linear increase in optimal pedal rate with increased power output in cycle ergometry. *Eur. J. Appl. Physiol.* **53**, 339–342.

Dillmann, U., Holzhoffer, C., Johann, Y., Bechtel, S., Gräber, S., Massing, C., Spiegel, J., Behnke, S., Bürmann, J. and Louis, A. K. (2014). Principal Component Analysis of gait in Parkinson's disease: Relevance of gait velocity. *Gait Posture* **39**, 882–887.

Di Prampero, P. E. (2000). Cycling on Earth, in space, on the Moon. *Eur. J. Appl. Physiol.* **82**, 345–360.

Dona, G., Preatoni, E., Cobelli, C., Rodano, R. and Harrison, A. J. (2009). Application of functional principal component analysis in race walking: an emerging methodology. *Sports Biomech.* **8**, 284–301.

Dorel, S., Couturier, A. and Hug, F. (2008). Intra-session repeatability of lower limb muscles activation pattern during pedaling. *J. Electromyogr. Kinesiol.* **18**, 857–865.

Dorel, S., Couturier, A., Lacour, J. R., Vandewalle, H., Hautier, C. and Hug, F. (2010). Force-velocity relationship in cycling revisited: benefit of two-dimensional pedal forces analysis. *Med. Sci. Sports Exerc.* **42**, 1174–1183.

Dorel, S., Guilhem, G., Couturier, A. and Hug, F. (2012). Adjustment of muscle coordination during an all-out sprint cycling task. *Med. Sci. Sports Exerc.* **44**, 2154–2164.

Edwards, R. G. and Lippold, O. C. J. (1956). The relation between force and integrated electrical activity in fatigued muscle. *J. Physiol.* **132**, 677.

Elert, J. E., Rantapää-Dahlqvist, S. B., Henriksson-Larsen, K., Lorentzon, R. and Gerdle, B. U. C. (1992). Muscle performance, electromyography and fibre type composition in fibromyalgia and work-related myalgia. *Scand. J. Rheumatol.* **21**, 28–34.

Enders, H., von Tscharner, V. and Nigg, B. M. (2014). Neuromuscular Strategies during Cycling at Different Muscular Demands. *Med. Sci. Sports Exerc.* **47**, 1450–1459.

Ericson, M. O. (1986). On the biomechanics of cycling. A study of joint and muscle load during exercise on the bicycle ergometer. *Scand. J. Rehabil. Med. Suppl.* **16**, 1–43.

Ericson, M. O., Nisell, R., Arborelius, U. P. and Ekholm, J. (1985). Muscular activity during ergometer cycling. *Scand. J. Rehabil. Med.* **17**, 53–61.

Ettema, G. and Loras, H. W. (2009). Efficiency in cycling: a review. *Eur. J. Appl. Physiol.* **106**, 1–14.

Farina, D. (2008). Counterpoint: spectral properties of the surface EMG do not provide information about motor unit recruitment and muscle fiber type. *J. Appl. Physiol.* **105**, 1673–1674.

Farina, D., Macaluso, A., Ferguson, R. A. and De Vito, G. (2004). Effect of power, pedal rate, and force on average muscle fiber conduction velocity during cycling. *J. Appl. Physiol.* **97**, 2035–2041.

Federolf, P. A., Boyer, K. A. and Andriacchi, T. P. (2013). Application of principal component analysis in clinical gait research: identification of systematic differences between healthy and medial knee-osteoarthritic gait. *J. Biomech.* **46**, 2173–2178.

Federolf, P., Reid, R., Gilgien, M., Haugen, P. and Smith, G. (2014). The application of principal component analysis to quantify technique in sports. *Scand. J. Med. Sci. Sports* **24**, 491–499.

Fetters, L. (2010). Perspective on variability in the development of human action. *Phys. Ther.* **90**, 1860–1867.

Foss, Ø. and Hallén, J. (2004). The most economical cadence increases with increasing workload. *Eur. J. Appl. Physiol.* **92**, 443–451.

Foss, M. L., Keteyian, S. J. and Fox, E. L. (1998). *Fox's physiological basis for exercise and sport*. 6th edition. McGraw-Hill, Dubuque (IA).

Friedman, W. A., Sypert, G. W., Munson, J. B. and Fleshman, J. W. (1981). Recurrent inhibition in type-identified motoneurons. *J. Neurophysiol.* **46**, 1349–1359.

Gerdle, B., Wretling, M. L. and Henriksson-Larsén, K. (1988). Do the fibre-type proportion and the angular velocity influence the mean power frequency of the electromyogram? *Acta Physiol. Scand.* **134**, 341–346.

Gillespie, C. A., Simpson, D. R. and Edgerton, V. R. (1974). Motor unit recruitment as reflected by muscle fibre glycogen loss in a prosimian (bushbaby) after running and jumping. *J. Neurol. Neurosurg. Psychiatry* **37**, 817–824.

Gollnick, P. D., Piehl, K. and Saltin, B. (1974). Selective glycogen depletion pattern in human muscle fibres after exercise of varying intensity and at varying pedalling rates. *J. Physiol.* **241**, 45–57.

Grimby, L. and Hannerz, J. (1977). Firing rate and recruitment order of toe extensor motor units in different modes of voluntary conraction. *J. Physiol.* **264**, 865–879.

Hagberg, J. M., Mullin, J. P., Giese, M. D. and Spitznagel, E. (1981). Effect of pedaling rate on submaximal exercise responses of competitive cyclists. *J. Appl. Physiol.* **51**, 447–451.

Hansen, E. A. and Sjogaard, G. (2007). Relationship between efficiency and pedal rate in cycling: significance of internal power and muscle fiber type composition. *Scand. J. Med. Sci. Sports* **17**, 408.

Hautier, C. A., Linossier, M. T., Belli, A., Lacour, J. R. and Arsac, L. M. (1996). Optimal velocity for maximal power production in non-isokinetic cycling is related to muscle fibre type composition. *Eur. J. Appl. Physiol.* **74**, 114–118.

Henneman, E., Somjen, G. and Carpenter, D. O. (1965a). Functional significance of cell size in spinal motoneurons. *J. Neurophysiol.* **28**, 560–580.

Henneman, E., Somjen, G. and Carpenter, D. O. (1965b). Excitability and inhibitability of motoneurons of different sizes. *J. Neurophysiol.* **28**, 599–620.

Hill, A. V. (1938). The heat of shortening and the dynamic constants of muscle. *Proc. R. Soc. Lond. B Biol. Sci.* **126**, 136–195.

Hodson-Tole, E. F. and Wakeling, J. M. (2008a). Motor unit recruitment patterns 1: responses to changes in locomotor velocity and incline. *J. Exp. Biol.* **211**, 1882–1892.

Hodson-Tole, E. F. and Wakeling, J. M. (2008b). Motor unit recruitment patterns 2: the influence of myoelectric intensity and muscle fascicle strain rate. *J. Exp. Biol.* **211**, 1893–1902.

Hoffer, J. A., O'Donovan, M. J., Pratt, C. A. and Loeb, G. E. (1981). Discharge patterns of hindlimb motoneurons during normal cat locomotion. *Science* **213**, 466–467.

Holt, N. C., Wakeling, J. M. and Biewener, A. A. (2014). The effect of fast and slow motor unit activation on whole-muscle mechanical performance: the size principle may not pose a mechanical paradox. *Proc. R. Soc. B Biol. Sci.* **281**, 20140002.

Hug, F. and Dorel, S. (2009). Electromyographic analysis of pedaling: a review. *J. Electromyogr. Kinesiol.* **19**, 182–198.

Hug, F., Decherchi, P., Marqueste, T. and Jammes, Y. (2004a). EMG versus oxygen uptake during cycling exercise in trained and untrained subjects. *J. Electromyogr. Kinesiol.* **14**, 187–195.

Hug, F., Bendahan, D., Le Fur, Y., Cozzone, P. J. and Grelot, L. (2004b). Heterogeneity of muscle recruitment pattern during pedaling in professional road cyclists: a magnetic resonance imaging and electromyography study. *Eur. J. Appl. Physiol.* **92**, 334–342.

Hug, F., Drouet, J. M., Champoux, Y., Couturier, A. and Dorel, S. (2008). Interindividual variability of electromyographic patterns and pedal force profiles in trained cyclists. *Eur. J. Appl. Physiol.* **104**, 667–678.

Ivy, J. L., Chi, M. M., Hintz, C. S., Sherman, W. M., Hellendall, R. P. and Lowry, O. H. (1987). Progressive metabolite changes in individual human muscle fibers with increasing work rates. *Am. J. Physiol.-Cell Physiol.* **252**, C630–C639.

Jammes, Y., Caquelard, F. and Badier, M. (1998). Correlation between surface electromyogram, oxygen uptake and blood lactate concentration during dynamic leg exercises. *Respir. Physiol.* **112**, 167–174.

Jayne, B. C. and Lauder, G. V. (1994). How swimming fish use slow and fast muscle fibers: implications for models of vertebrate muscle recruitment. *J. Comp. Physiol. A* **175**, 123–131.

Jones, A. M. and Poole, D. C. (2005). *Oxygen uptake kinetics in sport, exercise and medicine*. Routledge, London.

Jorge, M. and Hull, M. L. (1986). Analysis of EMG measurements during bicycle pedalling. *J. Biomech.* **19**, 683–694.

Josephson, R. K. (1999). Dissecting muscle power output. *J. Exp. Biol.* **202**, 3369–3375.

Josephson, R. K. and Edman, K. A. P. (1988). The consequences of fibre heterogeneity on the force-velocity relation of skeletal muscle. *Acta Physiol. Scand.* **132**, 341–352.

Kautz, S. A. and Hull, M. L. (1993). A theoretical basis for interpreting the force applied to the pedal in cycling. *J. Biomech.* **26**, 155.

Koh, C. E., Young, C. J., Young, J. M. and Solomon, M. J. (2008). Systematic review of randomized controlled trials of the effectiveness of biofeedback for pelvic floor dysfunction. *Br. J. Surg.* **95**, 1079–1087.

Kohler, G. and Boutellier, U. (2005). The generalized force–velocity relationship explains why the preferred pedaling rate of cyclists exceeds the most efficient one. *Eur. J. Appl. Physiol.* **94**, 188–195.

Korff, T., Romer, L. M., Mayhew, I. A. N. and Martin, J. C. (2007). Effect of Pedaling Technique on Mechanical Effectiveness and Efficiency in Cyclists. *Med. Sci. Sports Exerc.* **39**, 991.

Kupa, E. J., Roy, S. H., Kandarian, S. C. and De Luca, C. J. (1995). Effects of muscle fiber type and size on EMG median frequency and conduction velocity. *J. Appl. Physiol.* **79**, 23–32.

Lamarra, N., Whipp, B. J., Ward, S. A. and Wasserman, K. (1987). Effect of interbreath fluctuations on characterizing exercise gas exchange kinetics. *J. Appl. Physiol.* **62**, 2003–2012.

Lawrence, J. H. and De Luca, C. J. (1983). Myoelectric signal versus force relationship in different human muscles. *J. Appl. Physiol.* **54**, 1653–1659.

Lee, S. S. M., de Boef Miara, M., Arnold, A. S., Biewener, A. A. and Wakeling, J. M. (2011). EMG analysis tuned for determining the timing and level of activation in different motor units. *J. Electromyogr. Kinesiol.* **21**, 557–565.

Lee, S. S. M., de Boef Miara, M., Arnold, A. S., Biewener, A. A. and Wakeling, J. M. (2013). Recruitment of faster motor units is associated with greater rates of fascicle strain and rapid changes in muscle force during locomotion. *J. Exp. Biol.* **216**, 198–207.

Leirdal, S. and Ettema, G. (2011). Pedaling technique and energy cost in cycling. *Med. Sci. Sports Exerc.* **43**, 701–705.

Lucia, A., Hoyos, J. and Chicharro, J. L. (2001). Preferred pedalling cadence in professional cycling. *Med. Sci. Sports Exerc.* **33**, 1361–1366.

Lucia, A., Juan, A. F. S., Montilla, M., Canete, S., Santalla, A., Earnest, C. and Perez, M. (2004). In professional road cyclists, low pedaling cadences are less efficient. *Med. Sci. Sports Exerc.* **36**, 1048–1054.

MacIntosh, B. R., Neptune, R. R. and Horton, J. F. (2000). Cadence, power, and muscle activation in cycle ergometry. *Med. Sci. Sports Exerc.* **32**, 1281–1287.

Marsh, A. P. and Martin, P. E. (1995). The relationship between cadence and lower extremity EMG in cyclists and noncyclists. *Med. Sci. Sports Exerc.* **27**, 217–225.

Marsh, A. P., Martin, P. E. and Foley, K. O. (2000). Effect of cadence, cycling experience, and aerobic power on delta efficiency during cycling. *Med. Sci. Sports Exerc.* **32**, 1630.

Martin, J. C. and Brown, N. A. T. (2009). Joint-specific power production and fatigue during maximal cycling. *J. Biomech.* **42**, 474–479.

Moreland, J. D., Thomson, M. A. and Fuoco, A. R. (1998). Electromyographic biofeedback to improve lower extremity function after stroke: A meta-analysis. *Arch Phys Med Rehabil* **79**, 134–140.

Moseley, L., Achten, J., Martin, J. C. and Jeukendrup, A. E. (2004). No differences in cycling efficiency between world-class and recreational cyclists. *Int. J. Sports Med.* **25**, 374–379.

Muniz, A. M. S. and Nadal, J. (2009). Application of principal component analysis in vertical ground reaction force to discriminate normal and abnormal gait. *Gait Posture* **29**, 31–35.

Nardone, A., Romano, C. and Schieppati, M. (1989). Selective recruitment of high-threshold human motor units during voluntary isotonic lengthening of active muscles. *J. Physiol.* **409**, 451–471.

Neptune, R. R. and Herzog, W. (1999). The association between negative muscle work and pedaling rate. *J. Biomech.* **32**, 1021–1026.

Neptune, R. R. and Kautz, S. A. (2001). Muscle activation and deactivation dynamics: the governing properties in fast cyclical human movement performance? *Exerc. Sport Sci. Rev.* **29**, 76–81.

Neptune, R. R., Kautz, S. A. and Hull, M. L. (1997). The effect of pedaling rate on coordination in cycling. *J. Biomech.* **30**, 1051–1058.

Nestoriuc, Y., Martin, A., Rief, W. and Andrasik, F. (2008). Biofeedback treatment for headache disorders: a comprehensive efficacy review. *Appl Psychophysiol Biofeedback* **33**, 125–140.

Patterson, R. P., Pearson, J. L. and Fisher, S. V. (1983). The influence of flywheel weight and pedalling frequency on the biomechanics and physiological responses to bicycle exercise. *Ergonomics.* **26**, 659–668.

Petrofsky, J. S. (1979). Frequency and amplitude analysis of the EMG during exercise on the bicycle ergometer. *Eur. J. Appl. Physiol.* **41**, 1–15.

Poole, D. C., Gaesser, G. A., Hogan, M. C., Knight, D. R. and Wagner, P. D. (1992). Pulmonary and leg VO2 during submaximal exercise: implications for muscular efficiency. *J. Appl. Physiol.* **72**, 805–810.

Preatoni, E., Hamill, J., Harrison, A. J., Hayes, K., Van Emmerik, R. E., Wilson, C. and Rodano, R. (2013). Movement variability and skills monitoring in sports. *Sports Biomech.* **12**, 69–92.

Raasch, C. C., Zajac, F. E., Ma, B. and Levine, W. S. (1997). Muscle coordination of maximum-speed pedaling. *J. Biomech.* **30**, 595–602.

Ramsay, J. O. and Silverman, B. W. (2005). *Functional data analysis*. 2nd ed. New York ; Berlin: Springer.

Roberts, T. J. and Gabaldón, A. M. (2008). Interpreting muscle function from EMG: lessons learned from direct measurements of muscle force. *Integr. Comp. Biol.* **48**, 312–320.

Samozino, P., Horvais, N. and Hintzy, F. (2007). Why does power output decrease at high pedaling rates during sprint cycling? *Med. Sci. Sports Exerc.* **39**, 680–687.

Sanderson, D. J. (1991). The influence of cadence and power output on the biomechanics of force application during steady-rate cycling in competitive and recreational cyclists. *J Sports Sci* **9**, 191–203.

Sargeant, A. J. (1994). Human power output and muscle fatigue. *Int. J. Sports Med.* **15**, 116–121.

Sargeant, A. J. (2007). Structural and functional determinants of human muscle power. *Exp. Physiol.* **92**, 323–331.

Sargeant, A. J. and Beelen, A. (1993). Human muscle fatigue in dynamic exercise. In *Neuromuscular Fatigue*, pp. 81–92. Amsterdam: Academy Series, Royal Netherlands Academy of Arts and Sciences.

Sargeant, A. J., Hoinville, E. and Young, A. (1981). Maximum leg force and power output during short-term dynamic exercise. *J. Appl. Physiol.* **51**, 1175–1182.

Sarre, G. and Lepers, R. (2005). Neuromuscular function during prolonged pedalling exercise at different cadences. *Acta Physiol. Scand.* **185**, 321–328.

Sarre, G. and Lepers, R. (2007). Cycling exercise and the determination of electromechanical delay. *J. Electromyogr. Kinesiol.* **17**, 617–621.

Sarre, G., Lepers, R., Maffiuletti, N., Millet, G. and Martin, A. (2003). Influence of cycling cadence on neuromuscular activity of the knee extensors in humans. *Eur. J. Appl. Physiol.* **88**, 476–479.

Seabury, J. J., Adams, W. C. and Ramey, M. R. (1977). Influence of pedalling rate and power output on energy expenditure during bicycle ergometry. *Ergonomics* **20**, 491–498.

Sidossis, L. S., Horowitz, J. F. and Coyle, E. F. (1992). Load and velocity of contraction influence gross and delta mechanical efficiency. *Int. J. Sports Med.* **13**, 407–411.

Smith, J. L., Betts, B., Edgerton, V. R. and Zernicke, R. F. (1980). Rapid ankle extension during paw shakes: selective recruitment of fast ankle extensors. *J. Neurophysiol.* **43**, 612–620.

Solomonow, M., Baten, C., Smit, J., Baratta, R., Hermens, H., D'ambrosia, R. and Shoji, H. (1990). Electromyogram power spectra frequencies associated with motor unit recruitment strategies. *J. Appl. Physiol.* **68**, 1177–1185.

Takaishi, T., Yasuda, Y., Ono, T. and Moritani, T. (1996). Optimal pedaling rate estimated from neuromuscular fatigue for cyclists. *Med. Sci. Sports Exerc.* **28**, 1492–1497.

Takaishi, T., Yamamoto, T., Ono, T., Ito, T. and Moritani, T. (1998). Neuromuscular, metabolic, and kinetic adaptations for skilled pedaling performance in cyclists. *Med. Sci. Sports Exerc.* **30**, 442–449.

Troje, N. F. (2002). Decomposing biological motion: A framework for analysis and synthesis of human gait patterns. *J. Vis.* **2**, 371–387.

Van Emmerik, R. E., Hamill, J. and McDermott, W. J. (2005). Variability and coordinative function in human gait. *Quest* **57**, 102–123.

van Ingen Schenau, G. J., Boots, P. J. M., de Groot, G., Snackers, R. J. and van Woensel, W. W. L. M. (1992). The constrained control of force and position in multi-joint movements. *Neuroscience* **46**, 197–207.

Van Soest, A. J. and Casius, L. J. (2000). Which factors determine the optimal pedaling rate in sprint cycling? *Med. Sci. Sports Exerc.* **32**, 1927–1934.

Vereijken, B., Van Emmerik, R. E. A., Bongaardt, R., Beek, W. J. and Newell, K. M. (1997). Changing coordinative structures in complex skill acquisition. *Hum. Mov. Sci.* **16**, 823–844.

von Tscharner, V. (2000). Intensity analysis in time-frequency space of surface myoelectric signals by wavelets of specified resolution. *J. Electromyogr. Kinesiol.* **10**, 433–445.

von Tscharner, V. and Goepfert, B. (2003). Gender dependent EMGs of runners resolved by time/frequency and principal pattern analysis. *J. Electromyogr. Kinesiol.* **13**, 253–272.

von Tscharner, V. and Nigg, B. M. (2008). Point: Counterpoint: Spectral properties of the surface EMG can characterize/do not provide information about motor unit recruitment strategies and muscle fiber type. *J. Appl. Physiol.* **105**, 1671–1673.

Wakeling, J. M. (2004). Motor units are recruited in a task-dependent fashion during locomotion. *J. Exp. Biol.* **207**, 3883–3890.

Wakeling, J. M. (2009). Patterns of motor recruitment can be determined using surface EMG. *J. Electromyogr. Kinesiol.* **19**, 199–207.

Wakeling, J. M. and Horn, T. (2009). Neuromechanics of muscle synergies during cycling. *J. Neurophysiol.* **101**, 843–854.

Wakeling, J. M. and Rozitis, A. I. (2004). Spectral properties of myoelectric signals from different motor units in the leg extensor muscles. *J. Exp. Biol.* **207**, 2519–2528.

Wakeling, J. M., Pascual, S. A., Nigg, B. M. and Tscharner, V. (2001). Surface EMG shows distinct populations of muscle activity when measured during sustained sub-maximal exercise. *Eur. J. Appl. Physiol.* **86**, 40–47.

Wakeling, J. M., Kaya, M., Temple, G. K., Johnston, I. A. and Herzog, W. (2002). Determining patterns of motor recruitment during locomotion. *J. Exp. Biol.* **205**, 359–369.

Wakeling, J. M., Uehli, K. and Rozitis, A. I. (2006). Muscle fibre recruitment can respond to the mechanics of the muscle contraction. *J. R. Soc. Interface* **3**, 533–544.

Wakeling, J., Delaney, R. and Dudkiewicz, I. (2007). A method for quantifying dynamic muscle dysfunction in children and young adults with cerebral palsy. *Gait Posture* **25**, 580–589.

Wakeling, J. M., Blake, O. M. and Chan, H. K. (2010). Muscle coordination is key to the power output and mechanical efficiency of limb movements. *J. Exp. Biol.* **213**, 487–492.

Wakeling, J. M., Blake, O. M., Wong, I., Rana, M. and Lee, S. S. M. (2011). Movement mechanics as a determinate of muscle structure, recruitment and coordination. *Phil Trans R Soc B* **366**, 1554–1564.

Whipp, B. J., Ward, S. A., Lamarra, N., Davis, J. A. and Wasserman, K. (1982). Parameters of ventilatory and gas exchange dynamics during exercise. *J. Appl. Physiol.* **52**, 1506–1513.

Wilson, C., Simpson, S. E., Van Emmerik, R. E. and Hamill, J. (2008). Coordination variability and skill development in expert triple jumpers. *Sports Biomech.* **7**, 2–9.

Young, C. and Reinkensmeyer, D. J. (2014). Judging complex movement performances for excellence: A principal components analysis-based technique applied to competitive diving. *Hum. Mov. Sci.* **36**, 107–122.

Zajac, F. E. (1989). Muscle and tendon: properties, models, scaling, and application to biomechanics and motor control. *Crit Rev Biomed Eng* **17**, 359–411.